

8

Anthropogenic and Natural Radiative Forcing

Coordinating Lead Authors:

Gunnar Myhre (Norway), Drew Shindell (USA)

Lead Authors:

François-Marie Bréon (France), William Collins (UK), Jan Fuglestedt (Norway), Jianping Huang (China), Dorothy Koch (USA), Jean-François Lamarque (USA), David Lee (UK), Blanca Mendoza (Mexico), Teruyuki Nakajima (Japan), Alan Robock (USA), Graeme Stephens (USA), Toshihiko Takemura (Japan), Hua Zhang (China)

Contributing Authors:

Borgar Aamaas (Norway), Olivier Boucher (France), Stig B. Dalsøren (Norway), John S. Daniel (USA), Piers Forster (UK), Claire Granier (France), Joanna Haigh (UK), Øivind Hodnebrog (Norway), Jed O. Kaplan (Switzerland/Belgium/USA), George Marston (UK), Claus J. Nielsen (Norway), Brian C. O'Neill (USA), Glen P. Peters (Norway), Julia Pongratz (Germany), Michael Prather (USA), Venkatachalam Ramaswamy (USA), Raphael Roth (Switzerland), Leon Rotstayn (Australia), Steven J. Smith (USA), David Stevenson (UK), Jean-Paul Vernier (USA), Oliver Wild (UK), Paul Young (UK)

Review Editors:

Daniel Jacob (USA), A.R. Ravishankara (USA), Keith Shine (UK)

This chapter should be cited as:

Myhre, G., D. Shindell, F.-M. Bréon, W. Collins, J. Fuglestedt, J. Huang, D. Koch, J.-F. Lamarque, D. Lee, B. Mendoza, T. Nakajima, A. Robock, G. Stephens, T. Takemura and H. Zhang, 2013: Anthropogenic and Natural Radiative Forcing. In: *Climate Change 2013: The Physical Science Basis. Contribution of Working Group I to the Fifth Assessment Report of the Intergovernmental Panel on Climate Change* [Stocker, T.F., D. Qin, G.-K. Plattner, M. Tignor, S.K. Allen, J. Boschung, A. Nauels, Y. Xia, V. Bex and P.M. Midgley (eds.)]. Cambridge University Press, Cambridge, United Kingdom and New York, NY, USA.

Table of Contents

Executive Summary 661

8.1 Radiative Forcing 664

8.1.1 The Radiative Forcing Concept 664

Box 8.1: Definition of Radiative Forcing and Effective Radiative Forcing 665

Box 8.2: Grouping Forcing Compounds by Common Properties 668

8.1.2 Calculation of Radiative Forcing due to Concentration or Emission Changes 668

8.2 Atmospheric Chemistry 669

8.2.1 Introduction 669

8.2.2 Global Chemistry Modelling in Coupled Model Intercomparison Project Phase 5 670

8.2.3 Chemical Processes and Trace Gas Budgets 670

8.3 Present-Day Anthropogenic Radiative Forcing 675

8.3.1 Updated Understanding of the Spectral Properties of Greenhouse Gases and Radiative Transfer Codes 675

8.3.2 Well-mixed Greenhouse Gases 676

8.3.3 Ozone and Stratospheric Water Vapour 679

8.3.4 Aerosols and Cloud Effects 682

8.3.5 Land Surface Changes 686

8.4 Natural Radiative Forcing Changes: Solar and Volcanic 688

8.4.1 Solar Irradiance 688

8.4.2 Volcanic Radiative Forcing 691

Box 8.3: Volcanic Eruptions as Analogues 693

8.5 Synthesis of Global Mean Radiative Forcing, Past and Future 693

8.5.1 Summary of Radiative Forcing by Species and Uncertainties 694

8.5.2 Time Evolution of Historical Forcing 698

8.5.3 Future Radiative Forcing 700

8.6 Geographic Distribution of Radiative Forcing 702

8.6.1 Spatial Distribution of Current Radiative Forcing 702

8.6.2 Spatial Evolution of Radiative Forcing and Response over the Industrial Era 705

8.6.3 Spatial Evolution of Radiative Forcing and Response for the Future 708

8.7 Emission Metrics 710

8.7.1 Metric Concepts 710

Box 8.4: Choices Required When Using Emission Metrics 711

8.7.2 Application of Metrics 716

References 721

Appendix 8.A: Lifetimes, Radiative Efficiencies and Metric Values 731

Frequently Asked Questions

FAQ 8.1 How Important Is Water Vapour to Climate Change? 666

FAQ 8.2 Do Improvements in Air Quality Have an Effect on Climate Change? 684

Supplementary Material

Supplementary Material is available in online versions of the report.

Executive Summary

It is unequivocal that anthropogenic increases in the well-mixed greenhouse gases (WMGHGs) have substantially enhanced the greenhouse effect, and the resulting forcing continues to increase. Aerosols partially offset the forcing of the WMGHGs and dominate the uncertainty associated with the total anthropogenic driving of climate change.

As in previous IPCC assessments, AR5 uses the radiative forcing¹ (RF) concept, but it also introduces effective radiative forcing² (ERF). The RF concept has been used for many years and in previous IPCC assessments for evaluating and comparing the strength of the various mechanisms affecting the Earth's radiation balance and thus causing climate change. Whereas in the RF concept all surface and tropospheric conditions are kept fixed, the ERF calculations presented here allow all physical variables to respond to perturbations except for those concerning the ocean and sea ice. The inclusion of these adjustments makes ERF a better indicator of the eventual temperature response. ERF and RF values are significantly different for anthropogenic aerosols owing to their influence on clouds and on snow cover. These changes to clouds are rapid adjustments and occur on a time scale much faster than responses of the ocean (even the upper layer) to forcing. RF and ERF are estimated over the Industrial Era from 1750 to 2011 if other periods are not explicitly stated. {8.1, Box 8.1, Figure 8.1}

Industrial-Era Anthropogenic Forcing

The total anthropogenic ERF over the Industrial Era is 2.3 (1.1 to 3.3) W m⁻².³ It is certain that the total anthropogenic ERF is positive. Total anthropogenic ERF has increased more rapidly since 1970 than during prior decades. The total anthropogenic ERF estimate for 2011 is 43% higher compared to the AR4 RF estimate for the year 2005 owing to reductions in estimated forcing due to aerosols but also to continued growth in greenhouse gas RF. {8.5.1, Figures 8.15, 8.16}

Due to increased concentrations, RF from WMGHGs has increased by 0.20 (0.18 to 0.22) W m⁻² (8%) since the AR4 estimate for the year 2005. The RF of WMGHG is 2.83 (2.54 to 3.12) W m⁻². The majority of this change since AR4 is due to increases in the carbon dioxide (CO₂) RF of nearly 10%. The Industrial Era RF for CO₂ alone is 1.82 (1.63 to 2.01) W m⁻², and CO₂ is the component with the largest global mean RF. Over the last decade RF of CO₂ has an average growth rate of 0.27 (0.24 to 0.30) W m⁻² per decade. Emissions of CO₂ have made the largest contribution to the increased anthropogenic forcing in every decade since the 1960s. The best estimate for ERF of

WMGHG is the same as the RF but with a larger uncertainty ($\pm 20\%$). {8.3.2, 8.5.2, Figures 8.6, 8.18}

The net forcing by WMGHGs other than CO₂ shows a small increase since the AR4 estimate for the year 2005. A small growth in the CH₄ concentration has increased its RF by 2% to an AR5 value of 0.48 (0.43 to 0.53) W m⁻². RF of nitrous oxide (N₂O) has increased by 6% since AR4 and is now 0.17 (0.14 to 0.20) W m⁻². N₂O concentrations continue to rise while those of dichlorodifluoromethane (CFC-12), the third largest WMGHG contributor to RF for several decades, is falling due to its phase-out under the Montreal Protocol and amendments. Since 2011 N₂O has become the third largest WMGHG contributor to RF. The RF from all halocarbons (0.36 W m⁻²) is very similar to the value in AR4, with a reduced RF from chlorofluorocarbons (CFCs) but increases from many of their substitutes. Four of the halocarbons (trichlorofluoromethane (CFC-11), CFC-12, trichlorotrifluoroethane (CFC-113) and chlorodifluoromethane (HCFC-22)) account for around 85% of the total halocarbon RF. The first three of these compounds have declining RF over the last 5 years but their combined decrease is compensated for by the increased RF from HCFC-22. Since AR4, the RF from all HFCs has nearly doubled but still only amounts to 0.02 W m⁻². There is *high confidence*⁴ that the overall growth rate in RF from all WMGHG is smaller over the last decade than in the 1970s and 1980s owing to a reduced rate of increase in the combined non-CO₂ RF. {8.3.2; Figure 8.6}

Ozone and stratospheric water vapour contribute substantially to RF. The total RF estimated from modelled ozone changes is 0.35 (0.15 to 0.55) W m⁻², with RF due to tropospheric ozone changes of 0.40 (0.20 to 0.60) W m⁻² and due to stratospheric ozone changes of -0.05 (-0.15 to +0.05) W m⁻². Ozone is not emitted directly into the atmosphere but is formed by photochemical reactions. Tropospheric ozone RF is largely attributed to anthropogenic emissions of methane (CH₄), nitrogen oxides (NO_x), carbon monoxide (CO) and non-methane volatile organic compounds (NMVOCs), while stratospheric ozone RF results primarily from ozone depletion by halocarbons. Estimates are also provided attributing RF to emitted compounds. Ozone-depleting substances (ODS) cause ozone RF of -0.15 (-0.30 to 0.0) W m⁻², some of which is in the troposphere. Tropospheric ozone precursors cause ozone RF of 0.50 (0.30 to 0.70) W m⁻², some of which is in the stratosphere; this value is larger than that in AR4. There is *robust evidence* that tropospheric ozone also has a detrimental impact on vegetation physiology, and therefore on its CO₂ uptake, but there is a *low confidence* on quantitative estimates of the RF owing to this indirect effect. RF for stratospheric water vapour produced by CH₄ oxidation is 0.07 (0.02 to 0.12) W m⁻². The RF best estimates for ozone and stratospheric

¹ Change in net downward radiative flux at the tropopause after allowing for stratospheric temperatures to readjust to radiative equilibrium, while holding surface and tropospheric temperatures and state variables fixed at the unperturbed values.

² Change in net downward radiative flux at the top of the atmosphere (TOA) after allowing for atmospheric temperatures, water vapour, clouds and land albedo to adjust, but with global mean surface temperature or ocean and sea ice conditions unchanged (calculations presented in this chapter use the fixed ocean conditions method).

³ Uncertainties are given associated with best estimates of forcing. The uncertainty values represent the 5–95% (90%) confidence range.

⁴ In this Report, the following summary terms are used to describe the available evidence: limited, medium, or robust; and for the degree of agreement: low, medium, or high. A level of confidence is expressed using five qualifiers: very low, low, medium, high, and very high, and typeset in italics, e.g., *medium confidence*. For a given evidence and agreement statement, different confidence levels can be assigned, but increasing levels of evidence and degrees of agreement are correlated with increasing confidence (see Section 1.4 and Box TS.1 for more details).

water vapour are either identical or consistent with the range in AR4. {8.2, 8.3.3, Figure 8.7}

The magnitude of the aerosol forcing is reduced relative to AR4.

The RF due to aerosol–radiation interactions, sometimes referred to as *direct aerosol effect*, is given a best estimate of -0.35 (-0.85 to $+0.15$) W m^{-2} , and black carbon (BC) on snow and ice is 0.04 (0.02 to 0.09) W m^{-2} . The ERF due to aerosol–radiation interactions is -0.45 (-0.95 to $+0.05$) W m^{-2} . A total aerosol–cloud interaction⁵ is quantified in terms of the ERF concept with an estimate of -0.45 (-1.2 to 0.0) W m^{-2} . The total aerosol effect (excluding BC on snow and ice) is estimated as ERF of -0.9 (-1.9 to -0.1) W m^{-2} . The large uncertainty in aerosol ERF is the dominant contributor to overall net Industrial Era forcing uncertainty. Since AR4, more aerosol processes have been included in models, and differences between models and observations persist, resulting in similar uncertainty in the aerosol forcing as in AR4. Despite the large uncertainty range, there is a *high confidence* that aerosols have offset a substantial portion of WMGHG global mean forcing. {8.3.4, 8.5.1, Figures 8.15, 8.16}

There is *robust evidence* that anthropogenic land use change has increased the land surface albedo, which leads to an RF of $-0.15 \pm 0.10 \text{ W m}^{-2}$. There is still a large spread of estimates owing to different assumptions for the albedo of natural and managed surfaces and the fraction of land use changes before 1750. Land use change causes additional modifications that are not radiative, but impact the surface temperature, in particular through the hydrologic cycle. These are more uncertain and they are difficult to quantify, but tend to offset the impact of albedo changes. As a consequence, there is *low agreement* on the sign of the net change in global mean temperature as a result of land use change. {8.3.5}

Attributing forcing to emissions provides a more direct link from human activities to forcing. The RF attributed to methane emissions is *very likely*⁶ to be much larger ($\sim 1.0 \text{ W m}^{-2}$) than that attributed to methane concentration increases ($\sim 0.5 \text{ W m}^{-2}$) as concentration changes result from the partially offsetting impact of emissions of multiple species and subsequent chemical reactions. In addition, emissions of CO are *virtually certain* to have had a positive RF, while emissions of NO_x are *likely* to have had a net negative RF at the global scale. Emissions of ozone-depleting halocarbons are *very likely* to have caused a net positive RF as their own positive RF has outweighed the negative RF from the stratospheric ozone depletion that they have induced. {8.3.3, 8.5.1, Figure 8.17, FAQ 8.2}

Forcing agents such as aerosols, ozone and land albedo changes are highly heterogeneous spatially and temporally. These patterns generally track economic development; strong negative aerosol forcing appeared in eastern North America and Europe during the early

20th century, extending to Asia, South America and central Africa by 1980. Emission controls have since reduced aerosol pollution in North America and Europe, but not in much of Asia. Ozone forcing increased throughout the 20th century, with peak positive amplitudes around 15°N to 30°N due to tropospheric pollution but negative values over Antarctica due to stratospheric loss late in the century. The pattern and spatial gradients of forcing affect global and regional temperature responses as well as other aspects of climate response such as the hydrologic cycle. {8.6.2, Figure 8.25}

Natural Forcing

Satellite observations of total solar irradiance (TSI) changes from 1978 to 2011 show that the most recent solar cycle minimum was lower than the prior two. This *very likely* led to a small negative RF of -0.04 (-0.08 to 0.00) W m^{-2} between 1986 and 2008. The best estimate of RF due to TSI changes representative for the 1750 to 2011 period is 0.05 (to 0.10) W m^{-2} . This is substantially smaller than the AR4 estimate due to the addition of the latest solar cycle and inconsistencies in how solar RF has been estimated in earlier IPCC assessments. There is *very low confidence* concerning future solar forcing estimates, but there is *high confidence* that the TSI RF variations will be much smaller than the projected increased forcing due to GHG during the forthcoming decades. {8.4.1, Figures 8.10, 8.11}

The RF of volcanic aerosols is well understood and is greatest for a short period (~ 2 years) following volcanic eruptions. There have been no major volcanic eruptions since Mt Pinatubo in 1991, but several smaller eruptions have caused a RF for the years 2008–2011 of -0.11 (-0.15 to -0.08) W m^{-2} as compared to 1750 and -0.06 (-0.08 to -0.04) W m^{-2} as compared to 1999–2002. Emissions of CO₂ from volcanic eruptions since 1750 have been at least 100 times smaller than anthropogenic emissions. {8.4.2, 8.5.2, Figures 8.12, 8.13, 8.18}

There is *very high confidence* that industrial-era natural forcing is a small fraction of the anthropogenic forcing except for brief periods following large volcanic eruptions. In particular, *robust evidence* from satellite observations of the solar irradiance and volcanic aerosols demonstrates a near-zero (-0.1 to $+0.1 \text{ W m}^{-2}$) change in the natural forcing compared to the anthropogenic ERF increase of 1.0 (0.7 to 1.3) W m^{-2} from 1980 to 2011. The natural forcing over the last 15 years has *likely* offset a substantial fraction (at least 30%) of the anthropogenic forcing. {8.5.2; Figures 8.18, 8.19, 8.20}

Future Anthropogenic Forcing and Emission Metrics

Differences in RF between the emission scenarios considered here⁷ are relatively small for year 2030 but become very large by 2100 and are dominated by CO₂. The scenarios show a substantial

⁵ The aerosol–cloud interaction represents the portion of rapid adjustments to aerosols initiated by aerosol–cloud interactions, and is defined here as the total aerosol ERF minus the ERF due to aerosol–radiation–interactions (the latter includes cloud responses to the aerosol–radiation interaction RF)

⁶ In this Report, the following terms have been used to indicate the assessed likelihood of an outcome or a result: Virtually certain 99–100% probability, Very likely 90–100%, Likely 66–100%, About as likely as not 33–66%, Unlikely 0–33%, Very unlikely 0–10%, Exceptionally unlikely 0–1%. Additional terms (Extremely likely: 95–100%, More likely than not >50–100%, and Extremely unlikely 0–5%) may also be used when appropriate. Assessed likelihood is typeset in italics, e.g., *very likely* (see Section 1.4 and Box TS.1 for more details).

⁷ Chapter 1 describes the Representative Concentration Pathways (RCPs) that are the primary scenarios discussed in this report.

weakening of the negative total aerosol ERF. Nitrate aerosols are an exception to this reduction, with a substantial increase, which is a robust feature among the few available models for these scenarios. The scenarios emphasized in this assessment do not span the range of future emissions in the literature, however, particularly for near-term climate forcers. {8.2.2, 8.5.3, Figures 8.2, 8.21, 8.22}

Emission metrics such as Global Warming Potential (GWP) and Global Temperature change Potential (GTP) can be used to quantify and communicate the relative and absolute contributions to climate change of emissions of different substances, and of emissions from regions/countries or sources/sectors. The metric that has been used in policies is the GWP, which integrates the RF of a substance over a chosen time horizon, relative to that of CO₂. The GTP is the ratio of change in global mean surface temperature at a chosen point in time from the substance of interest relative to that from CO₂. There are significant uncertainties related to both GWP and GTP, and the relative uncertainties are larger for GTP. There are also limitations and inconsistencies related to their treatment of indirect effects and feedbacks. The values are very dependent on metric type and time horizon. The choice of metric and time horizon depends on the particular application and which aspects of climate change are considered relevant in a given context. Metrics do not define policies or goals but facilitate evaluation and implementation of multi-component policies to meet particular goals. All choices of metric contain implicit value-related judgements such as type of effect considered and weighting of effects over time. This assessment provides updated values of both GWP and GTP for many compounds. {8.7.1, 8.7.2, Table 8.7, Table 8.A.1, Supplementary Material Table 8.SM.16}

Forcing and temperature response can also be attributed to sectors. From this perspective and with the GTP metric, a single year's worth of current global emissions from the energy and industrial sectors have the largest contributions to global mean warming over the next approximately 50 to 100 years. Household fossil fuel and biofuel, biomass burning and on-road transportation are also relatively large contributors to warming over these time scales, while current emissions from sectors that emit large amounts of CH₄ (animal husbandry, waste/landfills and agriculture) are also important over shorter time horizons (up to 20 years). {8.7.2, Figure 8.34}

8.1 Radiative Forcing

There are a variety of ways to examine how various drivers contribute to climate change. In principle, observations of the climate response to a single factor could directly show the impact of that factor, or climate models could be used to study the impact of any single factor. In practice, however, it is usually difficult to find measurements that are influenced by only a single cause, and it is computationally prohibitive to simulate the response to every individual factor of interest. Hence various metrics intermediate between cause and effect are used to provide estimates of the climate impact of individual factors, with applications both in science and policy. Radiative forcing (RF) is one of the most widely used metrics, with most other metrics based on RF. In this chapter, we discuss RF from natural and anthropogenic components during the industrial period, presenting values for 2011 relative to 1750 unless otherwise stated, and projected values through 2100 (see also Annex II). In this section, we present the various definitions of RF used in this chapter, and discuss the utility and limitations of RF. These definitions are used in the subsequent sections quantifying the RF due to specific anthropogenic (Section 8.3) and natural (Section 8.4) causes and integrating RF due to all causes (Sections 8.5 and 8.6). Atmospheric chemistry relevant for RF is discussed in Section 8.2 and used throughout the chapter. Emission metrics using RF that are designed to facilitate rapid evaluation and comparison of the climate effects of emissions are discussed in Section 8.7.

8.1.1 The Radiative Forcing Concept

RF is the net change in the energy balance of the Earth system due to some imposed perturbation. It is usually expressed in watts per square meter averaged over a particular period of time and quantifies the energy imbalance that occurs when the imposed change takes place. Though usually difficult to observe, calculated RF provides a simple quantitative basis for comparing some aspects of the potential climate response to different imposed agents, especially global mean temperature, and hence is widely used in the scientific community. Forcing is often presented as the value due to changes between two particular times, such as pre-industrial to present-day, while its time evolution provides a more complete picture.

8.1.1.1 Defining Radiative Forcing

Alternative definitions of RF have been developed, each with its own advantages and limitations. The instantaneous RF refers to an instantaneous change in net (down minus up) radiative flux (shortwave plus longwave; in $W\ m^{-2}$) due to an imposed change. This forcing is usually defined in terms of flux changes at the top of the atmosphere (TOA) or at the climatological tropopause, with the latter being a better indicator of the global mean surface temperature response in cases when they differ.

Climate change takes place when the system responds in order to counteract the flux changes, and all such responses are explicitly

excluded from this definition of forcing. The assumed relation between a sustained RF and the equilibrium global mean surface temperature response (ΔT) is $\Delta T = \lambda RF$ where λ is the climate sensitivity parameter. The relationship between RF and ΔT is an expression of the energy balance of the climate system and a simple reminder that the steady-state global mean climate response to a given forcing is determined both by the forcing and the responses inherent in λ .

Implicit in the concept of RF is the proposition that the change in net irradiance in response to the imposed forcing alone can be separated from all subsequent responses to the forcing. These are not in fact always clearly separable and thus some ambiguity exists in what may be considered a forcing versus what is part of the climate response.

In both the Third Assessment Report (TAR) and AR4, the term radiative forcing (RF, also called stratospherically adjusted RF, as distinct from instantaneous RF) was defined as the change in net irradiance at the tropopause after allowing for stratospheric temperatures to readjust to radiative equilibrium, while holding surface and tropospheric temperatures and state variables such as water vapour and cloud cover fixed at the unperturbed values⁸. RF is generally more indicative of the surface and tropospheric temperature responses than instantaneous RF, especially for agents such as carbon dioxide (CO₂) or ozone (O₃) change that substantially alter stratospheric temperatures. To be consistent with TAR and AR4, RF is hereafter taken to mean the stratospherically adjusted RF.

8.1.1.2 Defining Effective Radiative Forcing

For many forcing agents the RF gives a very useful and appropriate way to compare the relative importance of their potential climate effect. Instantaneous RF or RF is not an accurate indicator of the temperature response for all forcing agents, however. Rapid adjustments in the troposphere can either enhance or reduce the flux perturbations, leading to substantial differences in the forcing driving long-term climate change. In much the same way that allowing for the relatively rapid adjustment of stratospheric temperatures provides a more useful characterization of the forcing due to stratospheric constituent changes, inclusion of rapid tropospheric adjustments has the potential to provide more useful characterization for drivers in the troposphere (see also Section 7.1.3).

Many of the rapid adjustments affect clouds and are not readily included into the RF concept. For example, for aerosols, especially absorbing ones, changes in the temperature distribution above the surface occur due to a variety of effects, including cloud response to changing atmospheric stability (Hansen et al., 2005; see Section 7.3.4.2) and cloud absorption effects (Jacobson, 2012), which affect fluxes but are not strictly part of RF. Similar adjustments take place for many forcings, including CO₂ (see Section 7.2.5.6).

Aerosols also alter cloud properties via microphysical interactions leading to indirect forcings (referred to as aerosol–cloud interactions;

⁸ Tropospheric variables were fixed except for the impact of aerosols on cloud albedo due to changes in droplet size with constant cloud liquid water which was considered an RF in AR4 but is part of ERF in AR5.

see Section 7.4). Although these adjustments are complex and not fully quantified, they occur both on the microphysical scale of the cloud particles as well as on a more macroscopic scale involving whole cloud systems (e.g., Shine et al., 2003; Penner et al., 2006; Quaas et al., 2009). A portion of these adjustments occurs over a short period, on cloud life cycle time scales, and is not part of a feedback arising from the surface temperature changes. Previously these type of adjustments were sometimes termed ‘fast feedbacks’ (e.g., Gregory et al., 2004; Hansen et al., 2005), whereas in AR5 they are denoted ‘rapid adjustments’ to emphasize their distinction from feedbacks involving surface temperature changes. Atmospheric chemistry responses have typically been included under the RF framework, and hence could also be included in a forcing encompassing rapid adjustments, which is important when evaluating forcing attributable to emissions changes (Section 8.1.2) and in the calculation of emission metrics (Section 8.7).

Studies have demonstrated the utility of including rapid adjustment in comparison of forcing agents, especially in allowing quantification of forcing due to aerosol-induced changes in clouds (e.g., effects previously denoted as cloud lifetime or semi-direct effects; see Figure 7.3) that are not amenable to characterization by RF (e.g., Rotstayn and Penner, 2001; Shine et al., 2003; Hansen et al., 2005; Lohmann et al., 2010; Ban-Weiss et al., 2012). Several measures of forcing have been introduced that include rapid adjustments. We term a forcing that accounts for rapid adjustments the effective radiative forcing (ERF). Conceptually, ERF represents the change in net TOA downward radiative flux after allowing for atmospheric temperatures, water vapour and clouds to adjust, but with global mean surface temperature or a portion of surface conditions unchanged. The primary methods in use for such calculations are (1) fixing sea surface temperatures (SSTs) and sea ice cover at climatological values while allowing all other parts of the system to respond until reaching steady state (e.g., Hansen et al., 2005) or (2) analyzing the transient global mean surface temperature response to an instantaneous perturbation and using the regression of the response extrapolated back to the start of the simulation to derive

the initial ERF (Gregory et al., 2004; Gregory and Webb, 2008). The ERF calculated using the regression technique has an uncertainty of about 10% (for the 5 to 95% confidence interval) for a single $4 \times \text{CO}_2$ simulation (ERF $\sim 7 \text{ W m}^{-2}$) due to internal variability in the transient climate (Andrews et al., 2012a), while given a similar length simulation the uncertainty due to internal variability in ERF calculated using the fixed-SST technique is much smaller and hence the latter may be more suitable for very small forcings. Analysis of both techniques shows that the fixed-SST method yields a smaller spread across models, even in calculations neglecting the uncertainty in the regression fitting procedure (Andrews et al., 2012a). As a portion of land area responses are included in the fixed-SST technique, however, that ERF is slightly less than it would be with surface temperature held fixed everywhere. It is possible to adjust for this in the global mean forcing, though we do not include such a correction here as we examine regional as well as global ERF, but the land response will also introduce artificial gradients in land–sea temperatures that could cause small local climate responses. In contrast, there is no global mean temperature response included in the regression method. Despite the low bias in fixed-SST ERF due to land responses, results from a multi-model analysis of the forcing due to CO_2 are 7% greater using this method than using the regression technique (Andrews et al., 2012a) though this is within the uncertainty range of the calculations. Although each technique has advantages, forcing diagnosed using the fixed-SST method is available for many more forcing agents in the current generation of climate models than forcing diagnosed using the regression method. Hence for practical purposes, ERF is hereafter used for results from the fixed-SST technique unless otherwise stated (see also Box 8.1).

The conceptual relation between instantaneous RF, RF and ERF is illustrated in Figure 8.1. It implies the adjustments to the instantaneous RF involve effects of processes that occur more rapidly than the time scale of the response of the global mean surface temperature to the forcing. However, there is no *a priori* time scale defined for adjustments to be rapid with the fixed-SST method. The majority take place on time scales

Box 8.1 | Definition of Radiative Forcing and Effective Radiative Forcing

The two most commonly used measures of radiative forcing in this chapter are the radiative forcing (RF) and the effective radiative forcing (ERF). RF is defined, as it was in AR4, as the change in net downward radiative flux at the tropopause after allowing for stratospheric temperatures to readjust to radiative equilibrium, while holding surface and tropospheric temperatures and state variables such as water vapor and cloud cover fixed at the unperturbed values.

ERF is the change in net TOA downward radiative flux after allowing for atmospheric temperatures, water vapour and clouds to adjust, but with surface temperature or a portion of surface conditions unchanged. Although there are multiple methods to calculate ERF, we take ERF to mean the method in which sea surface temperatures and sea ice cover are fixed at climatological values unless otherwise specified. Land surface properties (temperature, snow and ice cover and vegetation) are allowed to adjust in this method. Hence ERF includes both the effects of the forcing agent itself and the rapid adjustments to that agent (as does RF, though stratospheric temperature is the only adjustment for the latter). In the case of aerosols, the rapid adjustments of clouds encompass effects that have been referred to as indirect or semi-direct forcings (see Figure 7.3 and Section 7.5), with some of these same cloud responses also taking place for other forcing agents (see Section 7.2). Calculation of ERF requires longer simulations with more complex models than calculation of RF, but the inclusion of the additional rapid adjustments makes ERF a better indicator of the eventual global mean temperature response, especially for aerosols. When forcing is attributed to emissions or used for calculation of emission metrics, additional responses including atmospheric chemistry and the carbon cycle are also included in both RF and ERF (see Section 8.1.2). The general term *forcing* is used to refer to both RF and ERF.

FAQ 8.1 (continued)

Currently, water vapour has the largest greenhouse effect in the Earth's atmosphere. However, other greenhouse gases, primarily CO₂, are necessary to sustain the presence of water vapour in the atmosphere. Indeed, if these other gases were removed from the atmosphere, its temperature would drop sufficiently to induce a decrease of water vapour, leading to a runaway drop of the greenhouse effect that would plunge the Earth into a frozen state. So greenhouse gases other than water vapour provide the temperature structure that sustains current levels of atmospheric water vapour. Therefore, although CO₂ is the main anthropogenic control knob on climate, water vapour is a strong and fast feedback that amplifies any initial forcing by a typical factor between two and three. Water vapour is not a significant initial forcing, but is nevertheless a fundamental agent of climate change.

of seasons or less, but there is a spectrum of adjustment times. Changes in land ice and snow cover, for instance, may take place over many years. The ERF thus represents that part of the instantaneous RF that is maintained over long time scales and more directly contributes to the steady-state climate response. The RF can be considered a more limited version of ERF. Because the atmospheric temperature has been allowed to adjust, ERF would be nearly identical if calculated at the tropopause instead of the TOA for tropospheric forcing agents, as would RF. Recent work has noted likely advantages of the ERF framework for understanding model responses to CO₂ as well as to more complex forcing agents (see Section 7.2.5.6).

The climate sensitivity parameter λ derived with respect to RF can vary substantially across different forcing agents (Forster et al., 2007). The response to RF from a particular agent relative to the response to RF from CO₂ has been termed the *efficacy* (Hansen et al., 2005). By including many of the rapid adjustments that differ across forcing agents, the ERF concept includes much of their relative efficacy and therefore leads to more uniform climate sensitivity across agents. For example, the influence of clouds on the interaction of aerosols with sunlight and the effect of aerosol heating on cloud formation can lead to very large differences in the response per unit RF from black carbon (BC) located at different altitudes, but the response per unit ERF is nearly uniform with altitude (Hansen et al., 2005; Ming et al., 2010; Ban-Weiss et al., 2012). Hence as we use ERF in this chapter when it differs significantly from RF, efficacy is not used hereinafter. For inhomogeneous forcings, we note that the climate sensitivity parameter may also depend on the horizontal forcing distribution, especially with latitude (Shindell and Faluvegi, 2009; Section 8.6.2).

A combination of RF and ERF will be used in this chapter with RF provided to keep consistency with TAR and AR4, and ERF used to allow quantification of more complex forcing agents and, in some cases, provide a more useful metric than RF.

8.1.1.3 Limitations of Radiative Forcing

Both the RF and ERF concepts have strengths and weaknesses in addition to those discussed previously. Dedicated climate model simulations that are required to diagnose the ERF can be more computationally demanding than those for instantaneous RF or RF because many years are required to reduce the influence of climate variability. The presence of meteorological variability can also make it difficult to

isolate the ERF of small forcings that are easily isolated in the pair of radiative transfer calculations performed for RF (Figure 8.1). For RF, on the other hand, a definition of the tropopause is required, which can be ambiguous.

In many cases, however, ERF and RF are nearly equal. Analysis of 11 models from the current Coupled Model Intercomparison Project Phase 5 (CMIP5) generation finds that the rapid adjustments to CO₂ cause fixed-SST-based ERF to be 2% less than RF, with an intermodel standard deviation of 7% (Vial et al., 2013). This is consistent with an earlier study of six GCMs that found a substantial inter-model variation in the rapid tropospheric adjustment to CO₂ using regression analysis in slab ocean models, though the ensemble mean adjustment was less than 5% (Andrews and Forster, 2008). Part of the large uncertainty range arises from the greater noise inherent in regression analyses of single runs in comparison with fixed-SST experiments. Using fixed-SST simulations, Hansen et al. (2005) found that ERF is virtually identical to RF for increased CO₂, tropospheric ozone and solar irradiance, and within 6% for methane (CH₄), nitrous oxide (N₂O), stratospheric aerosols and for the aerosol–radiation interaction of reflective aerosols. Shindell et al. (2013b) also found that RF and ERF are statistically equal for tropospheric ozone. Lohmann et al. (2010) report a small increase in the forcing from CO₂ using ERF instead of RF based on the fixed-SST technique, while finding no substantial difference for CH₄, RF due to aerosol–radiation interactions or aerosol effects on cloud albedo. In the fixed-SST simulations of Hansen et al. (2005), ERF was about 20% less than RF for the atmospheric effects of BC aerosols (not including microphysical aerosol–cloud interactions), and nearly 300% greater for the forcing due to BC snow albedo forcing (Hansen et al., 2007). ERF was slightly greater than RF for stratospheric ozone in Hansen et al. (2005), but the opposite is true for more recent analyses (Shindell et al., 2013b), and hence it seems most appropriate at present to use RF for this small forcing. The various studies demonstrate that RF provides a good estimate of ERF in most cases, as the differences are very small, with the notable exceptions of BC-related forcings (Bond et al., 2013). ERF provides better characterization of those effects, as well as allowing quantification of a broader range of effects including all aerosol–cloud interactions. Hence while RF and ERF are generally quite similar for WMGHGs, ERF typically provides a more useful indication of climate response for near-term climate forcings (see Box 8.2). As the rapid adjustments included in ERF differ in strength across climate models, the uncertainty range for ERF estimates tends to be larger than the range for RF estimates.

Box 8.2 | Grouping Forcing Compounds by Common Properties

As many compounds cause RF when their atmospheric concentration is changed, it can be useful to refer to groups of compounds with similar properties. Here we discuss two primary groupings: well-mixed greenhouse gases (WMGHGs) and near-term climate forcers (NTCFs).

We define as ‘well-mixed’ those greenhouse gases that are sufficiently mixed throughout the troposphere that concentration measurements from a few remote surface sites can characterize the climate-relevant atmospheric burden; although these gases may still have local variation near sources and sinks and even small hemispheric gradients. Global forcing per unit emission and emission metrics for these gases thus do not depend on the geographic location of the emission, and forcing calculations can assume even horizontal distributions. These gases, or a subset of them, have sometimes been referred to as ‘long-lived greenhouse gases’ as they are well mixed because their atmospheric lifetimes are much greater than the time scale of a few years for atmospheric mixing, but the physical property that causes the aforementioned common characteristics is more directly associated with their mixing within the atmosphere. WMGHGs include CO₂, N₂O, CH₄, SF₆, and many halogenated species. Conversely, ozone is not a WMGHG.

We define ‘near-term climate forcers’ (NTCFs) as those compounds whose impact on climate occurs primarily within the first decade after their emission. This set of compounds is composed primarily of those with short lifetimes in the atmosphere compared to WMGHGs, and has been sometimes referred to as short-lived climate forcers or short-lived climate pollutants. However, the common property that is of greatest interest to a climate assessment is the time scale over which their impact on climate is felt. This set of compounds includes methane, which is also a WMGHG, as well as ozone and aerosols, or their precursors, and some halogenated species that are not WMGHGs. These compounds do not accumulate in the atmosphere at decadal to centennial time scales, and so their effect on climate is predominantly in the near term following their emission.

Whereas the global mean ERF provides a useful indication of the eventual change in global mean surface temperature, it does not reflect regional climate changes. This is true for all forcing agents, but is especially the case for the inhomogeneously distributed forcings because they activate climate feedbacks based on their regional distribution. For example, forcings over Northern Hemisphere (NH) middle and high latitudes induce snow and ice albedo feedbacks more than forcings at lower latitudes or in the Southern Hemisphere (SH) (e.g., Shindell and Faluvegi, 2009).

In the case of agents that strongly absorb incoming solar radiation (such as BC, and to a lesser extent organic carbon (OC) and ozone) the TOA forcing provides little indication of the change in solar radiation reaching the surface which can force local changes in evaporation and alter regional and general circulation patterns (e.g., Ramanathan and Carmichael, 2008; Wang et al., 2009). Hence the forcing at the surface, or the atmospheric heating, defined as the difference between surface and tropopause/TOA forcing, might also be useful metrics. Global mean precipitation changes can be related separately to ERF within the atmosphere and to a slower response to global mean temperature changes (Andrews et al., 2010; Ming et al., 2010; Ban-Weiss et al., 2012). Relationships between surface forcing and localized aspects of climate response have not yet been clearly quantified, however.

In general, most widely used definitions of forcing and most forcing-based metrics are intended to be proportional to the eventual temperature response, and most analyses to date have explored the global mean temperature response only. These metrics do not explicitly include impacts such as changes in precipitation, surface sunlight available for photosynthesis, extreme events, and so forth, or regional

temperatures, which can differ greatly from the global mean. Hence although they are quite useful for understanding the factors driving global mean temperature change, they provide only an imperfect and limited perspective on the factors driving broader climate change. In addition, a metric based solely on radiative perturbations does not allow comparison of non-RFs, such as effects of land cover change on evapotranspiration or physiological impacts of CO₂ and O₃ except where these cause further impacts on radiation such as through cloud cover changes (e.g., Andrews et al., 2012b).

8.1.2 Calculation of Radiative Forcing due to Concentration or Emission Changes

Analysis of forcing due to observed or modelled concentration changes between pre-industrial, defined here as 1750, and a chosen later year provides an indication of the importance of different forcing agents to climate change during that period. Such analyses have been a mainstay of climate assessments. This perspective has the advantage that observational data are available to accurately quantify the concentration changes for several of the largest forcing components. Atmospheric concentration changes, however, are the net result of variations in emissions of multiple compounds and any climate changes that have influenced processes such as wet removal, atmospheric chemistry or the carbon cycle. Characterizing forcing according to *concentration* changes thus mixes multiple root causes along with climate feedbacks. Policy decisions are better informed by analysis of forcing attributable to *emissions*, which the IPCC first presented in AR4. These analyses can be applied to historical emissions changes in a ‘backward-looking’ perspective, as done for example, for major WMGHGs (den Elzen et al., 2005; Hohne et al., 2011) and NTCFs (Shindell et al., 2009), or to current

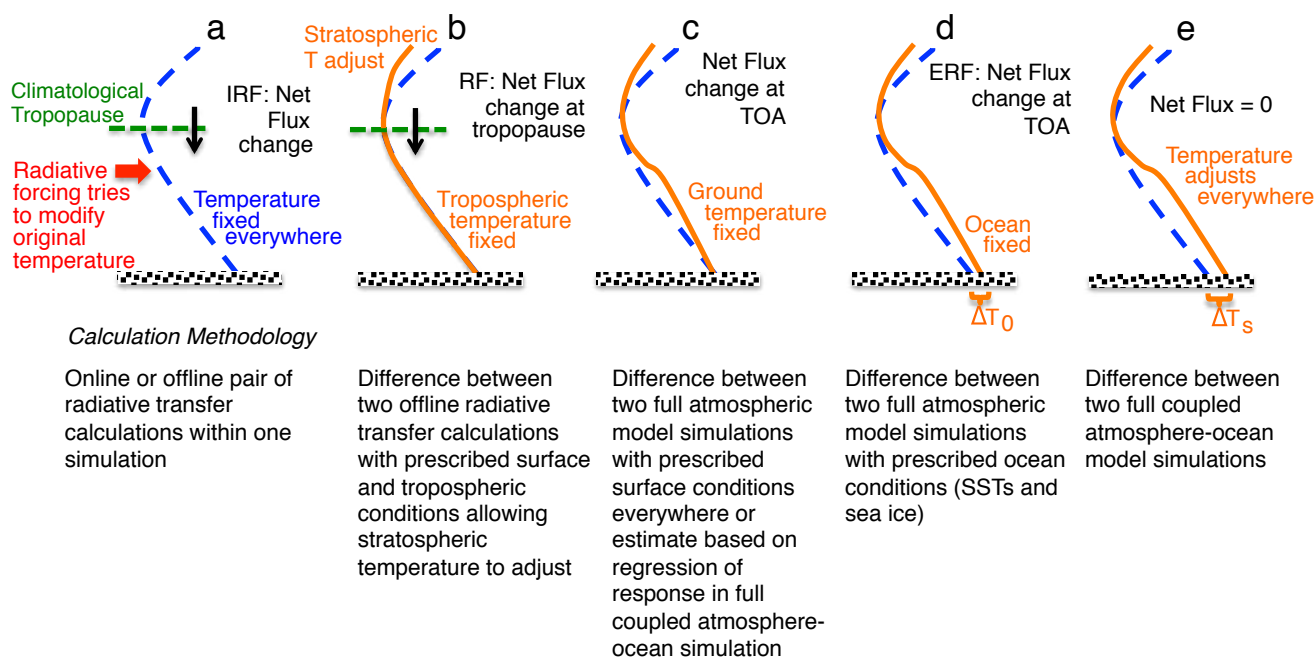


Figure 8.1 | Cartoon comparing (a) instantaneous RF, (b) RF, which allows stratospheric temperature to adjust, (c) flux change when the surface temperature is fixed over the whole Earth (a method of calculating ERF), (d) the ERF calculated allowing atmospheric and land temperature to adjust while ocean conditions are fixed and (e) the equilibrium response to the climate forcing agent. The methodology for calculation of each type of forcing is also outlined. ΔT_0 represents the land temperature response, while ΔT_s is the full surface temperature response. (Updated from Hansen et al., 2005.)

or projected future emissions in a ‘forward-looking’ view (see Section 8.7). Emissions estimates through time typically come from the scientific community, often making use of national reporting for recent decades.

With the greater use of emission-driven models, for example, in CMIP5, it is becoming more natural to estimate ERF resulting from emissions of a particular species rather than concentration-based forcing. Such calculations typically necessitate model simulations with chemical transport models or chemistry–climate models, however, and require careful consideration of which processes are included, especially when comparing results to concentration-based forcings. In particular, simulation of concentration responses to emissions changes requires incorporating models of the carbon cycle and atmospheric chemistry (gas and aerosol phases). The requisite expansion of the modelling realm for emissions-based forcing or emission metrics should in principle be consistent for all drivers. For example, as the response to aerosol or ozone precursor emissions includes atmospheric chemistry, the response to CO₂ emissions should as well. In addition, if the CO₂ concentration responses to CO₂ emissions include the impact of CO₂-induced climate changes on carbon uptake, then the effect of climate changes caused by any other emission on carbon uptake should also be included. Similarly, if the effects of atmospheric CO₂ concentration change on carbon uptake are included, the effects of other atmospheric composition or deposition changes on carbon uptake should be included as well (see also Section 6.4.1). Comparable issues are present for other forcing agents. In practice, the modelling realm used in studies of forcing attributable to emissions has not always been consistent. Furthermore, climate feedbacks have sometimes been included in the calculation of forcing due to ozone or aerosol changes, as when concentrations from a historical transient climate simulation are imposed for an ERF calculation. In this chapter, we endeavour to clarify which processes

have been included in the various estimates of forcing attributed to emissions (Sections 8.3 and 8.7).

RF or ERF estimates based on either historical emissions or concentrations provide valuable insight into the relative and absolute contribution of various drivers to historical climate change. Scenarios of changing future emissions and land use are also developed based on various assumptions about socioeconomic trends and societal choices. The forcing resulting from such scenarios is used to understand the drivers of potential future climate changes (Sections 8.5.3 and 8.6). As with historical forcings, the actual impact on climate depends on both the temporal and spatial structure of the forcings and the rate of response of various portions of the climate system.

8.2 Atmospheric Chemistry

8.2.1 Introduction

Most radiatively active compounds in the Earth’s atmosphere are chemically active, meaning that atmospheric chemistry plays a large role in determining their burden and residence time. In the atmosphere, a gaseous chemically active compound can be affected by (1) interaction with other species (including aerosols and water) in its immediate vicinity and (2) interaction with solar radiation (photolysis). Physical processes (wet removal and dry deposition) act on some chemical compounds (gas or aerosols) to further define their residence time in the atmosphere. Atmospheric chemistry is characterized by many interactions and patterns of temporal or spatial variability, leading to significant nonlinearities (Kleinman et al., 2001) and a wide range of time scales of importance (Isaksen et al., 2009).

This section assesses updates in understanding of processes, modelling and observations since AR4 (see Section 2.3) on key reactive species contributing to RF. Note that aerosols, including processes responsible for the formation of aerosols, are extensively described in Section 7.3.

8.2.2 Global Chemistry Modelling in Coupled Model Intercomparison Project Phase 5

Because the distribution of NTCFs cannot be estimated from observations alone, coupled chemistry-climate simulations are required to define their evolution and associated RF. While several CMIP5 modelling groups performed simulations with interactive chemistry (i.e., computed simultaneously within the climate model), many models used as input pre-computed distributions of radiatively active gases and/or aerosols. To assess the distributions of chemical species and their respective RF, many research groups participated in the Atmospheric Chemistry and Climate Model Intercomparison Project (ACCMIP).

The ACCMIP simulations (Lamarque et al., 2013) were defined to provide information on the long-term changes in atmospheric composition with a few, well-defined atmospheric simulations. Because of the nature of the simulations (pre-industrial, present-day and future climates), only a limited number of chemistry-transport models (models which require a full definition of the meteorological fields needed to simulate physical processes and transport) participated in the ACCMIP project, which instead drew primarily from the same General Circulation Models (GCMs) as CMIP5 (see Lamarque et al., 2013 for a list of the participating models and their configurations), with extensive model evaluation against observations (Bowman et al., 2013; Lee et al., 2013; Shindell et al., 2013c; Voulgarakis et al., 2013; Young et al., 2013).

In all CMIP5/ACCMIP chemistry simulations, anthropogenic and biomass burning emissions are specified. More specifically, a single set of historical anthropogenic and biomass burning emissions (Lamarque et al., 2010) and one set of emissions for each of the RCPs (van Vuuren et al., 2011) was defined (Figure 8.2). This was designed to increase the comparability of simulations. However, these uniform emission specifications mask the existing uncertainty (e.g., Bond et al., 2007; Lu et al., 2011), so that there is in fact a considerable range in the estimates and time evolution of recent anthropogenic emissions (Granier et al., 2011). Historical reconstructions of biomass burning (wildfires and deforestation) also exhibit quite large uncertainties (Kasischke and Penner, 2004; Ito and Penner, 2005; Schultz et al., 2008; van der Werf et al., 2010). In addition, the RCP biomass burning projections do not include the feedback between climate change and fires discussed in Bowman et al. (2009), Pechony and Shindell (2010) and Thonicke et al. (2010). Finally, the RCP anthropogenic precursor emissions of NTCFs tend to span a smaller range than available from existing scenarios (van Vuuren et al., 2011). The ACCMIP simulations therefore provide an estimate of the uncertainty due to range of representation of physical and chemical processes in models, but do not incorporate uncertainty in emissions.

8.2.3 Chemical Processes and Trace Gas Budgets

8.2.3.1 Tropospheric Ozone

The RF from tropospheric ozone is strongly height- and latitude-dependent through coupling of ozone change with temperature, water vapour and clouds (Lacis et al., 1990; Bernsten et al., 1997; Worden et al., 2008, 2011; Bowman et al., 2013). Consequently, it is necessary to accurately estimate the change in the ozone spatio-temporal structure using global models and observations. It is also well established that surface ozone detrimentally affects plant productivity (Ashmore, 2005; Fishman et al., 2010), albeit estimating this impact on climate, although possibly significant, is still limited to a few studies (Sitch et al., 2007; UNEP, 2011).

Tropospheric ozone is a by-product of the oxidation of carbon monoxide (CO), CH₄, and non-CH₄ hydrocarbons in the presence of nitrogen oxides (NO_x). As emissions of these precursors have increased (Figure 8.2), tropospheric ozone has increased since pre-industrial times (Volz and Kley, 1988; Marenco et al., 1994) and over the last decades (Parrish et al., 2009; Cooper et al., 2010; Logan et al., 2012), but with important regional variations (Section 2.2). Ozone production is usually limited by the supply of HO_x (OH + HO₂) and NO_x (NO + NO₂) (Levy, 1971; Logan et al., 1981). Ozone's major chemical loss pathways in the troposphere are through (1) photolysis (to O(¹D), followed by reaction with water vapour) and (2) reaction with HO₂ (Seinfeld and Pandis, 2006). The former pathway leads to couplings between stratospheric ozone (photolysis rate being a function of the overhead ozone column) and climate change (through water vapour). Observed surface ozone abundances typically range from less than 10 ppb over the tropical Pacific Ocean to more than 100 ppb downwind of highly emitting regions. The lifetime of ozone in the troposphere varies strongly with season and location: it may be as little as a few days in the tropical boundary layer, or as much as 1 year in the upper troposphere. Two recent studies give similar global mean lifetime of ozone: 22.3 ± 2 days (Stevenson et al., 2006) and 23.4 ± 2.2 days (Young et al., 2013).

For present (about 2000) conditions, the various components of the budget of global mean tropospheric ozone are estimated from the ACCMIP simulations and other model simulations since AR4 (Table 8.1). In particular, most recent models define a globally and annually averaged tropospheric ozone burden of (337 ± 23 Tg, 1-σ). Differences in the definition of the tropopause lead to inter-model variations of approximately 10% (Wild, 2007). This multi-model mean estimate of global annual tropospheric ozone burden has not significantly changed since the Stevenson et al. (2006) estimates (344 ± 39 Tg, 1-σ), and is consistent with the most recent satellite-based Ozone Monitoring Instrument–Microwave Limb Sounder (OMI-MLS; Ziemke et al., 2011) and Tropospheric Emission Spectrometer (TES; Osterman et al., 2008) climatologies.

Estimates of the ozone chemical sources and sinks (uncertainty estimates are quoted here as 1-σ) are less robust, with a net chemical production (production *minus* loss) of 618 ± 275 Tg yr⁻¹ (Table 8.1), larger than the Atmospheric Composition Change: a European Network (ACCENT) results (442 ± 309 Tg yr⁻¹; Stevenson et al., 2006). Estimates of ozone deposition (1094 ± 264 Tg yr⁻¹) are slightly increased

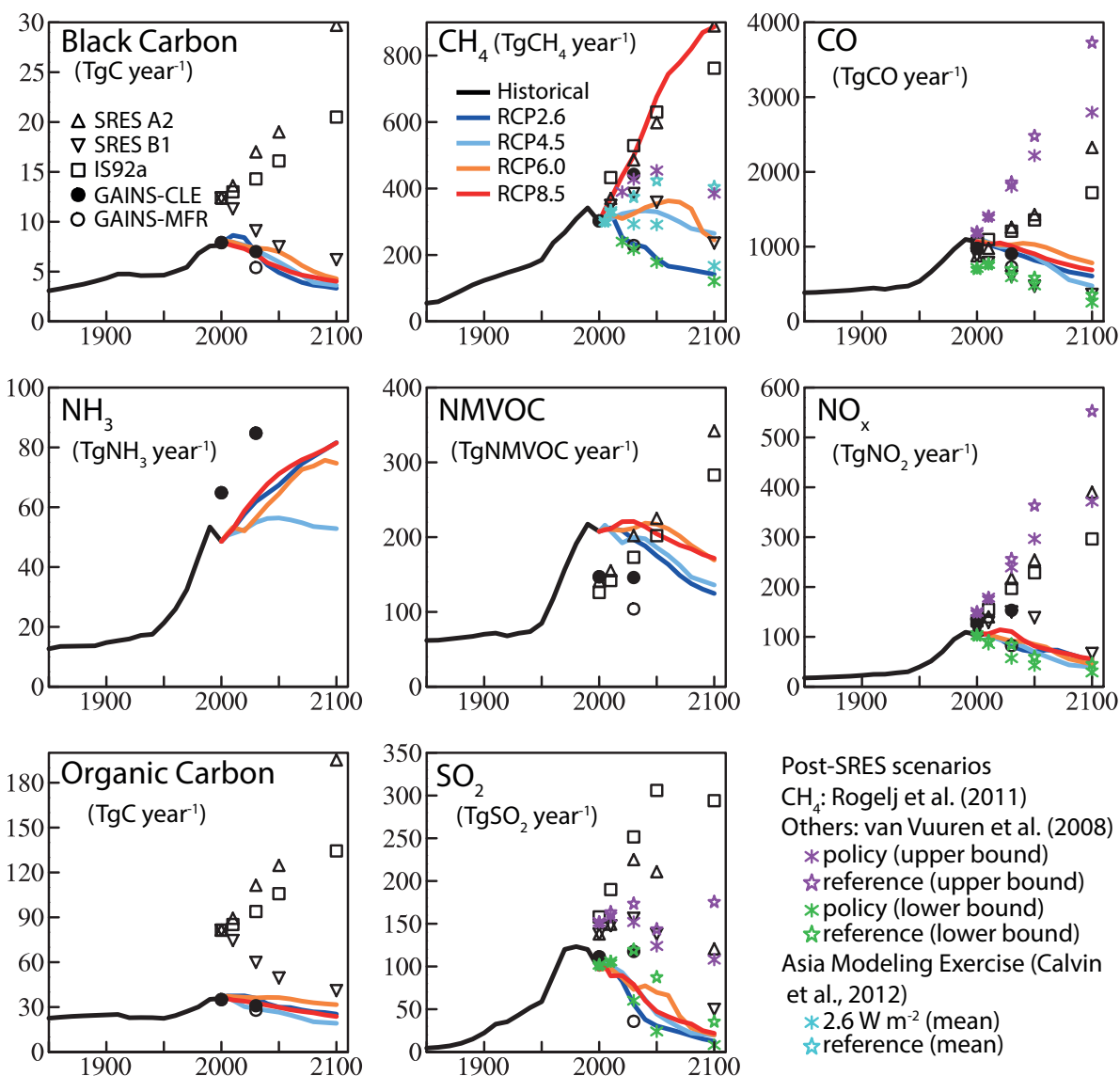


Figure 8.2 | Time evolution of global anthropogenic and biomass burning emissions 1850–2100 used in CMIP5/ACCIP following each RCP. Historical (1850–2000) values are from Lamarque et al. (2010). RCP values are from van Vuuren et al. (2011). Emissions estimates from Special Report on Emission Scenarios (SRES) are discussed in Annex II; note that black carbon and organic carbon estimates were not part of the SRES and are shown here only for completeness. The Maximum Feasible Reduction (MFR) and Current Legislation (CLE) are discussed in Cofala et al. (2007); as biomass burning emissions are not included in that publication, a fixed amount, equivalent to the value in 2000 from the RCP estimates, is added (see Annex II for more details; Dentener et al., 2006). The post-SRES scenarios are discussed in Van Vuuren et al. (2008) and Rogelj et al. (2011). For those, only the range (minimum to maximum) is shown. Global emissions from the Asian Modelling Exercise are discussed in Calvin et al. (2012). Regional estimates are shown in Supplementary Material Figure 8.SM.1 and Figure 8.SM.2 for the historical and RCPs.

since ACCENT ($1003 \pm 200 \text{ Tg yr}^{-1}$) while estimates of the net influx of ozone from the stratosphere to the troposphere ($477 \pm 96 \text{ Tg yr}^{-1}$) have slightly decreased since ACCENT ($552 \pm 168 \text{ Tg yr}^{-1}$). Additional model estimates of this influx (Hegglin and Shepherd, 2009; Hsu and Prather, 2009) fall within both ranges, as do estimates based on observations (Murphy and Fahey, 1994; Gettelman et al., 1997; Olsen et al., 2002), all estimates being sensitive to their choice of tropopause definition and interannual variability.

Model simulations for present-day conditions or the recent past are evaluated (Figure 8.3) against frequent ozonesonde measurements (Logan, 1999; Tilmes et al., 2012) and additional surface, aircraft and satellite measurements. The ACCMIP model simulations (Figure 8.3)

indicate 10 to 20% negative bias at 250 hPa in the SH tropical region, and a slight underestimate in NH tropical region. Comparison with satellite-based estimates of tropospheric ozone column (Ziemke et al., 2011) indicates an annual mean bias of $-4.3 \pm 29 \text{ Tg}$ (with a spatial correlation of $0.87 \pm 0.07, 1-\sigma$) for the ACCMIP simulations (Young et al., 2013). Overall, our ability to simulate tropospheric ozone burden for present (about 2000) has not substantially changed since AR4. Evaluation (using a subset of two ACCMIP models) of simulated trends (1960s to present or shorter) in surface ozone against observations at remote surface sites (see Section 2.2) indicates an underestimation, especially in the NH (Lamarque et al., 2010). Although this limits the ability to represent recent ozone changes, it is unclear how this translates into an uncertainty on changes since pre-industrial times.

Table 8.1 | Summary of tropospheric ozone global budget model and observation estimates for present (about 2000) conditions. Focus is on modelling studies published since AR4. STE stands for stratosphere–troposphere exchange. All uncertainties quoted as 1 standard deviation (68% confidence interval).

Burden	Production	Loss	Deposition	STE	Reference
Tg	Tg yr ⁻¹	Tg yr ⁻¹	Tg yr ⁻¹	Tg yr ⁻¹	
Modelling Studies					
337 ± 23	4877 ± 853	4260 ± 645	1094 ± 264	477 ± 96	Young et al. (2013); ACCMIP
323	N/A	N/A	N/A	N/A	Archibald et al. (2011)
330	4876	4520	916	560	Kawase et al. (2011)
312	4289	3881	829	421	Huijnen et al. (2010)
334	3826	3373	1286	662	Zeng et al. (2010)
324	4870	4570	801	502	Wild and Palmer (2008)
314	N/A	N/A	1035	452	Zeng et al. (2008)
319	4487	3999	N/A	500	Wu et al. (2007)
372	5042	4507	884	345	Horowitz (2006)
349	4384	3972	808	401	Liao et al. (2006)
344 ± 39	5110 ± 606	4668 ± 727	1003 ± 200	552 ± 168	Stevenson et al. (2006); ACCENT
314 ± 33	4465 ± 514	4114 ± 409	949 ± 222	529 ± 105	Wild (2007) (post-2000 studies)
N/A	N/A	N/A	N/A	515	Hsu and Prather (2009)
N/A	N/A	N/A	N/A	655	Hegglin and Shepherd (2009)
N/A	N/A	N/A	N/A	383–451	Clark et al. (2007)
Observational Studies					
333	N/A	N/A	N/A	N/A	Fortuin and Kelder (1998)
327	N/A	N/A	N/A	N/A	Logan (1999)
325	N/A	N/A	N/A	N/A	Ziemke et al. (2011); 60S–60N
319–351	N/A	N/A	N/A	N/A	Osterman et al. (2008); 60S–60N
N/A	N/A	N/A	N/A	449 (192–872)	Murphy and Fahey (1994)
N/A	N/A	N/A	N/A	510 (450–590)	Gottelman et al. (1997)
N/A	N/A	N/A	N/A	500 ± 140	Olsen et al. (2001)

In most studies ‘pre-industrial’ does not identify a specific year but is usually assumed to correspond to 1850s levels; no observational information on ozone is available for that time period. Using the Lamarque et al. (2010) emissions, the ACCMIP models (Young et al., 2013) are unable to reproduce the low levels of ozone observed at Montsouris 1876–1886 (Volz and Kley, 1988). The other early ozone measurements using the Schönbein paper are controversial (Marengo et al., 1994) and assessed to be of qualitative use only. The main uncertainty in estimating the pre-industrial to present-day change in ozone therefore remains the lack of constraint on emission trends because of the very incomplete knowledge of pre-industrial ozone concentrations, of which no new information is available. The uncertainty on pre-industrial conditions is not confined to ozone but applies to aerosols as well (e.g., Schmidt et al., 2012), although ice and lake core records provide some constraint on pre-industrial aerosol concentrations.

The ACCMIP results provide an estimated tropospheric ozone increase (Figure 8.4) from 1850 to 2000 of 98 ± 17 Tg (model range), similar to AR4 estimates. Skeie et al. (2011a) found an additional 5% increase in the anthropogenic contribution to the ozone burden between 2000 and 2010, which translates into an approximately 1.5% increase in tropospheric ozone burden. A best estimate of the change in ozone since 1850 is assessed at 100 ± 25 Tg (1- σ). Attribution simulations

(Stevenson et al., 2013) indicate unequivocally that anthropogenic changes in ozone precursor emissions are responsible for the increase between 1850 and present or into the future.

8.2.3.2 Stratospheric Ozone and Water Vapour

Stratospheric ozone has experienced significant depletion since the 1960s due to bromine and chlorine-containing compounds (Solomon, 1999), leading to an estimated global decrease of stratospheric ozone of 5% between the 1970s and the mid-1990s, the decrease being largest over Antarctica (Fioletov et al., 2002). Most of the ozone loss is associated with the long-lived bromine and chlorine-containing compounds (chlorofluorocarbons and substitutes) released by human activities, in addition to N₂O. This is in addition to a background level of natural emissions of short-lived halogens from oceanic and volcanic sources.

With the advent of the Montreal Protocol and its amendments, emissions of chlorofluorocarbons (CFCs) and replacements have strongly declined (Montzka et al., 2011), and signs of ozone stabilization and even possibly recovery have already occurred (Mader et al., 2010; Salby et al., 2012). A further consequence is that N₂O emissions (Section 8.2.3.4) *likely* dominate all other emissions in terms of ozone-depleting

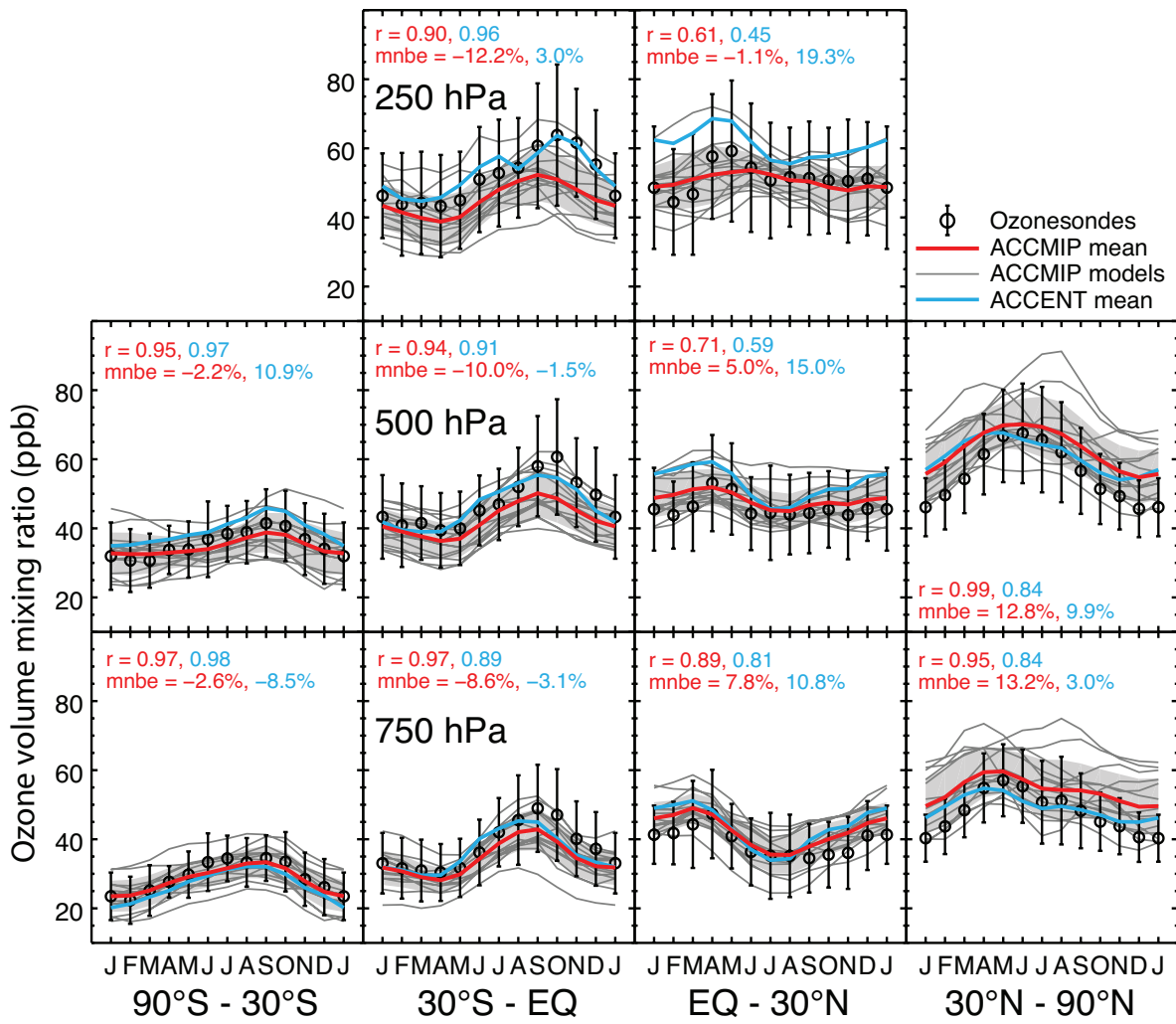


Figure 8.3 | Comparisons between observations and simulations for the monthly mean ozone for ACCMIP results (Young et al., 2013). ACCENT refers to the model results in Stevenson et al. (2006). For each box, the correlation of the seasonal cycle is indicated by the r value, while the mean normalized bias estimated is indicated by $mnbe$ value.

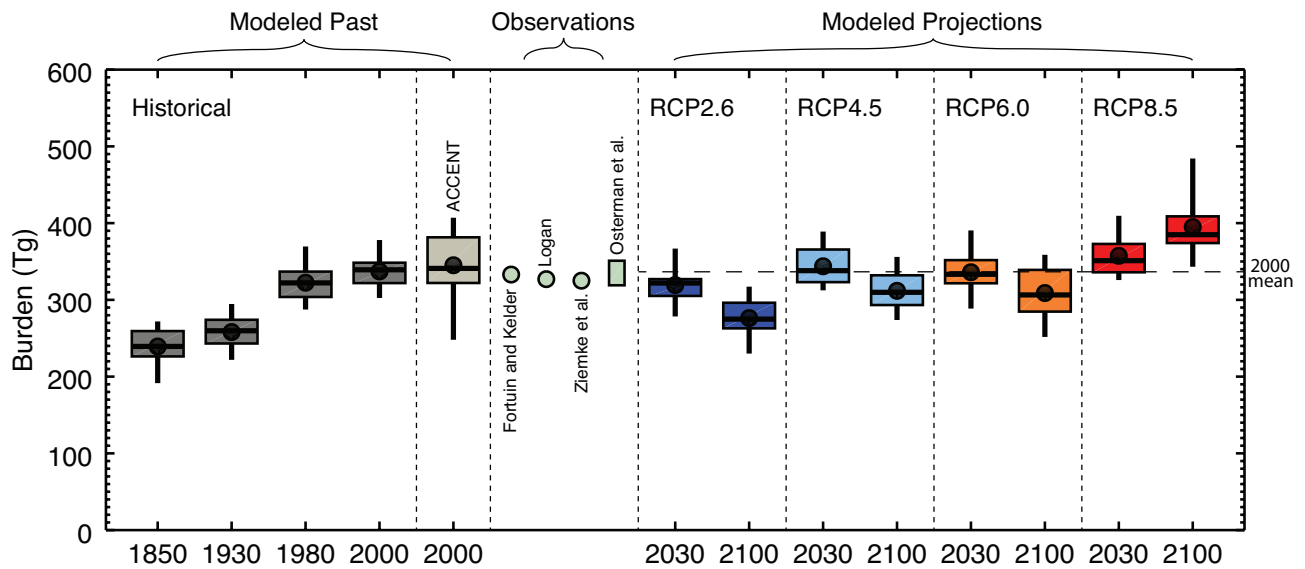


Figure 8.4 | Time evolution of global tropospheric ozone burden (in $Tg(O_3)$) from 1850 to 2100 from ACCMIP results, ACCENT results (2000 only), and observational estimates (see Table 8.1). The box, whiskers, line and dot show the interquartile range, full range, median and mean burdens and differences, respectively. The dashed line indicates the 2000 ACCMIP mean. (Adapted from Young et al., 2013.)

potential (Ravishankara et al., 2009). Chemistry-climate models with resolved stratospheric chemistry and dynamics recently predicted an estimated global mean total ozone column recovery to 1980 levels to occur in 2032 (multi-model mean value, with a range of 2024 to 2042) under the A1B scenario (Eyring et al., 2010a). Increases in the stratospheric burden and acceleration of the stratospheric circulation leads to an increase in the stratosphere–troposphere flux of ozone (Shindell et al., 2006c; Grewe, 2007; Hegglin and Shepherd, 2009; Zeng et al., 2010). This is also seen in recent RCP8.5 simulations, with the impact of increasing tropospheric burden (Kawase et al., 2011; Lamarque et al., 2011). However, observationally based estimates of recent trends in age of air (Engel et al., 2009; Stiller et al., 2012) do not appear to be consistent with the acceleration of the stratospheric circulation found in model simulations, possibly owing to inherent difficulties with extracting trends from SF₆ observations (Garcia et al., 2011).

Oxidation of CH₄ in the stratosphere (see Section 8.2.3.3) is a significant source of water vapour and hence the long-term increase in CH₄ leads to an anthropogenic forcing (see Section 8.3) in the stratosphere. Stratospheric water vapour abundance increased by an average of 1.0 ± 0.2 (1-σ) ppm during 1980–2010, with CH₄ oxidation explaining approximately 25% of this increase (Hurst et al., 2011). Other factors contributing to the long-term change in water vapour include changes in tropical tropopause temperatures (see Section 2.2.2.1).

8.2.3.3 Methane

The surface mixing ratio of CH₄ has increased by 150% since pre-industrial times (Sections 2.2.1.1.2 and 8.3.2.2), with some projections indicating a further doubling by 2100 (Figure 8.5). Bottom-up estimates of present CH₄ emissions range from 542 to 852 TgCH₄yr⁻¹ (see Table 6.8), while a recent top-down estimate with uncertainty analysis is 554 ± 56 TgCH₄yr⁻¹ (Prather et al., 2012). All quoted uncertainties in Section 8.2.3.3 are defined as 1-σ.

The main sink of CH₄ is through its reaction with the hydroxyl radical (OH) in the troposphere (Ehhalt and Heidt, 1973). A primary source of tropospheric OH is initiated by the photodissociation of ozone, followed by reaction with water vapour (creating sensitivity to humidity, cloud cover and solar radiation) (Levy, 1971; Crutzen, 1973). The

other main source of OH is through secondary reactions (Lelieveld et al., 2008), although some of those reactions are still poorly understood (Paulot et al., 2009; Peeters et al., 2009; Taraborrelli et al., 2012). A recent estimate of the CH₄ tropospheric chemical lifetime with respect to OH constrained by methyl chloroform surface observations is 11.2 ± 1.3 years (Prather et al., 2012). In addition, bacterial uptake in soils provides an additional small, less constrained loss (Fung et al., 1991); estimated lifetime = 120 ± 24 years (Prather et al., 2012), with another small loss in the stratosphere (Ehhalt and Heidt, 1973); estimated lifetime = 150 ± 50 years (Prather et al., 2012). Halogen chemistry in the troposphere also contributes to some tropospheric CH₄ loss (Allan et al., 2007), estimated lifetime = 200 ± 100 years (Prather et al., 2012).

The ACCMIP estimate for present CH₄ lifetime with respect to tropospheric OH varies quite widely (9.8 ± 1.6 years (Voulgarakis et al., 2013)), slightly shorter than the 10.2 ± 1.7 years in (Fiore et al. (2009)), but much shorter than the methyl chloroform-based estimate of 11.2 ± 1.3 years (Prather et al., 2012). A partial explanation for the range in CH₄ lifetime changes can be found in the degree of representation of chemistry in chemistry–climate models. Indeed, Archibald et al. (2010) showed that the response of OH to increasing nitrogen oxides strongly depends on the treatment of hydrocarbon chemistry in a model. The impact on CH₄ distribution in the ACCMIP simulations is, however, rather limited because most models prescribed CH₄ as a time-varying lower-boundary mixing ratio (Lamarque et al., 2013).

The chemical coupling between OH and CH₄ leads to a significant amplification of an emission impact; that is, increasing CH₄ emissions decreases tropospheric OH which in turn increases the CH₄ lifetime and therefore its burden. The OH-lifetime sensitivity for CH₄, $s_{OH} = -\delta \ln(OH)/\delta \ln(CH_4)$, was estimated in Chapter 4 of TAR to be 0.32, implying a 0.32% decrease in tropospheric mean OH (as weighted by CH₄ loss) for a 1% increase in CH₄. The Fiore et al. (2009) multi-model (12 models) study provides a slightly smaller value (0.28 ± 0.03). Holmes et al. (2013) gives a range 0.31 ± 0.04 by combining Fiore et al. (2009), Holmes et al. (2011) and three new model results (0.36, 0.31, 0.27). Only two ACCMIP models reported values (0.19 and 0.26; Voulgarakis et al., 2013). The projections of future CH₄ in Chapter 11 use the Holmes et al. (2013) range and uncertainty, which at the 2-σ level covers all but one model result. The feedback factor *f*, the ratio of the

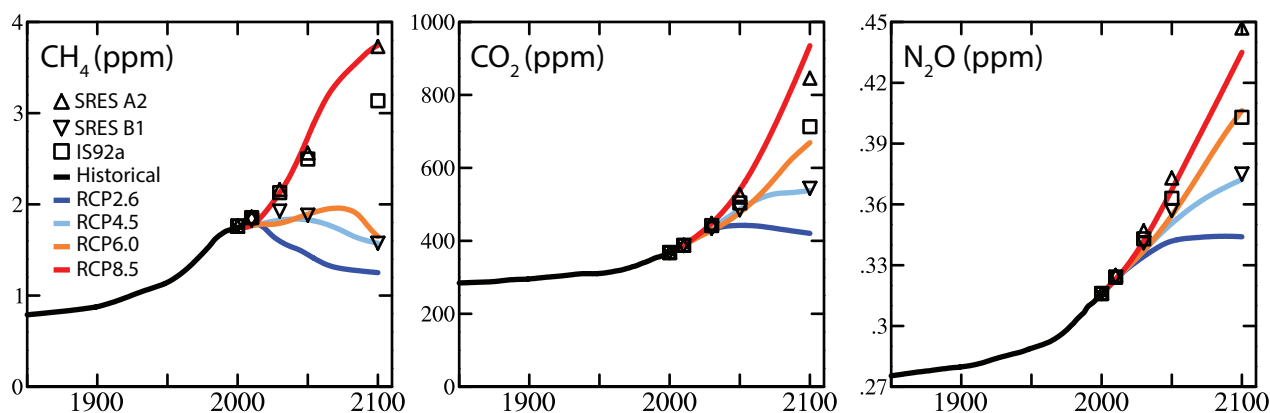


Figure 8.5 | Time evolution of global-averaged mixing ratio of long-lived species 1850–2100 following each RCP; blue (RCP2.6), light blue (RCP4.5), orange (RCP6.0) and red (RCP8.5). (Based on Meinshausen et al., 2011b.)

lifetime of a CH₄ perturbation to the lifetime of the total CH₄ burden, is calculated as $f = 1/(1-s)$. Other CH₄ losses, which are relatively insensitive to CH₄ burden, must be included so that $f = 1.34 \pm 0.06$, (slightly larger but within the range of the Stevenson et al. (2006) estimate of 1.29 ± 0.04 , based on six models), leading to an overall perturbation lifetime of 12.4 ± 1.4 years, which is used in calculations of metrics in Section 8.7. Additional details are provided in the Supplementary Material Section 8.SM.2.

8.2.3.4 Nitrous Oxide

Nitrous oxide (N₂O) in 2011 has a surface concentration 19% above its 1750 level (Sections 2.2.1.1.3 and 8.3.2.3). Increases in N₂O lead to depletion of mid- to upper-stratospheric ozone and increase in mid-latitude lower stratospheric ozone (as a result of increased photolysis rate from decreased ozone above). This impacts tropospheric chemistry through increase in stratosphere–troposphere exchange of ozone and odd nitrogen species and increase in tropospheric photolysis rates and OH formation (Prather and Hsu, 2010). Anthropogenic emissions represent around 30 to 45% of the present-day global total, and are mostly from agricultural and soil sources (Fowler et al., 2009) and fossil-fuel activities. Natural emissions come mostly from microbial activity in the soil. The main sink for N₂O is through photolysis and oxidation reactions in the stratosphere, leading to an estimated lifetime of 131 ± 10 years (Prather et al., 2012), slightly larger than previous estimates (Prather and Hsu, 2010; Montzka et al., 2011). The addition of N₂O to the atmosphere changes its own lifetime through feedbacks that couple N₂O to stratospheric NO_y and ozone depletion (Prather, 1998; Ravishankara et al., 2009; Prather and Hsu, 2010), so that the lifetime of a perturbation is less than that of the total burden, 121 ± 10 years (1- σ ; Prather et al., 2012) and is used in calculations of metrics (Section 8.7).

8.2.3.5 Halogenated Species

Halogenated species can be powerful greenhouse gases (GHGs). Those containing chlorine and bromine also deplete stratospheric ozone and are referred to as ozone-depleting substances (ODSs). Most of those compounds do not have natural emissions and, because of the implementation of the Montreal Protocol and its amendments, total emissions of ODSs have sharply decreased since the 1990s (Montzka et al., 2011). For CFCs, perfluorocarbons (PFCs) and SF₆ the main loss is through photolysis in the stratosphere. The CFC substitutes (hydrochlorofluorocarbons (HCFCs) and hydrofluorocarbons (HFCs)) are destroyed by OH oxidation in the troposphere. Their global concentration has steadily risen over the recent past (see Section 2.2.1.1.4).

8.2.3.6 Aerosols

Aerosol particles are present in the atmosphere with size ranges from a few nanometres to tens of micrometres. They are the results of direct emission (primary aerosols: BC, OC, sea salt, dust) into the atmosphere or as products of chemical reactions (secondary inorganic aerosols: sulphate, nitrate, ammonium; and secondary organic aerosols (SOAs)) occurring in the atmosphere. Secondary inorganic aerosols are the products of reactions involving sulphur dioxide, ammonia and nitric oxide emissions. SOAs are the result of chemical reactions

of non-methane hydrocarbons (and their products) with the hydroxyl radical (OH), ozone, nitrate (NO₃) or photolysis (Hallquist et al., 2009). Thus although many hydrocarbons in the atmosphere are of biogenic origin, anthropogenic pollutants can have impacts on their conversion to SOAs. There is tremendous complexity and still much uncertainty in the processes involved in the formation of SOAs (Hallquist et al., 2009; Carslaw et al., 2010). Additional information can be found in Section 7.3.2.

Once generated, the size and composition of aerosol particles can be modified by additional chemical reactions, condensation or evaporation of gaseous species and coagulation (Seinfeld and Pandis, 2006). It is this set of processes that defines their physical, chemical and optical properties, and hence their impact on radiation and clouds, with large regional and global differences (see Section 7.3.3). Furthermore, their distribution is affected by transport and deposition, defining a residence time in the troposphere of usually a few days (Textor et al., 2006).

8.3 Present-Day Anthropogenic Radiative Forcing

Human activity has caused a variety of changes in different forcing agents in the atmosphere or land surface. A large number of GHGs have had a substantial increase over the Industrial Era and some of these gases are entirely of anthropogenic origin. Atmospheric aerosols have diverse and complex influences on the climate. Human activity has modified the land cover and changed the surface albedo. Some of the gases and aerosols are directly emitted to the atmosphere whereas others are secondary products from chemical reactions of emitted species. The lifetimes of these different forcing agents vary substantially. This section discusses all known anthropogenic forcing agents of non-negligible importance and their quantification in terms of RF or ERF based on changes in abundance over the 1750–2011 period.

In this section we determine the RFs for WMGHGs and heterogeneously distributed species in fundamentally different ways. As described in Box 8.2, the concentrations of WMGHGs can be determined from observations at a few surface sites. For the pre-industrial concentrations these are typically from trapped air in polar ice or firn (see Section 2.2.1). Thus the RFs from WMGHGs are determined entirely from observations (Section 8.3.2). In contrast, we do not have sufficient pre-industrial or present-day observations of heterogeneously distributed forcing agents (e.g., ozone and aerosols) to be able to characterize their RF; therefore we instead have to rely on chemistry–climate models (Sections 8.3.3 and 8.3.4).

8.3.1 Updated Understanding of the Spectral Properties of Greenhouse Gases and Radiative Transfer Codes

RF estimates are performed with a combination of radiative transfer codes typical for GCMs as well as more detailed radiative transfer codes. Physical properties are needed in the radiative transfer codes such as spectral properties for gases. The HITRAN (High Resolution TRANsmission molecular absorption) database (Rothman, 2010) is widely used in radiative transfer models. Some researchers studied

the difference among different editions of HITRAN databases for diverse uses (Feng et al., 2007; Kratz, 2008; Feng and Zhao, 2009; Fomin and Falaleeva, 2009; Lu et al., 2012). Model calculations have shown that modifications of the spectroscopic characteristics tend to have a modest effect on the determination of RF estimates of order 2 to 3% of the calculated RF attributed to the combined doubling of CO₂, N₂O and CH₄. These results showed that even the largest overall RF induced by differences among the HITRAN databases is considerably smaller than the range reported for the modelled RF estimates; thus the line parameter updates to the HITRAN database are not a significant source for discrepancies in the RF calculations appearing in the IPCC reports. However, the more recent HITRAN data set is still recommended, as the HITRAN process offers internal verification and tends to progress closer to the best laboratory measurements. It is found that the differences among the water vapour continuum absorption formulations tend to be comparable to the differences among the various HITRAN databases (Paynter and Ramaswamy, 2011); but use of the older Robert continuum formula produces significantly larger flux differences, thus, replacement of the older continuum is warranted (Kratz, 2008) and there are still numerous unresolved issues left in the continuum expression, especially related to short-wave radiative transfer (Shine et al., 2012). Differences in absorption data from various HITRAN versions are *very likely* a small contributor to the uncertainty in RF of GHGs.

Line-by-line (LBL) models using the HITRAN data set as an input are the benchmark of radiative transfer models for GHGs. Some researchers compared different LBL models (Zhang et al., 2005; Collins et al., 2006) and line-wing cutoff, line-shape function and gas continuum absorption treatment effects on LBL calculations (Zhang et al., 2008; Fomin and Falaleeva, 2009). The agreement between LBL codes has been investigated in many studies and found to generally be within a few percent (e.g., Collins et al., 2006; Iacono et al., 2008; Forster et al., 2011a) and to compare well to observed radiative fluxes under controlled situations (Oreopoulos et al., 2012). Forster et al. (2011a) evaluated global mean radiatively important properties of chemistry climate models (CCMs) and found that the combined WMGHG global annual mean instantaneous RF at the tropopause is within 30% of LBL models for all CCM radiation codes tested. The accuracies of the LW RF due to CO₂ and tropospheric ozone increase are generally very good and within 10% for most of the participation models, but problems remained in simulating RF for stratospheric water vapour and ozone changes with errors between 3% and 200% compared to LBL models. Whereas the differences in the results from CCM radiation codes were large, the agreement among the LW LBL codes was within 5%, except for stratospheric water vapour changes.

Most intercomparison studies of the RF of GHGs are for clear-sky and aerosol-free conditions; the introduction of clouds would greatly complicate the targets of research and are usually omitted in the intercomparison exercises of GCM radiation codes and LBL codes (e.g., Collins et al., 2006; Iacono et al., 2008). It is shown that clouds can reduce the magnitude of RF due to GHGs by about 25% (Forster et al., 2005; Worden et al., 2011; Zhang et al., 2011), but the influence of clouds on the diversity in RF is found to be within 5% in four detailed radiative transfer schemes with realistic cloud distributions (Forster et al., 2005). Estimates of GHG RF are based on the LBL codes or the radiative

transfer codes compared and validated against LBL models, and the uncertainty range from AR4 in the RF of GHG of 10% is retained. We underscore that uncertainty in RF calculations in many GCMs is substantially higher owing both to radiative transfer codes and meteorological data such as clouds adopted in the simulations.

8.3.2 Well-mixed Greenhouse Gases

AR4 assessed the RF from 1750 to 2005 of the WMGHGs to be 2.63 W m⁻². The four most important gases were CO₂, CH₄, dichlorodifluoromethane (CFC-12) and N₂O in that order. Halocarbons, comprising CFCs, HCFCs, HFCs, PFCs and SF₆, contributed 0.337 W m⁻² to the total. Uncertainties (90% confidence ranges) were assessed to be approximately 10% for the WMGHGs. The major changes to the science since AR4 are the updating of the atmospheric concentrations, the inclusion of new species (NF₃ and SO₂F₂) and discussion of ERF for CO₂. Since AR4 N₂O has overtaken CFC-12 as the third largest contributor to RF. The total WMGHG RF is now 2.83 (2.54 to 3.12) W m⁻².

The RFs in this section are derived from the observed differences in concentrations of the WMGHGs between 1750 and 2011. The concentrations of CO₂, CH₄ and N₂O vary throughout the pre-industrial era, mostly due to varying climate, with a possible small contribution from anthropogenic emissions (MacFarling Meure et al., 2006). These variations do not contribute to uncertainty in the RF as strictly defined here, but do affect the RF attribution to anthropogenic emissions. On centennial time scales, variations in late Holocene concentrations of CO₂ are around 10 ppm (see note to Table 2.1), much larger than the uncertainty in the 1750 concentration. This would equate to a variation in the RF of 10%. For CH₄ and N₂O the centennial variations are comparable to the uncertainties in the 1750 concentrations and so do not significantly affect the estimate of the 1750 value used in calculating RF.

8.3.2.1 Carbon Dioxide

The tropospheric mixing ratio of CO₂ has increased globally from 278 (276–280) ppm in 1750 to 390.5 (390.3 to 390.7) ppm in 2011 (see Section 2.2.1.1.1). Here we assess the RF due to changes in atmospheric concentration rather than attributing it to anthropogenic emissions. Section 6.3.2.6 describes how only a fraction of the historical CO₂ emissions have remained in the atmosphere. The impact of land use change on CO₂ from 1850 to 2000 was assessed in AR4 to be 12 to 35 ppm (0.17 to 0.51 W m⁻²).

Using the formula from Table 3 of Myhre et al. (1998), and see Supplementary Material Table 8.SM.1, the CO₂ RF (as defined in Section 8.1) from 1750 to 2011 is 1.82 (1.63 to 2.01) W m⁻². The uncertainty is dominated by the radiative transfer modelling which is assessed to be 10% (Section 8.3.1). The uncertainty in the knowledge of 1750 concentrations contributes only 2% (see Supplementary Material Table 8.SM.2)

Table 8.2 shows the concentrations and RF in AR4 (2005) and 2011 for the most important WMGHGs. Figure 8.6 shows the time evolution of RF and its rate of change. Since AR4, the RF of CO₂ has increased by 0.16 W m⁻² and continues the rate noted in AR4 of almost 0.3 W m⁻² per decade. As shown in Figure 8.6(d) the rate of increase in the RF

from the WMGHGs over the last 15 years has been dominated by CO_2 . Since AR4, CO_2 has accounted for more than 80% of the WMGHG RF increase. The interannual variability in the rate of increase in the CO_2 RF is due largely to variation in the natural land uptake whereas the trend is driven by increasing anthropogenic emissions (see Figure 6.8 in Section 6.3.1).

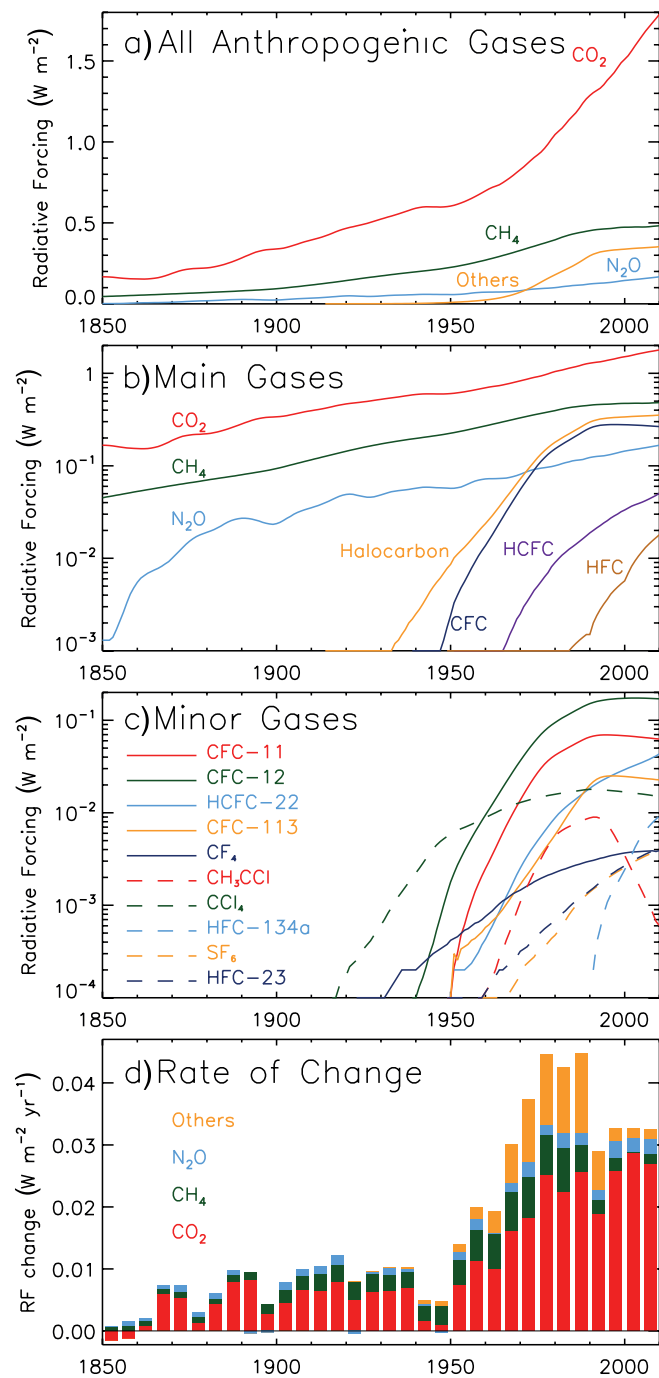


Figure 8.6 | (a) Radiative forcing (RF) from the major well-mixed greenhouse gases (WMGHGs) and groups of halocarbons from 1850 to 2011 (data from Tables A.II.1.1 and A.II.4.16), (b) as (a) but with a logarithmic scale, (c) RF from the minor WMGHGs from 1850 to 2011 (logarithmic scale). (d) Rate of change in forcing from the major WMGHGs and groups of halocarbons from 1850 to 2011.

As described in Section 8.1.1.3, CO_2 can also affect climate through physical effects on lapse rates and clouds, leading to an ERF that will be different from the RF. Analysis of CMIP5 models (Vial et al., 2013) found a large negative contribution to the ERF (20%) from the increase in land surface temperatures which was compensated for by positive contributions from the combined effects on water vapour, lapse rate, albedo and clouds. It is therefore not possible to conclude with the current information whether the ERF for CO_2 is higher or lower than the RF. Therefore we assess the ratio ERF/RF to be 1.0 and assess our uncertainty in the CO_2 ERF to be (−20% to 20%). We have *medium confidence* in this based on our understanding that the physical processes responsible for the differences between ERF and RF are small enough to be covered within the 20% uncertainty.

There are additional effects mediated through plant physiology, reducing the conductance of the plant stomata and hence the transpiration of water. Andrews et al. (2012b) find a physiological enhancement of the adjusted forcing by 3.5% due mainly to reductions in low cloud. This is smaller than a study with an earlier model by Doutriaux-Boucher et al. (2009) which found a 10% effect. Longer-term impacts of CO_2 on vegetation distributions also affect climate (O’ishi et al., 2009; Andrews et al., 2012b) but because of the longer time scale we choose to class these as feedbacks rather than rapid adjustments.

8.3.2.2 Methane

Globally averaged surface CH_4 concentrations have risen from 722 ± 25 ppb in 1750 to 1803 ± 2 ppb by 2011 (see Section 2.2.1.1.2). Over that time scale the rise has been due predominantly to changes in anthropogenic-related CH_4 . Anthropogenic emissions of other compounds have also affected CH_4 concentrations by changing its removal rate (Section 8.2.3.3). Using the formula from Myhre et al. (1998) (see Supplementary Material Table 8.SM.1) the RF for CH_4 from 1750 to 2011 is $0.48 \pm 0.05 \text{ W m}^{-2}$, with an uncertainty dominated by the radiative transfer calculation. This increase of 0.01 W m^{-2} since AR4 is due to the 29 ppb increase in the CH_4 mixing ratio. This is much larger than the 11 ppb increase between TAR and AR4, and has been driven by increases in net natural and anthropogenic emissions, but the relative contributions are not well quantified. Recent trends in CH_4 and their causes are discussed in Sections 2.2.1.1.2 and 6.3.3.1. CH_4 concentrations do vary with latitude and decrease above the tropopause; however, this variation contributes only 2% to the uncertainty in RF (Freckleton et al., 1998).

In this section only the direct forcing from changing CH_4 concentrations is addressed. CH_4 emissions can also have indirect effects on climate through impacts on CO_2 , stratospheric water vapour, ozone, sulphate aerosol and lifetimes of HFCs and HCFCs (Boucher et al., 2009; Shindell et al., 2009; Collins et al., 2010). Some of these are discussed further in Sections 8.3.3, 8.5.1 and 8.7.2.

8.3.2.3 Nitrous Oxide

Concentrations of nitrous oxide have risen from 270 ± 7 ppb in 1750 to 324.2 ± 0.1 ppb in 2011, an increase of 5 ppb since 2005 (see Section 2.2.1.1.3). N_2O now has the third largest forcing of the anthropogenic gases, at $0.17 \pm 0.03 \text{ W m}^{-2}$ an increase of 6% since 2005 (see Table

8.2) where the uncertainty is due approximately equally to the pre-industrial concentration and radiative transfer. Only the direct RF from changing nitrous oxide concentrations is included. Indirect effects of N₂O emissions on stratospheric ozone are not taken into account here but are discussed briefly in Section 8.7.2.

8.3.2.4 Other Well-mixed Greenhouse Gases

RFs of the other WMGHG are shown in Figure 8.6 (b and c) and Table 8.2. The contribution of groups of halocarbons to the rate of change

of WMGHG RF is shown in Figure 8.6 (d). Between 1970 and 1990 halocarbons made a significant contribution to the rate of change of RF. The rate of change in the total WMGHG RF was higher in 1970 to 1990 with *high confidence* compared to the present owing to higher contribution from non-CO₂ gases especially the halocarbons. Since the Montreal Protocol and its amendments, the rate of change of RF from halocarbons and related compounds has been much less, but still just positive (total RF of 0.360 W m⁻² in 2011 compared to 0.351 W m⁻² in 2005) as the growth of HCFCs, HFCs, PFCs and other halogens (SF₆, SO₂F₂, NF₃) RFs (total 0.022 W m⁻² since 2005) more than compensates

Table 8.2 | Present-day mole fractions (in ppt(pmol mol⁻¹) except where specified) and RF (in W m⁻²) for the WMGHGs. Concentration data are averages of National Oceanic and Atmospheric Administration (NOAA) and Advanced Global Atmospheric Gases Experiment (AGAGE) observations where available. CO₂ concentrations are the average of NOAA and SIO. See Table 2.1 for more details of the data sources. The data for 2005 (the time of the AR4 estimates) are also shown. Some of the concentrations vary slightly from those reported in AR4 owing to averaging different data sources. Radiative efficiencies for the minor gases are given in Table 8.A.1. Uncertainties in the RF for all gases are dominated by the uncertainties in the radiative efficiencies. We assume the uncertainties in the radiative efficiencies to be perfectly correlated between the gases, and the uncertainties in the present day and 1750 concentrations to be uncorrelated.

Species	Concentrations (ppt)		Radiative forcing ^a (W m ⁻²)	
	2011	2005	2011	2005
CO ₂ (ppm)	391 ± 0.2	379	1.82 ± 0.19	1.66
CH ₄ (ppb)	1803 ± 2	1774	0.48 ± 0.05	0.47 ^e
N ₂ O (ppb)	324 ± 0.1	319	0.17 ± 0.03	0.16
CFC-11	238 ± 0.8	251	0.062	0.065
CFC-12	528 ± 1	542	0.17	0.17
CFC-13	2.7		0.0007	
CFC-113	74.3 ± 0.1	78.6	0.022	0.024
CFC-115	8.37	8.36	0.0017	0.0017
HCFC-22	213 ± 0.1	169	0.0447	0.0355
HCFC-141b	21.4 ± 0.1	17.7	0.0034	0.0028
HCFC-142b	21.2 ± 0.2	15.5	0.0040	0.0029
HFC-23	24.0 ± 0.3	18.8	0.0043	0.0034
HFC-32	4.92	1.15	0.0005	0.0001
HFC-125	9.58 ± 0.04	3.69	0.0022	0.0008
HFC-134a	62.7 ± 0.3	34.3	0.0100	0.0055
HFC-143a	12.0 ± 0.1	5.6	0.0019	0.0009
HFC-152a	6.4 ± 0.1	3.4	0.0006	0.0003
SF ₆	7.28 ± 0.03	5.64	0.0041	0.0032
SO ₂ F ₂	1.71	1.35	0.0003	0.0003
NF ₃	0.9	0.4	0.0002	0.0001
CF ₄	79.0 ± 0.1	75.0	0.0040	0.0036
C ₂ F ₆	4.16 ± 0.02	3.66	0.0010	0.0009
CH ₃ CCl ₃	6.32 ± 0.07	18.32	0.0004	0.0013
CCl ₄	85.8 ± 0.8	93.1	0.0146	0.0158
CFCs			0.263 ± 0.026 ^b	0.273 ^c
HCFCs			0.052 ± 0.005	0.041
Montreal gases ^d			0.330 ± 0.033	0.331
Total halogens			0.360 ± 0.036	0.351 ^f
Total			2.83 ± 0.029	2.64

Notes:

^a Pre-industrial values are zero except for CO₂ (278 ppm), CH₄ (722 ppb), N₂O (270 ppb) and CF₄ (35 ppt).

^b Total includes 0.007 W m⁻² to account for CFC-114, Halon-1211 and Halon-1301.

^c Total includes 0.009 W m⁻² forcing (as in AR4) to account for CFC-13, CFC-114, CFC-115, Halon-1211 and Halon-1301.

^d Defined here as CFCs + HCFCs + CH₃CCl₃ + CCl₄.

^e The value for the 1750 methane concentrations has been updated from AR4 in this report, thus the 2005 methane RF is slightly lower than reported in AR4.

^f Estimates for halocarbons given in the table may have changed from estimates reported in AR4 owing to updates in radiative efficiencies and concentrations.

for the decline in the CFCs, CH_3CCl_3 and CCl_4 RFs (-0.013 W m^{-2} since 2005). The total halocarbon RF is dominated by four gases, namely CFC-12, trichlorofluoromethane (CFC-11), chlorodifluoromethane (HCFC-22) and trichlorofluoroethane (CFC-113) in that order, which account for about 85% of the total halocarbon RF (see Table 8.2). The indirect RF from the impacts of ODSs is discussed in Section 8.3.3.2.

8.3.2.4.1 Chlorofluorocarbons and hydrochlorofluorocarbons

The CFCs and HCFCs contribute approximately 11% of the WMGHG RF. Although emissions have been drastically reduced for CFCs, their long lifetimes mean that reductions take substantial time to affect their concentrations. The RF from CFCs has declined since 2005 (mainly due to a reduction in the concentrations of CFC-11 and CFC-12), whereas the RF from HCFCs is still rising (mainly due to HCFC-22).

8.3.2.4.2 Hydrofluorocarbons

The RF of HFCs is 0.02 W m^{-2} and has close to doubled since AR4 (2005 concentrations). HFC-134a is the dominant contributor to RF of the HFCs, with an RF of 0.01 W m^{-2} .

8.3.2.4.3 Perfluorocarbons and sulphur hexafluoride

These gases have lifetimes of thousands to tens of thousands of years (Table 8.A.1); therefore emissions essentially accumulate in the atmosphere on the time scales considered here. CF_4 has a natural source and a 1750 concentration of 35 ppt (see Section 2.2.1.1.4). These gases currently contribute 0.01 W m^{-2} of the total WMGHG RF.

8.3.2.4.4 New species

Nitrogen trifluoride (NF_3) is used in the electronics industry and sulfur dioxide (SO_2) is used as a fumigant. Both have rapidly increasing emissions and high GWPs, but currently contribute only around 0.0002 W m^{-2} and 0.0003 W m^{-2} to anthropogenic RF, respectively (Weiss et al., 2008; Andersen et al., 2009; Muhle et al., 2009; Arnold et al., 2013).

8.3.3 Ozone and Stratospheric Water Vapour

Unlike for the WMGHGs, the estimate of the tropospheric and stratospheric ozone concentration changes are almost entirely model based for the full pre-industrial to present-day interval (though, especially for the stratosphere, more robust observational evidence on changes is available for recent decades; see Section 2.2).

AR4 assessed the RF (for 1750–2005) from tropospheric ozone to be 0.35 W m^{-2} from multi-model studies with a high 95th percentile of 0.65 W m^{-2} to allow for the possibility of model overestimates of the pre-industrial tropospheric ozone levels. The stratospheric ozone RF was assessed from observational trends from 1979 to 1998 to be $-0.05 \pm 0.1 \text{ W m}^{-2}$, with the 90% confidence range increased to reflect uncertainty in the trend prior to 1979 and since 1998. In AR4 the RF from stratospheric water vapour generated by CH_4 oxidation was assessed to be $+0.07 \pm 0.05 \text{ W m}^{-2}$ based on Hansen et al. (2005).

Since AR4, there have been a few individual studies of tropospheric or stratospheric ozone forcing (Shindell et al., 2006a, 2006c, 2013a; Skeie et al., 2011a; Søvde et al., 2011), a multi-model study of stratospheric ozone RF in the 2010 WMO stratospheric ozone assessment (Forster et al., 2011b), and the ACCMIP multi-model study of tropospheric and tropospheric + stratospheric chemistry models (Conley et al., 2013; Stevenson et al., 2013). There is now greater understanding of how tropospheric ozone precursors can affect stratospheric ozone, and how ODSs can affect tropospheric ozone (Shindell et al., 2013a). We assess the total ozone RF to be $+0.35$ (0.15 to 0.55) W m^{-2} . This can be split according to altitude or by emitted species (Shindell et al., 2013a). We assess these contributions to be 0.40 (0.20 to 0.60) W m^{-2} for ozone in the troposphere and $-0.05 \pm 0.10 \text{ W m}^{-2}$ for ozone in the stratosphere based on the studies presented in Table 8.3. Alternatively, the contributions to the total ozone forcing can be attributed as 0.50 (0.30 to 0.70) W m^{-2} from ozone precursors and -0.15 (-0.3 to 0.0) W m^{-2} from the effect of ODSs. The value attributed to ODSs is assessed to be slightly smaller in magnitude than in the two studies quoted in Table 8.3 (Søvde et al., 2011; Shindell et al., 2013a) because the models used for these had stratospheric ozone RFs with higher magnitudes than the ACCMIP mean (Conley et al., 2013). Differences between the ERFs and RFs for tropospheric and stratospheric ozone are *likely* to be small compared to the uncertainties in the RFs (Shindell et al., 2013b), so the assessed values for the ERFs are the same as those for the RFs.

The influence of climate change is typically included in ozone RF estimates as those are based on modelled concentration changes, but the available literature provides insufficient evidence for the sign and magnitude of the impact and we therefore refrain from giving an estimate except to assess that it is *very likely* to be smaller than the overall uncertainty in the total RF. Unlike the WMGHGs, there are significant latitudinal variations in the RFs from changes in tropospheric and stratospheric ozone. The implications of inhomogeneous RFs are explored in more detail in Section 8.6.

There has been one study since AR4 (Myhre et al., 2007) on the RF from water vapour formed from the stratospheric oxidation of CH_4 (Section 8.3.3.3). This is consistent with the AR4 value and so has not led to any change in the recommended value of 0.07 (0.02 to 0.12) W m^{-2} since AR4.

8.3.3.1 Tropospheric Ozone

Ozone is formed in the troposphere by photochemical reactions of natural and anthropogenic precursor species (Section 8.2.3.1). Changes in ozone above the tropopause due to emissions of stratospheric ODSs can also affect ozone in the troposphere either by transport across the tropopause or modification of photolysis rates. Changes in climate have also affected tropospheric ozone concentrations (medium evidence, low agreement) through changes in chemistry, natural emissions and transport from the stratosphere (Isaksen et al., 2009).

The most recent estimates of tropospheric ozone RF come from multi-model studies under ACCMIP (Conley et al., 2013; Lamarque et al., 2013; Stevenson et al., 2013). The model ensemble reported only 1850–2000 RFs (0.34 W m^{-2}) so the single-model results from Skeie et

al. (2011a) were used to expand the timespan to 1750–2010, adding 0.04 W m^{-2} , and 0.02 W m^{-2} to account for the periods 1750–1850 and 2000–2010 respectively. The best estimate of tropospheric ozone RF taking into account the ACCMIP models and the Søvde et al. (2011) results (the Skeie et al. (2011a) and Shindell et al. (2013a) models are included in ACCMIP) is 0.40 (0.20 to 0.60) W m^{-2} . The quantifiable uncertainties come from the inter-model spread (-0.11 to 0.11 W m^{-2}) and the differences between radiative transfer models (-0.07 to 0.07 W m^{-2}); all 5 to 95% confidence interval. Additional uncertainties arise from the lack of knowledge of pre-industrial emissions and the representation of chemical and physical processes beyond those included in the current models. The tropospheric ozone RF is sensitive to the assumed ‘pre-industrial’ levels. As described in Section 8.2.3.1, very limited late 19th and early 20th century observations of surface ozone concentrations are lower than the ACCMIP models for the same period; however, we assess that those observations are very uncertain. Skeie et al. (2011a) and Stevenson et al. (2013) increase their uncertainty ranges to 30% for 1 standard deviation which is equivalent to (-50% to $+50\%$) for the 5 to 95% confidence range and we adopt this for AR5. The overall *confidence* in the tropospheric ozone RF is assessed as *high*.

Because we have *low confidence* in the pre-industrial ozone observations, and these were extremely limited in spatial coverage, it is not possible to calculate a purely observationally based ozone RF. However, modern observations can be used to assess the performance of the chemistry models. Bowman et al. (2013) used satellite retrievals from the TES instrument to constrain the RF from the ACCMIP models. This reduced the inter-model uncertainty by 30%; however, we still maintain overall the (-50% to $+50\%$) 5 to 95% confidence range for AR5.

The time evolution of the tropospheric ozone forcing is shown in Figure 8.7. There is a noticeable acceleration in the forcing after 1950 and a deceleration in the 1990s reflecting the time evolution of anthropogenic precursor emissions. Observational evidence for trends in ozone concentrations is discussed in Section 2.2.2.3.

It can be useful to calculate a normalized radiative forcing (NRF) which is an RF per change in ozone column in $\text{W m}^{-2} \text{DU}^{-1}$ or W mol^{-1} . This is only an approximation as the NRF is sensitive to the vertical profile of the ozone change and to the latitudinal profile to a smaller extent. From Table 8.3 we assess the NRF to be 0.042 (0.037 to 0.047) $\text{W m}^{-2} \text{DU}^{-1}$ (94 (83 to 105) W mol^{-1}) similar to the value of $0.042 \text{ W m}^{-2} \text{DU}^{-1}$ (94 W mol^{-1}) in TAR (Ramaswamy et al., 2001).

A small number of studies have looked at attributing the ozone changes among the anthropogenically emitted species. Søvde et al. (2011) report a tropospheric ozone RF of 0.38 W m^{-2} , 0.44 W m^{-2} from ozone precursors and -0.06 W m^{-2} from the impact of stratospheric ozone depletion on the troposphere. Shindell et al. (2013a) also calculate that ODSs are responsible for about -0.06 W m^{-2} of the tropospheric ozone RF, and ozone precursors for about 0.41 W m^{-2} . Six of the models in Stevenson et al. (2013) and Shindell et al. (2009) performed experiments to attribute the ozone RF to the individual precursor emissions. An average of these seven model results leads to attributions of $0.24 \pm 0.13 \text{ W m}^{-2}$ due to CH_4 emissions, $0.14 \pm 0.09 \text{ W m}^{-2}$ from NO_x emissions, $0.07 \pm 0.03 \text{ W m}^{-2}$ from CO , and $0.04 \pm 0.03 \text{ W m}^{-2}$ from

non-methane volatile organic compounds (NMVOCs). These results were calculated by reducing the precursor emissions individually from 2000 to pre-industrial levels. The results were scaled by the total ozone RFs attributed to ozone precursors (0.50 W m^{-2}) to give the contributions to the full 1750–2010 RF. Because of the nonlinearity of the chemistry an alternative method of starting from pre-industrial conditions and increasing precursor emissions singly may give a different result. Note that as well as inducing an ozone RF, these ozone precursor species can also strongly affect the concentrations of CH_4 and aerosols, adding extra terms (both positive and negative) to their total indirect forcings. The contributions to the 1750–2010 CH_4 RF are again based on Stevenson et al. (2013) and Shindell et al. (2009). The Stevenson et al. (2013) values are for 1850–2000 rather than 1750 to 2011 so for these we distribute the CH_4 RF for 1750–1850 and 2000–2011 (0.06 W m^{-2}) by scaling the CH_4 and CO contributions (assuming these were the most significant contributors over those time periods). This gives contributions of 0.58 ± 0.08 , -0.29 ± 0.18 , 0.07 ± 0.02 and $0.02 \pm 0.02 \text{ W m}^{-2}$ for changes from historical to present day emissions of CH_4 (inferred emissions), NO_x , CO and VOCs respectively (uncertainties are 5 to 95% confidence intervals). The difference between the total CH_4 RF attributed to ozone precursors here (0.38 W m^{-2}) and the value calculated from CH_4 concentration changes in Table 8.2 (0.48 W m^{-2}) is due to nonlinearities in the CH_4 chemistry because large single-step changes were used. To allow an easier comparison between the concentration-based and emission-based approaches in Section 8.5.1 the nonlinear term ($+0.1 \text{ W m}^{-2}$) is distributed between the four emitted species according to their absolute magnitude so that they total 0.48 W m^{-2} . The scaled results still lie within the uncertainty bounds of the values quoted above. The impact of climate change over the historical period on CH_4 oxidation is not accounted for in these calculations.

Tropospheric ozone can also affect the natural uptake of CO_2 by decreasing plant productivity (see Sections 6.4.8.2 and 8.2.3.1) and it is found that this indirect effect could have contributed to the total CO_2 RF (Section 8.3.2.1; Sitch et al., 2007), roughly doubling the overall RF attributed to ozone precursors. Although we assess there to be

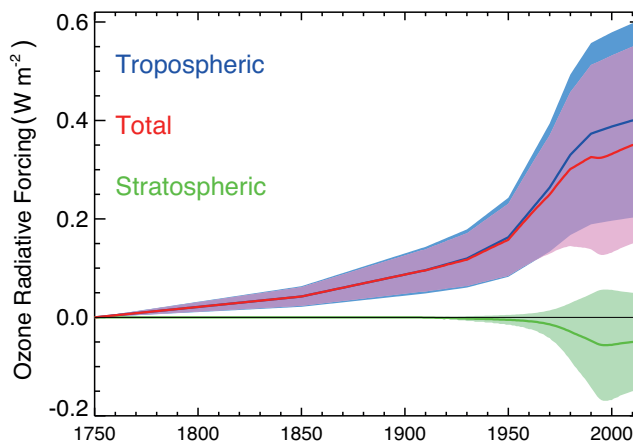


Figure 8.7 | Time evolution of the radiative forcing from tropospheric and stratospheric ozone from 1750 to 2010. Tropospheric ozone data are from Stevenson et al. (2013) scaled to give 0.40 W m^{-2} at 2010. The stratospheric ozone RF follow the functional shape of the Effective Equivalent Stratospheric Chlorine assuming a 3-year age of air (Daniel et al., 2010) scaled to give -0.05 W m^{-2} at 2010.

Table 8.3 | Contributions of tropospheric and stratospheric ozone changes to radiative forcing (W m^{-2}) from 1750 to 2011.

	Troposphere				Stratosphere		
	Longwave	Shortwave	Total	Normalized Radiative Forcing $\text{m W m}^{-2} \text{DU}^{-1}$	Longwave	Shortwave	Total
AR4 (Forster et al. (2007))			0.35 (0.25 to 0.65)				-0.05 (-0.15 to 0.05)
Shindell et al. (2013a) ^f			0.33 (0.31 to 0.35)				-0.08 (-0.10 to -0.06)
WMO (Forster et al., 2011b)							-0.03 ^a (-0.23 to +0.17) +0.03 ^b
Søvde et al. (2011)			0.45 ^c 0.38 ^d	40 39			-0.12 -0.12
Skeie et al. (2011a)			0.41 (0.21 to 0.61)	38			
ACCMIP ^e	0.33 (0.24 to 0.42)	0.08 (0.06 to 0.10)	0.41 (0.21 to 0.61)	42 (37 to 47)	-0.13 (-0.26 to 0)	0.11 (0.03 to 0.19)	-0.02 (-0.09 to 0.05)
AR5			0.40 (0.20 to 0.60)	42 (37 to 47)			-0.05 (-0.15 to 0.05)

Notes:

- ^a From multi-model results.
^b From Randel and Wu (2007) observation-based data set.
^c Using the REF chemistry, see Søvde et al. (2011).
^d Using the R2 chemistry.
^e The Atmospheric Chemistry and Climate Model Intercomparison Project (ACCMIP) tropospheric ozone RFs are from Stevenson et al. (2013). The stratospheric ozone values are from Conley et al. (2013) calculations for 1850–2005 disregarding the *Modèle de Chimie Atmosphérique à Grande Echelle* (MOCAGE) model which showed excessive ozone depletion.
^f Only the Goddard Institute for Space Studies (GISS)-E2-R results (including bias correction) from the Shindell et al. (2013a) study are shown here rather than the multi-model result presented in that paper.

robust evidence of an effect, we make no assessment of the magnitude because of lack of further corroborating studies.

8.3.3.2 Stratospheric Ozone

The decreases in stratospheric ozone due to anthropogenic emissions of ODSs have a positive RF in the shortwave (increasing the flux into the troposphere) and a negative RF in the longwave. This leaves a residual forcing that is the difference of two larger terms. In the lower stratosphere the longwave effect tends to be larger, whereas in the upper stratosphere the shortwave dominates. Thus whether stratospheric ozone depletion has contributed an overall net positive or negative forcing depends on the vertical profile of the change (Forster and Shine, 1997). WMO (2011) assessed the RF from 1979 to 2005 from observed ozone changes (Randel and Wu, 2007) and results from 16 models for the 1970s average to 2004. The observed and modelled mean ozone changes gave RF values of different signs (see Table 8.3). Negative net RFs arise from models with ozone decline in the lowermost stratosphere, particularly at or near the tropopause.

The ACCMIP study also included some models with stratospheric chemistry (Conley et al., 2013). One model in that study stood out as having excessive ozone depletion. Removing that model leaves a stratospheric ozone RF of -0.02 (-0.09 to 0.05) W m^{-2} . These results are in good agreement with the model studies from WMO (2011). Forster et al. (2007) in AR4 calculated a forcing of -0.05 W m^{-2} from observations over the period 1979–1998 and increased the uncertainty to 0.10 W m^{-2} to encompass changes between the pre-industrial period and

2005. The RF from stratospheric ozone due to changes in emissions of ozone precursors and ODSs is here assessed to be -0.05 (-0.15 to 0.05) taking into account all the studies listed in Table 8.3. This is in agreement with AR4, although derived from different data. The time-line of stratospheric ozone forcing is shown in Figure 8.7, making the assumption that it follows the trajectory of the changes in EESC. It reaches a minimum in the late 1990s and starts to recover after that.

The net global RF from ODSs taking into account the compensating effects on ozone and their direct effects as WMGHGs is 0.18 (0.03 to 0.33) W m^{-2} . The patterns of RF for these two effects are different so the small net global RF comprises areas of positive and negative RF.

8.3.3.3 Stratospheric Water Vapour

Stratospheric water vapour is dependent on the amount entering from the tropical troposphere and from direct injection by volcanic plumes (Joshi and Jones, 2009) and aircraft, and the *in situ* chemical production from the oxidation of CH_4 and hydrogen. This contrasts with tropospheric water vapour which is almost entirely controlled by the balance between evaporation and precipitation (see FAQ 8.1). We consider trends in the transport (for instance, due to the Brewer–Dobson circulation or tropopause temperature changes) to be climate feedback rather than a forcing so the anthropogenic RFs come from oxidation of CH_4 and hydrogen, and emissions from stratospheric aircraft.

Myhre et al. (2007) used observations of the vertical profile of CH_4 to deduce a contribution from oxidation of anthropogenic CH_4 of 0.083

$W\ m^{-2}$ which compares with the value of $0.07\ W\ m^{-2}$ from calculations in a 2D model in Hansen et al. (2005). Both of these values are consistent with AR4 which obtained the stratospheric water vapour forcing by scaling the CH_4 direct forcing by 15%. Thus the time evolution of this forcing is also obtained by scaling the CH_4 forcing by 15%. The best estimate and uncertainty range from AR4 of 0.07 (0.02 to 0.12) $W\ m^{-2}$ remain unchanged and the large uncertainty range is due to large differences found in the intercomparison studies of radiative transfer modelling for changes in stratospheric water vapour (see Section 8.3.1).

RF from the current aircraft fleet through stratospheric water vapour emissions is very small. Wilcox et al. (2012) estimate a contribution from civilian aircraft in 2005 of 0.0009 (0.0003 to 0.0013) $W\ m^{-2}$ with *high confidence* in the upper limit. Water vapour emissions from aircraft in the troposphere also contribute to contrails which are discussed in Section 8.3.4.5.

8.3.4 Aerosols and Cloud Effects

8.3.4.1 Introduction and Summary of AR4

In AR4 (Forster et al., 2007), RF estimates were provided for three aerosol effects. These were the RF of aerosol–radiation interaction (previously denoted as direct aerosol effect), RF of the aerosol–cloud interaction (previously denoted as the cloud albedo effect), and the impact of BC on snow and ice surface albedo. See Chapter 7 and Figure 7.3 for an explanation of the change in terminology between AR4 and AR5. The RF due to aerosol–radiation interaction is scattering and absorption of shortwave and longwave radiation by atmospheric aerosols. Several different aerosol types from various sources are present in the atmosphere (see Section 8.2). Most of the aerosols primarily scatter solar radiation, but some components absorb solar radiation to various extents with BC as the most absorbing component. RF of aerosols in the troposphere is often calculated at the TOA because it is similar to tropopause values (Forster et al., 2007). A best estimate RF of $-0.5 \pm 0.4\ W\ m^{-2}$ was given in AR4 for the change in the net aerosol–radiation interaction between 1750 and 2005 and a medium to low level of scientific understanding (LOSU).

An increase in the hygroscopic aerosol abundance may enhance the concentration of cloud condensation nuclei (CCN). This may increase the cloud albedo and under the assumption of fixed cloud water content this effect was given a best estimate of $-0.7\ W\ m^{-2}$ (range from -1.8 to -0.3) in AR4 and a low LOSU.

BC in the snow or ice can lead to a decrease of the surface albedo. This leads to a positive RF. In AR4 this mechanism was given a best RF estimate of $0.1 \pm 0.1\ W\ m^{-2}$ and a low LOSU.

Impacts on clouds from the ERF of aerosol–cloud interaction (including both effects previously denoted as cloud lifetime and cloud albedo effect) and the ERF of aerosol–radiation interaction (including both effects previously denoted as direct aerosol effect and semi-direct effect) were not strictly in accordance with the RF concept, because they involve tropospheric changes in variables other than the forcing agent at least in the available model estimates, so no best RF estimates

were provided in AR4 (see Section 8.1). However, the ERF of aerosol–cloud and aerosol–radiation interactions were included in the discussion of total aerosol effect in Chapter 7 in AR4 (Denman et al., 2007). The mechanisms influenced by anthropogenic aerosol including the aerosol cloud interactions are discussed in detail in this assessment in Section 7.5 and summarized in the subsections that follow.

8.3.4.2 Radiation Forcing of the Aerosol–Radiation Interaction by Component

Based on a combination of global aerosol models and observation-based methods, the best RF estimate of the aerosol–radiation interaction in AR5 is -0.35 (-0.85 to $+0.15$) $W\ m^{-2}$ (see Section 7.5). This estimate is thus smaller in magnitude than in AR4, however; with larger uncertainty range. Overall, the estimate compared to AR4 is more robust because the agreement between estimates from models and observation-based methods is much greater (see Section 7.5). The larger range arises primarily from analysis by observation-based methods (see Section 7.5).

The main source of the model estimate is based on updated simulations in AeroCom (Myhre et al., 2013), which is an intercomparison exercise of a large set of global aerosol models that includes extensive evaluation against measurements. The assessment in Chapter 7 relies to a large extent on this study for the separation in the various aerosol components, except for BC where the assessment in Chapter 7 relies in addition on Bond et al. (2013). The RF of aerosol–radiation interaction is separated into seven components in this report; namely sulphate, BC from fossil fuel and biofuel, OA from fossil fuel and biofuel, BC and OA combined from biomass burning (BB), nitrate, SOA and mineral dust. BC and OA from biomass burning are combined due to the joint sources, whereas treated separately for fossil fuel and biofuel because there is larger variability in the ratio of BC to OA in the fossil fuel and biofuel emissions. This approach is consistent with TAR and AR4. Table 8.4 compares the best estimates of RF due to aerosol–radiation interaction for various components in this report with values in SAR, TAR and AR4. In magnitude the sulphate and BC from use of fossil fuel and biofuel dominate. It is important to note that the BB RF is small in magnitude but consists of larger, offsetting terms in magnitude from OA and BC (see Section 7.5.2). Changes in the estimates of RF due to aerosol–radiation interaction of the various components have been rather modest compared to AR4, except for BC from fossil fuel and biofuel (see Section 7.5). SOA is a new component compared to AR4. Anthropogenic SOA precursors contribute only modestly to the anthropogenic change in SOA. The increase in SOA is mostly from biogenic precursors and enhanced partitioning of SOA into existing particles from anthropogenic sources and changes in the atmospheric oxidation (Carlton et al., 2010). This change in SOA is therefore of anthropogenic origin, but natural emission of SOA precursors is important (Hoyle et al., 2011).

Note that the best estimate and the uncertainty for the total is not equal to the sum of the aerosol components because the total is estimated based on a combination of methods (models and observation-based methods), whereas the estimates for the components rely mostly on model estimates.

Table 8.4 | Global and annual mean RF ($W m^{-2}$) due to aerosol–radiation interaction between 1750 and 2011 of seven aerosol components for AR5. Values and uncertainties from SAR, TAR, AR4 and AR5 are provided when available. Note that for SAR, TAR and AR4 the end year is somewhat different than for AR5 with 1993, 1998 and 2005, respectively.

Global Mean Radiative Forcing ($W m^{-2}$)				
	SAR	TAR	AR4	AR5
Sulphate aerosol	-0.40 (-0.80 to -0.20)	-0.40 (-0.80 to -0.20)	-0.40 (-0.60 to -0.20)	-0.40 (-0.60 to -0.20)
Black carbon aerosol from fossil fuel and biofuel	+0.10 (+0.03 to +0.30)	+0.20 (+0.10 to +0.40)	+0.20 (+0.05 to +0.35)	+0.40 (+0.05 to +0.80)
Primary organic aerosol from fossil fuel and biofuel	Not estimated	-0.10 (-0.30 to -0.03)	-0.05 (0.00 to -0.10)	-0.09 (-0.16 to -0.03)
Biomass burning	-0.20 (-0.60 to -0.07)	-0.20 (-0.60 to -0.07)	+0.03(-0.09 to +0.15)	-0.0 (-0.20 to +0.20)
Secondary organic aerosol	Not estimated	Not estimated	Not estimated	-0.03 (-0.27 to +0.20)
Nitrate	Not estimated	Not estimated	-0.10 (-0.20 to 0.00)	-0.11 (-0.30 to -0.03)
Dust	Not estimated	-0.60 to +0.40	-0.10 (-0.30 to +0.10)	-0.10 (-0.30 to +0.10)
Total	Not estimated	Not estimated	-0.50 (-0.90 to -0.10)	-0.35 (-0.85 to +0.15)

The RF due to aerosol–radiation interaction during some time periods is more uncertain than the current RF. Improvements in the observations of aerosols have been substantial with availability of remote sensing from the ground-based optical observational network AEROSOL ROBOTIC NETWORK (AERONET) and the launch of the Moderate Resolution Imaging Spectrometer (MODIS) and Multi-angle Imaging Spectro-Radiometer (MISR) instruments (starting in 2000) as well as other satellite data. This has contributed to constraining the current RF using aerosol observations. The aerosol observations are very limited backward in time, although there is growing constraint coming from new ice and

lake core records, and uncertainties in the historical emission of aerosols and their precursors used in the global aerosol modeling are larger than for current conditions. Emissions of carbonaceous aerosols are particularly uncertain in the 1800s due to a significant biofuel source in this period, in contrast to the SO_2 emissions which were very small until the end of the 1800s. The uncertainty in the biomass burning emissions also increases backward in time. Note that, for 1850, the biomass burning emissions from Lamarque et al. (2010) are quite different from the previous estimates, but RF due to aerosol–radiation interaction is close to zero for this component. Figure 8.8 shows an example of the time evolution of the RF due to aerosol–radiation interaction as a total and separated into six aerosol components. From 1950 to 1990 there was a strengthening of the total RF due to aerosol–radiation interaction, mainly due to a strong enhancement of the sulphate RF. After 1990 the change has been small with even a weakening of the RF due to aerosol–radiation interaction, mainly due to a stronger BC RF as a result of increased emissions in East and Southeast Asia.

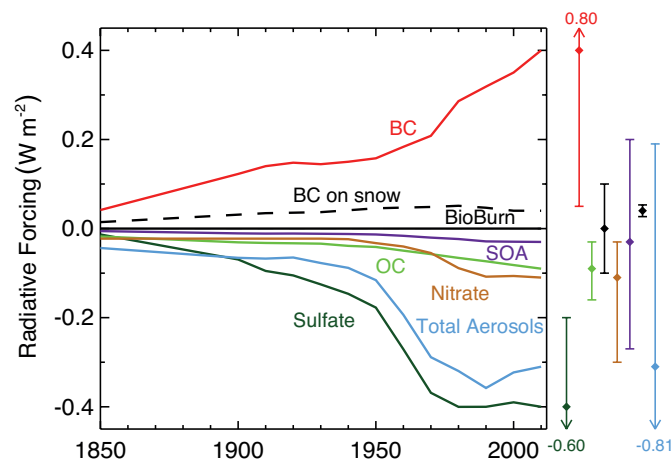


Figure 8.8 | Time evolution of RF due to aerosol–radiation interaction and BC on snow and ice. Multi-model results for 1850, 1930, 1980 and 2000 from ACCMIP for aerosol–radiation interaction (Shindell et al., 2013c) and BC on snow and ice (Lee et al., 2013) are combined with higher temporal-resolution results from the Goddard Institute for Space Studies (GISS)-E2 and Oslo-Chemical Transport Model 2 (OsloCTM2) models (aerosol–radiation interaction) and OsloCTM2 (BC on snow and ice). Uncertainty ranges (5 to 95%) for year 2010 are shown with vertical lines. Values next to the uncertainty lines are for cases where uncertainties go beyond the scale. The total includes the RF due to aerosol–radiation interaction for six aerosol components and RF due to BC on snow and ice. All values have been scaled to the best estimates for 2011 given in Table 8.4. Note that time evolution for mineral dust is not included and the total RF due to aerosol–radiation interaction is estimated based on simulations of the six other aerosol components.

8.3.4.3 Aerosol–Cloud Interactions

The RF by aerosol effects on cloud albedo was previously referred to as the Twomey or cloud albedo effect (see Section 7.1). Although this RF can be calculated, no estimate of this forcing is given because it has heuristic value only and does not simply translate to the ERF due to aerosol–cloud interaction. The total aerosol ERF, namely ERF due to aerosol–radiation and aerosol–cloud interactions (excluding BC on snow and ice) provided in Chapter 7 is estimated with a 5 to 95% uncertainty between -1.9 and $-0.1 W m^{-2}$ with a best estimate value of $-0.9 W m^{-2}$ (medium confidence). The likely range of this forcing is between -1.5 and $-0.4 W m^{-2}$. The estimate of ERF due to aerosol–radiation and aerosol–cloud interaction is lower (i.e., less negative) than the corresponding AR4 RF estimate of $-1.2 W m^{-2}$ because the latter was based mainly on GCM studies that did not take secondary processes (such as aerosol effects on mixed-phase and/or convective clouds and effects on longwave radiation) into account. This new best estimate of ERF due to aerosol–radiation and aerosol–cloud interaction is also consistent with the studies allowing cloud-scale processes and related responses and with the lower estimates of this forcing inferred from satellite observations.

Frequently Asked Questions

FAQ 8.2 | Do Improvements in Air Quality Have an Effect on Climate Change?

Yes they do, but depending on which pollutant(s) they limit, they can either cool or warm the climate. For example, whereas a reduction in sulphur dioxide (SO₂) emissions leads to more warming, nitrogen oxide (NO_x) emission control has both a cooling (through reducing of tropospheric ozone) and a warming effect (due to its impact on methane lifetime and aerosol production). Air pollution can also affect precipitation patterns.

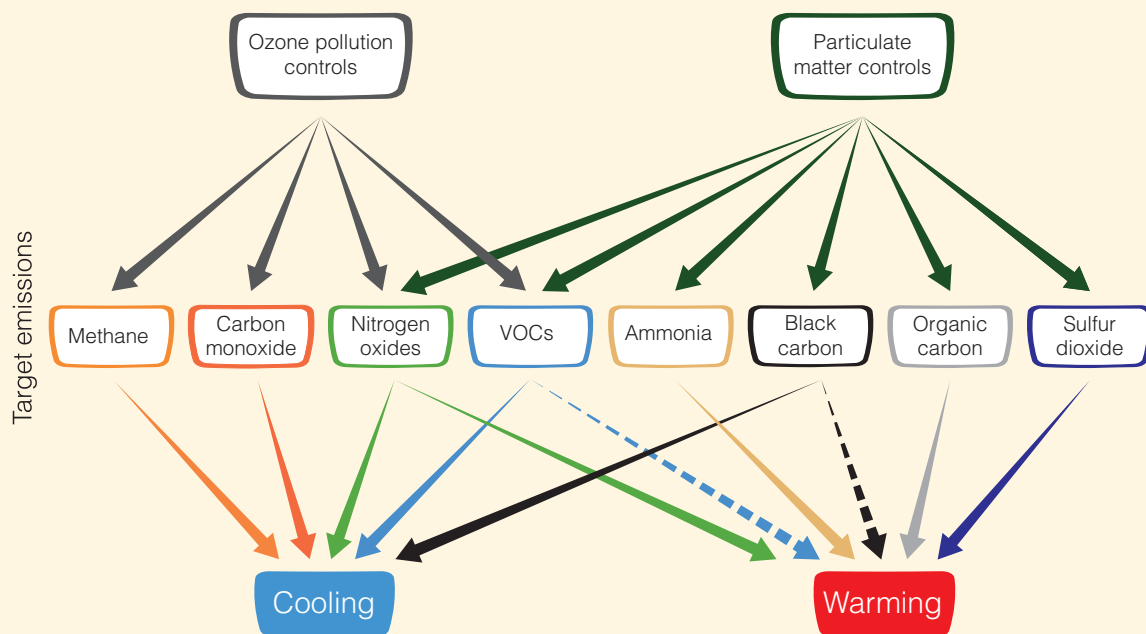
Air quality is nominally a measure of airborne surface pollutants, such as ozone, carbon monoxide, NO_x and aerosols (solid or liquid particulate matter). Exposure to such pollutants exacerbates respiratory and cardiovascular diseases, harms plants and damages buildings. For these reasons, most major urban centres try to control discharges of airborne pollutants.

Unlike carbon dioxide (CO₂) and other well-mixed greenhouse gases, tropospheric ozone and aerosols may last in the atmosphere only for a few days to a few weeks, though indirect couplings within the Earth system can prolong their impact. These pollutants are usually most potent near their area of emission or formation, where they can force local or regional perturbations to climate, even if their globally averaged effect is small.

Air pollutants affect climate differently according to their physical and chemical characteristics. Pollution-generated greenhouse gases will impact climate primarily through shortwave and longwave radiation, while aerosols can in addition affect climate through cloud–aerosol interactions.

Controls on anthropogenic emissions of methane (FAQ 8.2, Figure 1) to lower surface ozone have been identified as ‘win–win’ situations. Consequences of controlling other ozone precursors are not always as clear. NO_x emission controls, for instance, might be expected to have a cooling effect as they reduce tropospheric ozone, but their impact on CH₄ lifetime and aerosol formation is more likely instead to cause overall warming.

Satellite observations have identified increasing atmospheric concentrations of SO₂ (the primary precursor to scattering sulphate aerosols) from coal-burning power plants over eastern Asia during the last few decades. The most recent power plants use scrubbers to reduce such emissions (albeit not the concurrent CO₂ emissions and associated long-term climate warming). This improves air quality, but also reduces the cooling effect of sulphate aerosols and therefore exacerbates warming. Aerosol cooling occurs through aerosol–radiation and aerosol–cloud interactions and is estimated at -0.9 W m^{-2} (all aerosols combined, Section 8.3.4.3) since pre-industrial, having grown especially during the second half of the 20th century when anthropogenic emissions rose sharply. (continued on next page)



FAQ 8.2, Figure 1 | Schematic diagram of the impact of pollution controls on specific emissions and climate impact. Solid black line indicates known impact; dashed line indicates uncertain impact.

FAQ 8.2 (continued)

Black carbon or soot, on the other hand, absorbs heat in the atmosphere (leading to a 0.4 W m^{-2} radiative forcing from anthropogenic fossil and biofuel emissions) and, when deposited on snow, reduces its albedo, or ability to reflect sunlight. Reductions of black carbon emissions can therefore have a cooling effect, but the additional interaction of black carbon with clouds is uncertain and could lead to some counteracting warming.

Air quality controls might also target a specific anthropogenic activity sector, such as transportation or energy production. In that case, co-emitted species within the targeted sector lead to a complex mix of chemistry and climate perturbations. For example, smoke from biofuel combustion contains a mixture of both absorbing and scattering particles as well as ozone precursors, for which the combined climate impact can be difficult to ascertain.

Thus, surface air quality controls will have some consequences on climate. Some couplings between the targeted emissions and climate are still poorly understood or identified, including the effects of air pollutants on precipitation patterns, making it difficult to fully quantify these consequences. There is an important twist, too, in the potential effect of climate change on air quality. In particular, an observed correlation between surface ozone and temperature in polluted regions indicates that higher temperatures from climate change alone could worsen summertime pollution, suggesting a 'climate penalty'. This penalty implies stricter surface ozone controls will be required to achieve a specific target. In addition, projected changes in the frequency and duration of stagnation events could impact air quality conditions. These features will be regionally variable and difficult to assess, but better understanding, quantification and modelling of these processes will clarify the overall interaction between air pollutants and climate.

One reason an expert judgment estimate of ERF due to aerosol–radiation and aerosol–cloud interaction is provided rather than ERF due to aerosol–cloud interaction specifically is that the individual contributions are very difficult to disentangle. These contributions are the response of processes that are the outputs from a system that is constantly readjusting to multiple nonlinear forcings. Assumptions of independence and linearity are required to deduce ERF due to aerosol–radiation interaction and ERF due to aerosol–cloud interaction (although there is no *a priori* reason why the individual ERFs should be simply additive). Under these assumptions, ERF due to aerosol–cloud interaction is deduced as the difference between ERF due to aerosol–radiation and aerosol–cloud interaction and ERF due to aerosol–radiation interaction alone. This yields an ERF due to aerosol–cloud interaction estimate of -0.45 W m^{-2} which is much smaller in magnitude than the -1.4 W m^{-2} median forcing value of the models summarized in Figure 7.19 and is also smaller in magnitude than the AR4 estimates of -0.7 W m^{-2} for RF due to aerosol–cloud interaction.

8.3.4.4 Black Carbon Deposition in Snow and Ice

Because absorption by ice is very weak at visible and ultraviolet (UV) wavelengths, BC in snow makes the snow darker and increases absorption. This is not enough darkening to be seen by eye, but it is enough to be important for climate (Warren and Wiscombe, 1980; Clarke and Noone, 1985). Several studies since AR4 have re-examined this issue and find that the RF may be weaker than the estimates of Hansen and Nazarenko (2004) in AR4 (Flanner et al., 2007; Koch et al., 2009a; Rypdal et al., 2009; Lee et al., 2013). The anthropogenic BC on snow/ice is assessed to have a positive global and annual mean RF of $+0.04 \text{ W m}^{-2}$, with a $0.02\text{--}0.09 \text{ W m}^{-2}$ 5 to 95% uncertainty range (see fur-

ther description in Section 7.5.2.3). This RF has a two to four times larger global mean surface temperature change per unit forcing than a change in CO_2 .

In Figure 8.8, the time evolution of global mean RF due to BC on snow and ice is shown based on multi-model simulations in ACCMIP (Lee et al., 2013) for 1850, 1930, 1980 and 2000. The results show a maximum in the RF in 1980 with a small increase since 1850 and a 20% lower RF in 2000 compared to 1980. Those results are supported by observations. The BC concentration in the Arctic atmosphere is observed to be declining since 1990, at least in the Western Hemisphere portion (Sharma et al., 2004), which should lead to less deposition of BC on the snow surface. Surveys across Arctic during 1998 and 2005 to 2009 showed that the BC content of Arctic snow appears to be lower than in 1984 (Doherty et al., 2010) and found BC concentrations in Canada, Alaska and the Arctic Ocean (e.g., Hegg et al., 2009), about a factor of 2 lower than measured in the 1980s (e.g., Clarke and Noone, 1985). Large-area field campaigns (Huang et al., 2011; Ye et al., 2012) found that the BC content of snow in northeast China is comparable to values found in Europe. The steep drop off in BC content of snow with latitude in northeast China may indicate that there is not much BC in the Arctic coming from China (Huang et al., 2011; Ye et al., 2012; Wang et al., 2013). The change in the spatial pattern of emission of BC is a main cause for the difference in the temporal development of RF due to BC on snow and ice compared to the BC from RF due to aerosol–radiation interaction over the last decades.

8.3.4.5 Contrails and Contrail-Induced Cirrus

AR4 assessed the RF of contrails (persistent linear contrails) as $+0.01$ (-0.007 to $+0.02$) W m^{-2} and provided no estimate for contrail induced cirrus. In AR5, Chapter 7 gives a best estimate of RF due to contrails of $+0.01$ ($+0.005$ to $+0.03$) W m^{-2} and an ERF estimate of the combined contrails and contrail-induced cirrus of $+0.05$ ($+0.02$ to $+0.15$) W m^{-2} . Since AR4, the evidence for contrail-induced cirrus has increased because of observational studies (for further details see Section 7.2.7).

8.3.5 Land Surface Changes

8.3.5.1 Introduction

Anthropogenic land cover change has a direct impact on the Earth radiation budget through a change in the surface albedo. It also impacts the climate through modifications in the surface roughness, latent heat flux and river runoff. In addition, human activity may change the water cycle through irrigation and power plant cooling, and also generate direct input of heat to the atmosphere by consuming energy. Land use change, and in particular deforestation, also has significant impacts on WMGHG concentration, which are discussed in Section 6.3.2.2. Potential geo-engineering techniques that aim at increasing the surface albedo are discussed in Section 7.7.2.3.

AR4 referenced a large number of RF estimates resulting from a change in land cover albedo. It discussed the uncertainties due to the reconstruction of historical vegetation, the characterization of present-day vegetation and the surface radiation processes. On this basis, AR4 gave a best estimate of RF relative to 1750 due to land use related surface albedo at $-0.2 \pm 0.2 \text{ W m}^{-2}$ with a level of scientific understanding at medium-low.

8.3.5.2 Land Cover Changes

Hurt et al. (2006) estimates that 42 to 68% of the global land surface was impacted by land use activities (crop, pasture, wood harvest) during the 1700–2000 period. Until the mid-20th century most land use change took place over the temperate regions of the NH. Since then, reforestation is observed in Western Europe, North America and China as a result of land abandonment and afforestation efforts, while deforestation is concentrated in the tropics. After a rapid increase of the rate of deforestation during the 1980s and 1990s, satellite data indicate a slowdown in the past decade (FAO, 2012).

Since AR4, Pongratz et al. (2008) and Kaplan et al. (2011) extended existing reconstructions on land use back in time to the past millennium, accounting for the progress of agriculture technique and historical events such as the black death or war invasions. As agriculture was already widespread over Europe and South Asia by 1750, the RF, which is defined with respect to this date, is weaker than the radiative flux change from the state of natural vegetation cover (see Figure 8.9). Deforestation in Europe and Asia during the last millennium led to a significant regional negative forcing. Betts et al. (2007) and Goosse et al. (2006) argue that it probably contributed to the 'Little Ice Age', together with natural solar and volcanic activity components, before the increase in GHG concentration led to temperatures similar to those

experienced in the early part of the second millennium. There is still significant uncertainty in the anthropogenic land cover change, and in particular its time evolution (Gaillard et al., 2010).

8.3.5.3 Surface Albedo and Radiative Forcing

Surface albedo is the ratio between reflected and incident solar flux at the surface. It varies with the surface cover. Most forests are darker (i.e., lower albedo) than grasses and croplands, which are darker than barren land and desert. As a consequence, deforestation tends to increase the Earth albedo (negative RF) while cultivation of some bright surfaces may have the opposite effect. Deforestation also leads to a large increase in surface albedo in case of snow cover as low vegetation accumulates continuous snow cover more readily in early winter allowing it to persist longer in spring. This causes average winter albedo in deforested areas to be generally much higher than that of a tree-covered landscape (Bernier et al., 2011).

The pre-industrial impact of the Earth albedo increase due to land use change, including the reduced snow masking by tall vegetation, is estimated to be on the order of -0.05 W m^{-2} (Pongratz et al., 2009). Since then, the increase in world population and agriculture development led to additional forcing. Based on reconstruction of land use since the beginning of the Industrial Era, Betts et al. (2007) and Pongratz et al. (2009) computed spatially and temporally distributed estimates of the land use RF. They estimate that the shortwave flux change induced by the albedo variation, from fully natural vegetation state to 1992, is on the order of -0.2 W m^{-2} (range -0.24 to -0.21 W m^{-2}). The RF, defined with respect to 1750, is in the range -0.17 to -0.18 W m^{-2} . A slightly stronger value (-0.22 W m^{-2}) was found by Davin et al. (2007) for the period 1860–1992.

In recent years, the availability of global scale MODIS data (Schaaf et al., 2002) has improved surface albedo estimates (Rechid et al., 2009). These data have been used by Myhre et al. (2005a) and Kvilevåg et al. (2010). They argue that the observed albedo difference between natural vegetation and croplands is less than usually assumed in climate simulations, so that the RF due to land use change is weaker than in estimates that do not use the satellite data. On the other hand, Nair et al. (2007) show observational evidence of an underestimate of the surface albedo change in land use analysis in southwest Australia. Overall, there is still a significant range of RF estimates for the albedo component of land use forcing. This is mostly due to the range of albedo change as a result of land use change, as shown in an inter-comparison of seven atmosphere–land models (de Noblet-Ducoudre et al., 2012).

Deforestation has a direct impact on the atmospheric CO_2 concentration and therefore contributes to the WMGHG RF as quantified in Section 8.3.2. Conversely, afforestation is a climate mitigation strategy to limit the CO_2 concentration increase. Several authors have compared the radiative impact of deforestation/afforestation that results from the albedo change with the greenhouse effect of CO_2 released/sequestered. Pongratz et al. (2010) shows that the historic land use change has had a warming impact (i.e., greenhouse effect dominates) at the global scale and over most regions with the exception of Europe and India. Bala et al. (2007) results show latitudinal contrast where the greenhouse effect dominates for low-latitude deforestation while

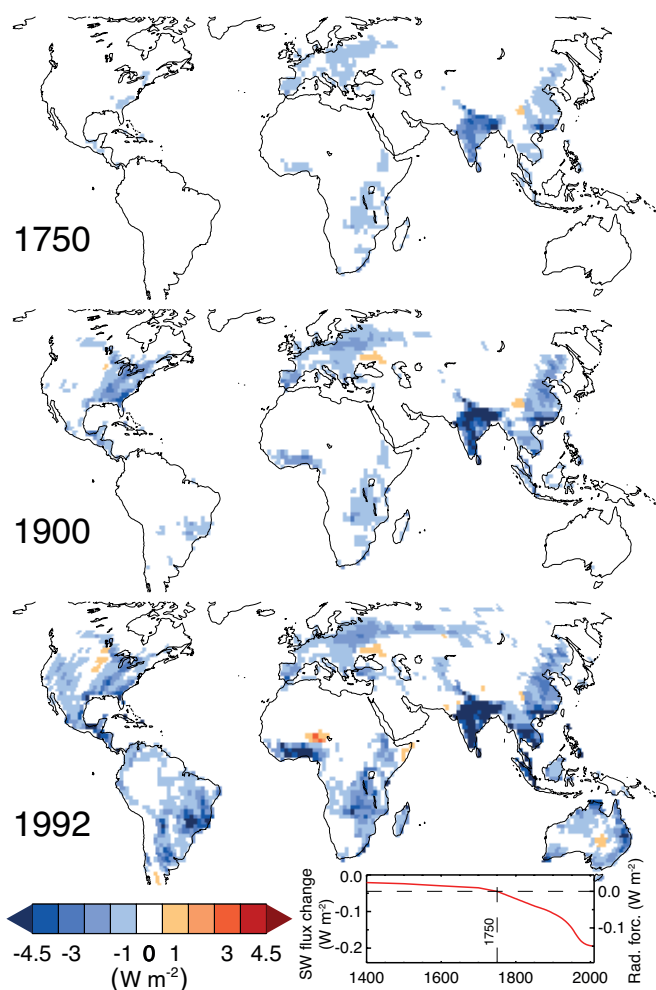


Figure 8.9 | Change in top of the atmosphere (TOA) shortwave (SW) flux (W m^{-2}) following the change in albedo as a result of anthropogenic Land Use Change for three periods (1750, 1900 and 1992 from top to bottom). By definition, the RF is with respect to 1750, but some anthropogenic changes had already occurred in 1750. The lower right inset shows the globally averaged impact of the surface albedo change to the TOA SW flux (left scale) as well as the corresponding RF (right scale) after normalization to the 1750 value. Based on simulations by Pongratz et al. (2009).

the combined effect of albedo and evapotranspiration impact does at high latitude. These results are also supported by Bathiany et al. (2010). Similarly, Lohila et al. (2010) shows that the afforestation of boreal peatlands results in a balanced RF between the albedo and greenhouse effect. Overall, because of the opposite impacts, the potential of afforestation to mitigate climate change is limited (Arora and Montenegro, 2011) while it may have undesired impacts on the atmospheric circulation, shifting precipitation patterns (Swann et al., 2012).

8.3.5.4 Other Impacts of Land Cover Change on the Earth's Albedo

Burn scars resulting from agriculture practices, uncontrolled fires or deforestation (Bowman et al., 2009) have a lower albedo than unperturbed vegetation (Jin and Roy, 2005). On the other hand, at high latitude, burnt areas are more easily covered by snow, which may result in an overall increase of the surface albedo. Surface blackening of natural vegetation due to fire is relatively short lived and typically disap-

pears within one to a few years (Jin et al., 2012). Myhre et al. (2005b) estimates a global albedo-related radiative effect due to African fires of 0.015 W m^{-2} .

Over semi-arid areas, the development of agriculture favours the generation of dust. Mulitza et al. (2010) demonstrates a very large increase of dust emission and deposition in the Sahel concomitant with the development of agriculture in this area. This, together with the analysis of dust sources (Ginoux et al., 2010), suggests that a significant fraction of the dust that is transported over the Atlantic has an anthropogenic origin and impacts the Earth albedo. There is no full estimate of the resulting RF, however. The dust RF estimate in Section 8.3.4.2 includes both land use contributions and change in wind-driven emissions. Both dust and biomass burning aerosol may impact the Earth surface albedo as these particles can be deposited on snow, which has a large impact on its absorption, in particular for soot. This is discussed in Section 8.3.4.4.

Urban areas have an albedo that is 0.01 to 0.02 smaller than adjacent croplands (Jin et al., 2005). There is the potential for a strong increase through white roof coating with the objective of mitigating the heat island effect (Oleson et al., 2010). Although the global scale impact is small, local effects can be very large, as shown by Campa et al. (2008) that reports a regional (260 km^2) 0.09 increase in albedo and -20 W m^{-2} RF as a consequence of greenhouse horticulture development.

8.3.5.5 Impacts of Surface Change on Climate

Davin et al. (2007) argues that the climate sensitivity to land use forcing is lower than that for other forcings, due to its spatial distribution but also the role of non-radiative processes. Indeed, in addition to the impact on the surface albedo, land use change also modifies the evaporation and surface roughness, with counterbalancing consequences on the lower atmosphere temperature. There is increasing evidence that the impact of land use on evapotranspiration—a non-RF on climate—is comparable to, but of opposite sign than, the albedo effect, so that RF is not as useful a metric as it is for gases and aerosols. For instance, Findell et al. (2007) climate simulations show a negligible impact of land use change on the global mean temperature, although there are some significant regional changes.

Numerical climate experiments demonstrate that the impact of land use on climate is much more complex than just the RF. This is due in part to the very heterogeneous nature of land use change (Barnes and Roy, 2008), but mostly due to the impact on the hydrological cycle through evapotranspiration, root depth and cloudiness (van der Molen et al., 2011). As a consequence, the forcing on climate is not purely radiative and the net impact on the surface temperature may be either positive or negative depending on the latitude (Bala et al., 2007). Davin and de Noblet-Ducoudre (2010) analyses the impact on climate of large-scale deforestation; the albedo cooling effect dominates for high latitude whereas reduced evapotranspiration dominates in the tropics. This latitudinal trend is confirmed by observations of the temperature difference between open land and nearby forested land (Lee et al., 2011).

Irrigated areas have continuously increased during the 20th century although a slowdown has been observed in recent decades (Bonfils

and Lobell, 2007). There is clear evidence that irrigation leads to local cooling of several degrees (Kueppers et al., 2007). Irrigation also affects cloudiness and precipitation (Puma and Cook, 2010). In the United States, DeAngelis et al. (2010) found that irrigation in the Great Plains in the summer produced enhanced precipitation in the Midwest 1000 km to the northeast.

8.3.5.6 Conclusions

There is still a rather wide range of estimates of the albedo change due to anthropogenic land use change, and its RF. Although most published studies provide an estimate close to -0.2 W m^{-2} , there is convincing evidence that it may be somewhat weaker as the albedo difference between natural and anthropogenic land cover may have been overestimated. In addition, non-radiative impact of land use have a similar magnitude, and may be of opposite sign, as the albedo effect (though these are not part of RF). A comparison of the impact of land use change according to seven climate models showed a wide range of results (Pitman et al., 2009), partly due to difference in the implementation of land cover change, but mostly due to different assumptions on ecosystem albedo, plant phenology and evapotranspiration. There is no agreement on the sign of the temperature change induced by anthropogenic land use change. It is *very likely* that land use change led to an increase of the Earth albedo with a RF of $-0.15 \pm 0.10 \text{ W m}^{-2}$, but a net cooling of the surface—accounting for processes that are not limited to the albedo—is *about as likely as not*.

8.4 Natural Radiative Forcing Changes: Solar and Volcanic

Several natural drivers of climate change operate on multiple time scales. Solar variability takes place at many time scales that include centennial and millennial scales (Helama et al., 2010), as the radiant energy output of the Sun changes. Also, variations in the astronomical alignment of the Sun and the Earth (Milankovitch cycles) induce cyclical changes in RF, but this is substantial only at millennial and longer time scales (see Section 5.2.1.1). Volcanic forcing is highly episodic, but can have dramatic, rapid impacts on climate. No major asteroid impacts occurred during the reference period (1750–2012) and thus this effect is not considered here. This section discusses solar and volcanic forcings, the two dominant natural contributors of climate change since the pre-industrial time.

8.4.1 Solar Irradiance

In earlier IPCC reports the forcing was estimated as the instantaneous RF at TOA. However, due to wavelength-albedo dependence, solar radiation-wavelength dependence and absorption within the stratosphere and the resulting stratospheric adjustment, the RF is reduced to about 78% of the TOA instantaneous RF (Gray et al., 2009). There is *low confidence* in the exact value of this number, which can be model and time scale dependent (Gregory et al., 2004; Hansen et al., 2005). AR4 gives an 11-year running mean instantaneous TOA RF between 1750 and the present of 0.12 W m^{-2} with a range of estimates of 0.06 to 0.30 W m^{-2} , equivalent to a RF of 0.09 W m^{-2} with a range of 0.05 to 0.23 W m^{-2} . For a consistent treatment of all forcing agents, hereafter we use

RF while numbers quoted from AR4 will be provided both as RF and instantaneous RF at TOA.

8.4.1.1 Satellite Measurements of Total Solar Irradiance

Total solar irradiance (TSI) measured by the Total Irradiance Monitor (TIM) on the spaceborne Solar Radiation and Climate Experiment (SORCE) is $1360.8 \pm 0.5 \text{ W m}^{-2}$ during 2008 (Kopp and Lean, 2011) which is $\sim 4.5 \text{ W m}^{-2}$ lower than the Physikalisch-Meteorologisches Observatorium Davos (PMOD) TSI composite during 2008 (Frohlich, 2009). The difference is probably due to instrumental biases in measurements prior to TIM. Measurements with the PREcision MONitor Sensor (PREMOS) instrument support the TIM absolute values (Kopp and Lean, 2011). The TIM calibration is also better linked to national standards which provides further support that it is the most accurate (see Supplementary Material Section 8.SM.6). Given the lower TIM TSI values relative to currently used standards, most general circulation models are calibrated to incorrectly high values. However, the few tenths of a percent bias in the absolute TSI value has minimal consequences for climate simulations because the larger uncertainties in cloud properties have a greater effect on the radiative balance. As the maximum-to-minimum TSI relative change is well-constrained from observations, and historical variations are calculated as changes relative to modern values, a revision of the absolute value of TSI affects RF by the same fraction as it affects TSI. The downward revision of TIM TSI with respect to PMOD, being 0.3%, thus has a negligible impact on RF, which is given with a relative uncertainty of several tenths of a percent.

Since 1978, several independent space-based instruments have directly measured the TSI. Three main composite series were constructed, referred to as the Active Cavity Radiometer Irradiance Monitor (ACRIM) (Willson and Mordvinov, 2003), the Royal Meteorological Institute of Belgium (RMIB) (Dewitte et al., 2004) and the PMOD (Frohlich, 2006) series. There are two major differences between ACRIM and PMOD. The first is the rapid drift in calibration between PMOD and ACRIM before 1981. This arises because both composites employ the Hickey–Frieden (HF) radiometer data for this interval, while a re-evaluation of the early HF degradation has been implemented by PMOD but not by ACRIM. The second one, involving also RMIB, is the bridging of the gap between the end of ACRIM I (mid-1989) and the beginning of ACRIM II (late 1991) observations, as it is possible that a change in HF data occurred during this gap. This possibility is neglected in ACRIM and thus its TSI increases by more than 0.5 W m^{-2} during solar cycle (SC) 22. These differences lead to different long-term TSI trends in the three composites (see Figure 8.10): ACRIM rises until 1996 and subsequently declines, RMIB has an upward trend through 2008 and PMOD shows a decline since 1986 which unlike the other two composites, follows the solar-cycle-averaged sunspot number (Lockwood, 2010). Moreover, the ACRIM trend implies that the TSI on time scales longer than the SC is positively correlated with the cosmic ray variation indicating a decline in TSI throughout most of the 20th century (the opposite to most TSI reconstructions produced to date; see Section 8.4.1.2). Furthermore, extrapolating the ACRIM TSI long-term drift would imply a brighter Sun in the Maunder minimum (MM) than now, again opposite to most TSI reconstructions (Lockwood and Frohlich, 2008). Finally, analysis of instrument degradation and pointing issues (Lee et al., 1995) and independent modeling based on solar magnetograms (Wenzler et al.,

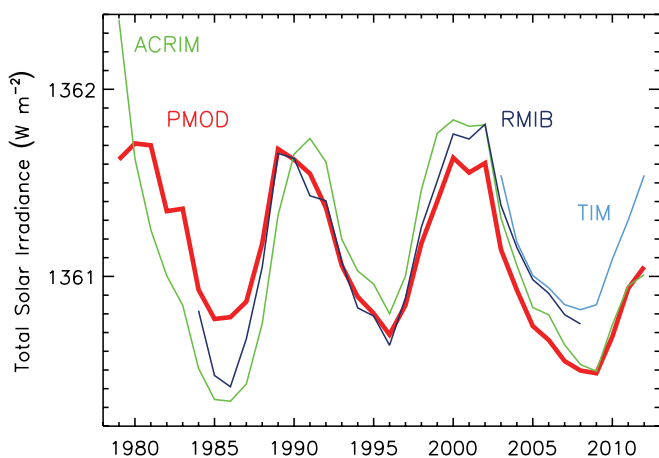


Figure 8.10 | Annual average composites of measured total solar irradiance: The Active Cavity Radiometer Irradiance Monitor (ACRIM) (Willson and Mordvinov, 2003), the Physikalisch-Meteorologisches Observatorium Davos (PMOD) (Frohlich, 2006) and the Royal Meteorological Institute of Belgium (RMIB) (Dewitte et al., 2004). These composites are standardized to the annual average (2003–2012) Total Irradiance Monitor (TIM) (Kopp and Lean, 2011) measurements that are also shown.

2009; Ball et al., 2012), confirm the need for correction of HF data, and we conclude that PMOD is more accurate than the other composites.

TSI variations of approximately 0.1% were observed between the maximum and minimum of the 11-year SC in the three composites mentioned above (Kopp and Lean, 2011). This variation is mainly due to an interplay between relatively dark sunspots, bright faculae and bright network elements (Foukal and Lean, 1988; see Section 5.2.1.2). A declining trend since 1986 in PMOD solar minima is evidenced in Figure 8.10. Considering the PMOD solar minima values of 1986 and 2008, the RF is -0.04 W m^{-2} . Our assessment of the uncertainty range of changes in TSI between 1986 and 2008 is -0.08 to 0.0 W m^{-2} and thus *very likely* negative, and includes the uncertainty in the PMOD data (Frohlich, 2009; see Supplementary Material Section 8.SM.6) but is extended to also take into account the uncertainty of combining the satellite data.

For incorporation of TIM data with the previous and overlapping data, in Figure 8.10 we have standardized the composite time series to the TIM series (over 2003–2012, the procedure is explained in Supplementary Material Section 8.SM.6. Moreover as we consider annual averages, ACRIM and PMOD start at 1979 because for 1978 both composites have only two months of data.

8.4.1.2 Total Solar Irradiance Variations Since Preindustrial Time

The year 1750, which is used as the preindustrial reference for estimating RF, corresponds to a maximum of the 11-year SC. Trend analysis are usually performed over the minima of the solar cycles that are more stable. For such trend estimates, it is then better to use the closest SC minimum, which is in 1745. To avoid trends caused by comparing different portions of the solar cycle, we analyze TSI changes using multi-year running means. For the best estimate we use a recent TSI reconstruction by Krivova et al. (2010) between 1745 and 1973 and from 1974 to 2012 by Ball et al. (2012). The reconstruction is based

on physical modeling of the evolution of solar surface magnetic flux, and its relationship with sunspot group number (before 1974) and sunspot umbra and penumbra and faculae afterwards. This provides a more detailed reconstruction than other models (see the time series in Supplementary Material Table 8.SM.3). The best estimate from our assessment of the most reliable TSI reconstruction gives a 7-year running mean RF between the minima of 1745 and 2008 of 0.05 W m^{-2} . Our assessment of the range of RF from TSI changes is 0.0 to 0.10 W m^{-2} which covers several updated reconstructions using the same 7-year running mean past-to-present minima years (Wang et al., 2005; Steinhilber et al., 2009; Delaygue and Bard, 2011), see Supplementary Material Table 8.SM.4. All reconstructions rely on indirect proxies that inherently do not give consistent results. There are relatively large discrepancies among the models (see Figure 8.11). With these considerations, we adopt this value and range for AR5. This RF is almost half of that in AR4, in part because the AR4 estimate was based on the previous solar cycle minimum while the AR5 estimate includes the drop of TSI in 2008 compared to the previous two SC minima (see 8.4.1). Concerning the uncertainty range, in AR4 the upper limit corresponded to the reconstruction of Lean (2000), based on the reduced brightness of non-cycling Sun-like stars assumed typical of a Maunder minimum (MM) state. The use of such stellar analogues was based on the work of Baliunas and Jastrow (1990), but more recent surveys have not reproduced their results and suggest that the selection of the original set was flawed (Hall and Lockwood, 2004; Wright, 2004); the lower limit from 1750 to present in AR4 was due to the assumed increase in the amplitude of the 11-year cycle only. Thus the RF and uncertainty range have been obtained in a different way in AR5 compared to AR4. Maxima to maxima RF give a higher estimate than minima to minima RF, but the latter is more relevant for changes in solar activity. Given the *medium agreement* and *medium evidence*, this RF value has a *medium confidence level* (although confidence is higher for the last three decades). Figure 8.11 shows several TSI reconstructions modelled using sunspot group numbers (Wang et al., 2005; Krivova et al., 2010;

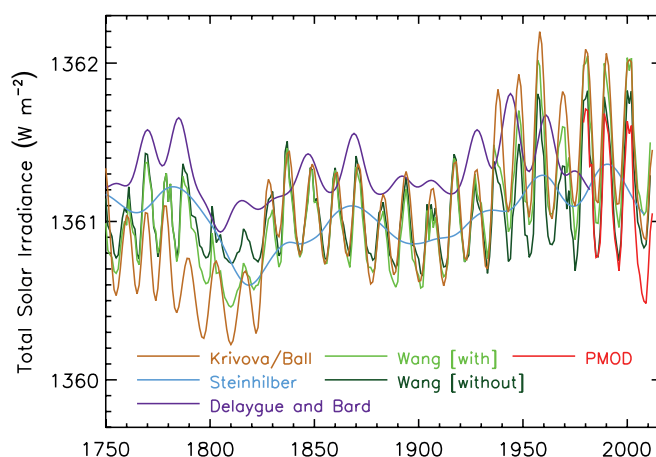


Figure 8.11 | Reconstructions of total solar irradiance since 1745; annual resolution series from Wang et al. (2005) with and without an independent change in the background level of irradiance, Krivova et al. (2010) combined with Ball et al. (2012) and 5-year time resolution series from Steinhilber et al. (2009) and Delaygue and Bard (2011). The series are standardized to the Physikalisch-Meteorologisches Observatorium Davos (PMOD) measurements of solar cycle 23 (1996–2008) (PMOD is already standardized to Total Irradiance Monitor).

Ball et al., 2012) and sunspot umbra and penumbra and faculae (Ball et al., 2012), or cosmogenic isotopes (Steinhilber et al., 2009; Delaygue and Bard, 2011). These reconstructions are standardized to PMOD SC 23 (1996–2008) (see also Supplementary Material Section 8.SM.6).

For the MM-to-present AR4 gives a TOA instantaneous RF range of 0.1 to 0.28 W m⁻², equivalent to 0.08 to 0.22 W m⁻² with the RF definition used here. The reconstructions in Schmidt et al. (2011) indicate a MM-to-present RF range of 0.08 to 0.18 W m⁻², which is within the AR4 range although narrower. As discussed above, the estimates based on irradiance changes in Sun-like stars are not included in this range because the methodology has been shown to be flawed. A more detailed explanation of this is found in Supplementary Material Section 8.SM.6. For details about TSI reconstructions on millennia time scales see Section 5.2.1.2.

8.4.1.3 Attempts to Estimate Future Centennial Trends of Total Solar Irradiance

Cosmogenic isotope and sunspot data (Rigozo et al., 2001; Solanki and Krivova, 2004; Abreu et al., 2008) reveal that currently the Sun is in a grand activity maximum that began about 1920 (20th century grand maximum). However, SC 23 showed an activity decline not previously seen in the satellite era (McComas et al., 2008; Smith and Balogh, 2008; Russell et al., 2010). Most current estimations suggest that the forthcoming solar cycles will have lower TSI than those for the past 30 years (Abreu et al., 2008; Lockwood et al., 2009; Rigozo et al., 2010; Russell et al., 2010). Also there are indications that the mean magnetic field in sunspots may be diminishing on decadal level. A linear expansion of the current trend may indicate that of the order of half the sunspot activity may disappear by about 2015 (Penn and Livingston, 2006). These studies only suggest that the Sun may have left the 20th century grand maximum and not that it is entering another grand minimum. But other works propose a grand minimum during the 21st century, estimating an RF within a range of -0.16 to 0.12 W m⁻² between this future minimum and the present-day TSI (Jones et al., 2012). However, much more evidence is needed and at present there is *very low confidence* concerning future solar forcing estimates.

Nevertheless, even if there is such decrease in the solar activity, there is a *high confidence* that the TSI RF variations will be much smaller in magnitude than the projected increased forcing due to GHG (see Section 12.3.1).

8.4.1.4 Variations in Spectral Irradiance

8.4.1.4.1 Impacts of ultraviolet variations on the stratosphere

Ozone is the main gas involved in stratospheric radiative heating. Ozone production rate variations are largely due to solar UV irradiance changes (HAIGH, 1994), with observations showing statistically significant variations in the upper stratosphere of 2 to 4% along the SC (Soukharev and Hood, 2006). UV variations may also produce transport-induced ozone changes due to indirect effects on circulation (Shindell et al., 2006b). In addition, statistically significant evidence for an 11-year variation in stratospheric temperature and zonal winds is attributed to UV radiation (Frame and Gray, 2010). The direct UV heat-

ing of the background ozone is dominant and over twice as large as the ozone heating in the upper stratosphere and above, while indirect solar and terrestrial radiation through the SC-induced ozone change is dominant below about 5 hPa (Shibata and Kodera, 2005). The RF due to solar-induced ozone changes is a small fraction of the solar RF discussed in Section 8.4.1.1 (Gray et al., 2009).

8.4.1.4.2 Measurements of spectral irradiance

Solar spectral irradiance (SSI) variations in the far (120 to 200 nm) and middle (200 to 300 nm) ultraviolet (UV) are the primary driver for heating, composition, and dynamic changes of the stratosphere, and although these wavelengths compose a small portion of the incoming radiation they show large relative variations between the maximum and minimum of the SC compared to the corresponding TSI changes. As UV heating of the stratosphere over a SC has the potential to influence the troposphere indirectly, through dynamic coupling, and therefore climate (Haigh, 1996; Gray et al., 2010), the UV may have a more significant impact on climate than changes in TSI alone would suggest. Although this indicates that metrics based only on TSI are not appropriate, UV measurements present several controversial issues and modelling is not yet robust.

Multiple space-based measurements made in the past 30 years indicated that UV variations account for about 30% of the SC TSI variations, while about 70% were produced within the visible and infrared (Rottman, 2006). However, current models and data provide the range of 30 to 90% for the contribution of the UV variability below 400 nm to TSI changes (Ermolli et al., 2013), with a more probable value of ~60% (Morrill et al., 2011; Ermolli et al., 2013). The Spectral Irradiance Monitor (SIM) on board SORCE (Harder et al., 2009) shows, over the SC 23 declining phase, measurements that are rather inconsistent with prior understanding, indicating that additional validation and uncertainty estimates are needed (DeLand and Cebula, 2012; Lean and Deland, 2012). A wider exposition can be found in Supplementary Material Section 8.SM.6.

8.4.1.4.3 Reconstructions of preindustrial ultraviolet variations

The Krivova et al. (2010) reconstruction is based on what is known about spectral contrasts of different surface magnetic features and the relationship between TSI and magnetic fields. The authors interpolated backwards to the year 1610 based on sunspot group numbers and magnetic information. The Lean (2000) model is based on historical sunspot number and area and is scaled in the UV using measurements from the Solar Stellar Irradiance Comparison Experiment (SOLSTICE) on board the Upper Atmosphere Research Satellite (UARS). The results show smoothed 11-year UV SSI changes between 1750 and the present of about 25% at about 120 nm, about 8% at 130 to 175 nm, ~4% at 175 to 200 nm, and about 0.5% at 200 to 350 nm. Thus, the UV SSI appears to have generally increased over the past four centuries, with larger trends at shorter wavelengths. As few reconstructions are available, and recent measurements suggest a poor understanding of UV variations and their relationship with solar activity, there is *very low confidence* in these values.

8.4.1.5 The Effects of Cosmic Rays on Clouds

Changing cloud amount or properties modify the Earth's albedo and therefore affect climate. It has been hypothesized that cosmic ray flux create atmospheric ions which facilitates aerosol nucleation and new particle formation with a further impact on cloud formation (Dickinson, 1975; Kirkby, 2007). High solar activity means a stronger heliospheric magnetic field and thus a more efficient screen against cosmic rays. Under the hypothesis underlined above, the reduced cosmic ray flux would promote fewer clouds amplifying the warming effect expected from high solar activity. There is evidence from laboratory, field and modelling studies that ionization from cosmic ray flux may enhance aerosol nucleation in the free troposphere (Merikanto et al., 2009; Mirme et al., 2010; Kirkby et al., 2011). However, there is *high confidence (medium evidence and high agreement)* that the cosmic ray-ionization mechanism is too weak to influence global concentrations of cloud condensation nuclei or their change over the last century or during a SC in a climatically significant way (Harrison and Ambaum, 2010; Erlykin and Wolfendale, 2011; Snow-Kropla et al., 2011). A detailed exposition is found in Section 7.4.6.

8.4.2 Volcanic Radiative Forcing

8.4.2.1 Introduction

Volcanic eruptions that inject substantial amounts of SO₂ gas into the stratosphere are the dominant natural cause of externally forced climate change on the annual and multi-decadal time scales, both because of the multi-decadal variability of eruptions and the time scale of the climate system response, and can explain much of the pre-industrial climate change of the last millennium (Schneider et al., 2009; Brovkin et al., 2010; Legras et al., 2010; Miller et al., 2012). Although volcanic eruptions inject both mineral particles (called ash or tephra) and sulphate aerosol precursor gases (predominantly SO₂) into the atmosphere, it is the sulphate aerosols, which because of their small size are effective scatterers of sunlight and have long lifetimes, that are responsible for RF important for climate. Global annually averaged emissions of CO₂ from volcanic eruptions since 1750 have been at least 100 times smaller than anthropogenic emissions and inconsequential for climate on millennial and shorter time scales (Gerlach, 2011). To be important for climate change, sulphur must be injected into the stratosphere, as the lifetime of aerosols in the troposphere is only about one week, whereas sulphate aerosols in the stratosphere from tropical eruptions have a lifetime of about one year, and those from high-latitude eruptions last several months. Most stratospheric aerosols are from explosive eruptions that directly put sulphur into the stratosphere, but Bourassa et al. (2012, 2013) showed that sulphur injected into the upper troposphere can then be lifted into the stratosphere over the next month or two by deep convection and large scale Asian summer monsoon circulation, although Vernier et al. (2013) and Fromm et al. (2013) suggested that direct injection was also important. Robock (2000), AR4 (Forster et al., 2007) and Timmreck (2012) provide summaries of this relatively well understood forcing agent.

There have been no major volcanic eruptions since Mt Pinatubo in 1991 (Figure 8.12), but several smaller eruptions have caused a RF for the years 2008–2011 of -0.11 (-0.15 to -0.08) W m⁻², approximately

twice the magnitude of the 1999–2002 RF of -0.06 (-0.08 to -0.04) W m⁻², consistent with the trends noted in Solomon et al. (2011). However, the CMIP5 simulations discussed elsewhere in this report did not include the recent small volcanic forcing in their calculations. New work has also produced a better understanding of high latitude eruptions, the hydrological response to volcanic eruptions (Trenberth and Dai, 2007; Anchukaitis et al., 2010), better long-term records of past volcanism and better understanding of the effects of very large eruptions.

There are several ways to measure both the SO₂ precursor and sulphate aerosols in the stratosphere, using balloons, airplanes, and both ground- and satellite-based remote sensing. Both the infrared and ultraviolet signals sensed by satellite instruments can measure SO₂, and stratospheric aerosol measurements by space-based sensors have been made on a continuous basis since 1978 by a number of instruments employing solar and stellar occultation, limb scattering, limb emission, and lidar strategies (Thomason and Peter, 2006; Kravitz et al., 2011; Solomon et al., 2011).

Forster et al. (2007) described four mechanisms by which volcanic forcing influences climate: RF due to aerosol–radiation interaction; differential (vertical or horizontal) heating, producing gradients and changes in circulation; interactions with other modes of circulation, such as El Niño–Southern Oscillation (ENSO); and ozone depletion with its effects on stratospheric heating, which depends on anthropogenic chlorine (stratospheric ozone would increase with a volcanic eruption under low-chlorine conditions). In addition, the enhanced diffuse light from volcanic aerosol clouds impacts vegetation and hence the carbon cycle (Mercado et al., 2009) and aerosol–cloud interaction of sulphate aerosols on clouds in the troposphere can also be important (Schmidt et al., 2010), though Frolicher et al. (2011) showed that the impacts of the 1991 Mt Pinatubo eruption on the carbon cycle were small.

8.4.2.2 Recent Eruptions

The background stratospheric aerosol concentration was affected by several small eruptions in the first decade of the 21st century (Nagai et al., 2010; Vernier et al., 2011; Neely et al., 2013; see also Figure 8.13), with a very small contribution from tropospheric pollution (Siddaway and Petelina, 2011; Vernier et al., 2011), and had a small impact on RF (Solomon et al., 2011). Two recent high-latitude eruptions, of Kasatochi Volcano (52.1°N, 175.3°W) on August 8, 2008 and of Sarychev Volcano (48.1°N, 153.2°E) on June 12–16, 2009, each injected ~ 1.5 Tg(SO₂) into the stratosphere, but did not produce detectable climate response. Their eruptions, however, led to better understanding of the dependence of the amount of material and time of year of high-latitude injections to produce climate impacts (Haywood et al., 2010; Kravitz et al., 2010, 2011). The RF from high-latitude eruptions is a function of seasonal distribution of insolation and the 3- to 4-month lifetime of high-latitude volcanic aerosols. Kravitz and Robock (2011) showed that high-latitude eruptions must inject at least 5 Tg(SO₂) into the lower stratosphere in the spring or summer, and much more in fall or winter, to have a detectable climatic response.

On April 14, 2010 the Eyjafjallajökull volcano in Iceland (63.6°N, 19.6°W) began an explosive eruption phase that shut down air traffic

in Europe for 6 days and continued to disrupt it for another month. The climatic impact of Eyjafjallajökull was about 10,000 times less than that of Mt Pinatubo; however, because it emitted less than 50 ktonnes SO₂ and its lifetime in the troposphere was 50 times less than if it had been injected into the stratosphere, and was therefore undetectable amidst the chaotic weather noise in the atmosphere (Robock, 2010). 2011 saw the continuation of a number of small eruptions with significant tropospheric SO₂ and ash injections, including Puyehue-Cordón Caulle in Chile, Nabro in Eritrea, and Grimsvötn in Iceland. None have been shown to have produced an important RF, but the June 13, 2011 Nabro eruption resulted in the largest stratospheric aerosol cloud since the 1991 Mt Pinatubo eruption (Bourassa et al., 2012), more than 1.5 Tg(SO₂).

Figure 8.12 shows reconstructions of volcanic aerosol optical depth since 1750. Figure 8.13 shows details of the vertical distribution of stratospheric aerosols in the tropics since 1985. The numerous small eruptions in the past decade are evident, but some of them were at higher latitudes and their full extent is not captured in this plot.

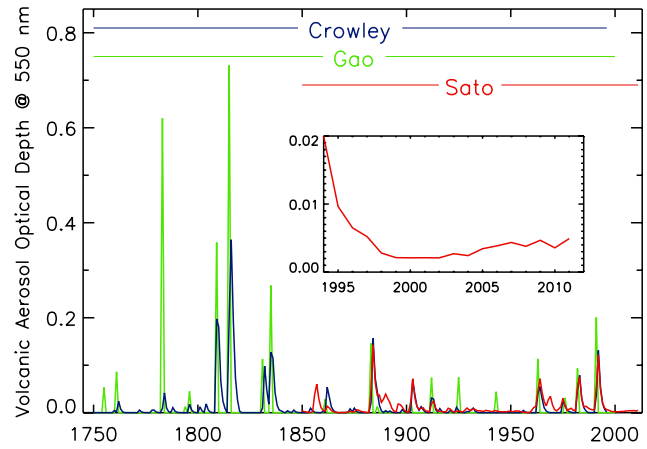


Figure 8.12 | Volcanic reconstructions of global mean aerosol optical depth (at 550 nm). Gao et al. (2008) and Crowley and Unterman (2013) are from ice core data, and end in 2000 for Gao et al. (2008) and 1996 for Crowley and Unterman (2013). Sato et al. (1993) includes data from surface and satellite observations, and has been updated through 2011. (Updated from Schmidt et al., 2011.)

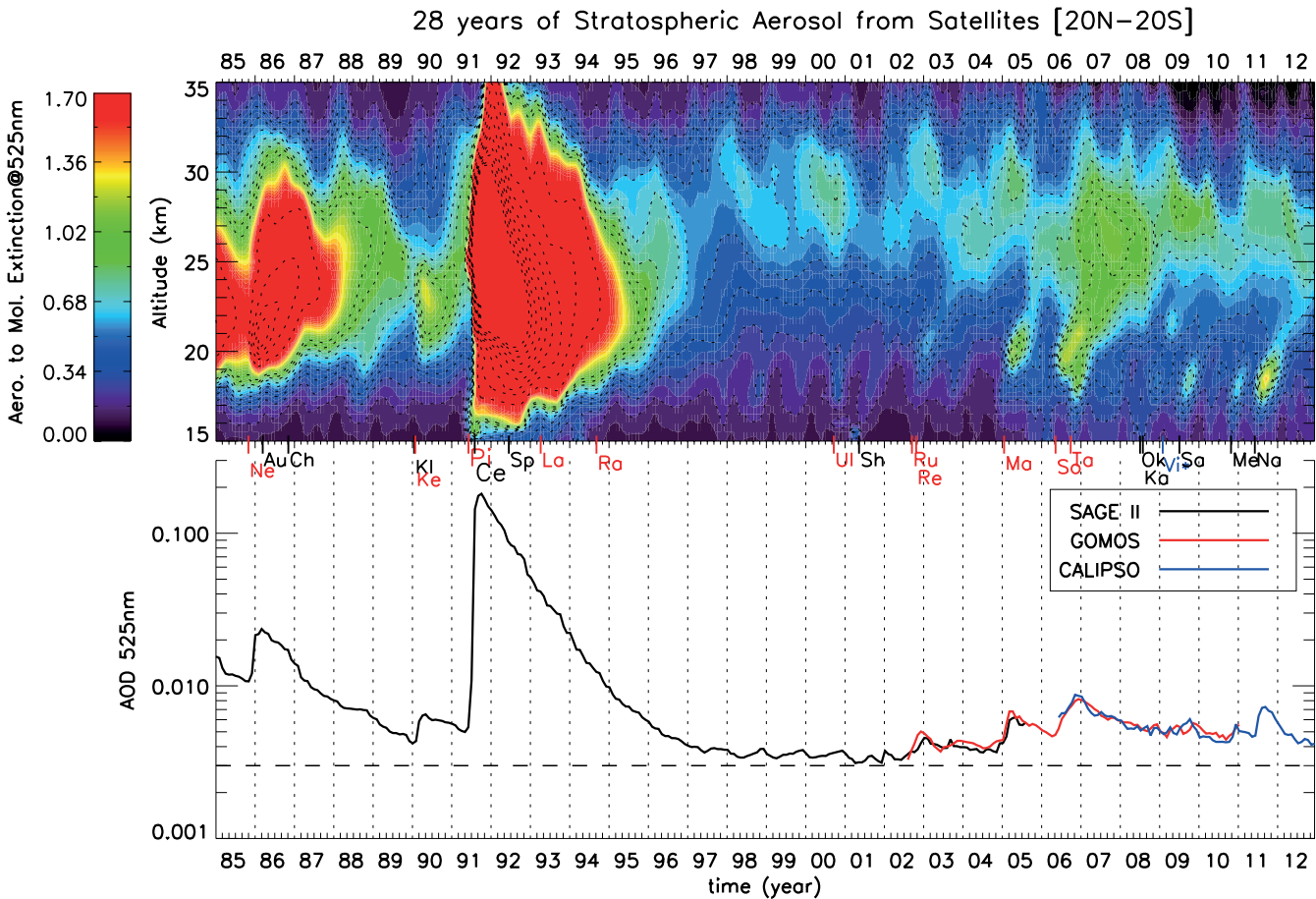


Figure 8.13 | (Top) Monthly mean extinction ratio (525 nm) profile evolution in the tropics [20°N to 20°S] from January 1985 through December 2012 derived from Stratospheric Aerosol and Gas Experiment (SAGE) II extinction in 1985–2005 and Cloud-Aerosol Lidar and Infrared Pathfinder Satellite Observation (CALIPSO) scattering ratio in 2006–2012, after removing clouds below 18 km based on their wavelength dependence (SAGE II) and depolarization properties (CALIPSO) compared to aerosols. Black contours represent the extinction ratio in log-scale from 0.1 to 100. The position of each volcanic eruption occurring during the period is displayed with its first two letters on the horizontal axis, where tropical eruptions are noted in red. The eruptions were Nevado del Ruiz (Ne), Augustine (Au), Chikurachki (Ch), Kliuchevskoi (Kl), Kelut (Ke), Pinatubo (Pi), Cerro Hudson (Ce), Spur (Sp), Lascar (La), Rabaul (Ra), Ulawun (Ul), Shiveluch (Sh), Ruang (Ru), Reventador (Re), Manam (Ma), Soufrière Hills (So), Tavorvur (Ta), Okmok (Ok), Kasatochi (Ka), Victoria (Vi)*—forest fires with stratospheric aerosol injection), Sarychev (Sa), Merapi (Me), Nabro (Na). (Updated from Figure 1 from Vernier et al., 2011.) (Bottom) Mean stratospheric aerosol optical depth (AOD) in the tropics [20°N to 20°S] between the tropopause and 40 km since 1985 from the SAGE II (black line), the Global Ozone Monitoring by Occultation of Stars (GOMOS) (red line), and CALIPSO (blue line). (Updated from Figure 5 from Vernier et al., 2011.)

Box 8.3 | Volcanic Eruptions as Analogues

Volcanic eruptions provide a natural experiment of a stratospheric aerosol cloud that can serve to inform us of the impacts of the proposed production of such a cloud as a means to control the climate, which is one method of geoengineering (Rasch et al., 2008); see Section 7.7. For example, Trenberth and Dai (2007) showed that the Asian and African summer monsoon, as well as the global hydrological cycle, was weaker for the year following the 1991 Mt Pinatubo eruption, which is consistent with climate model simulations (Robock et al., 2008). MacMynowski et al. (2011) showed that because the climate system response of the hydrological cycle is rapid, forcing from volcanic eruptions, which typically last about a year, can serve as good analogues for longer-lived forcing. The formation of sulphate aerosols, their transport and removal, their impacts on ozone chemistry, their RF, and the impacts on whitening skies all also serve as good analogues for geoengineering proposals. Volcanic impacts on the carbon cycle because of more diffuse radiation (Mercado et al., 2009) and on remote sensing can also be useful analogues, and the impacts of contrail-generated sub-visual cirrus (Long et al., 2009) can be used to test the long-term impacts of a permanent stratospheric cloud.

Smoke from fires generated by nuclear explosions on cities and industrial areas, which could be lofted into the stratosphere, would cause surface cooling and a reduction of stratospheric ozone (Mills et al., 2008). Volcanic eruptions that produce substantial stratospheric aerosol clouds also serve as an analogue that supports climate model simulations of the transport and removal of stratospheric aerosols, their impacts on ozone chemistry, their RF, and the climate response. The use of the current global nuclear arsenal still has the potential to produce nuclear winter, with continental temperatures below freezing in summer (Robock et al., 2007a; Toon et al., 2008), and the use of only 100 nuclear weapons could produce climate change unprecedented in recorded human history (Robock et al., 2007b), with significant impacts on global agriculture (Özdoğan et al., 2013; Xia and Robock, 2013).

8.4.2.3 Records of Past Volcanism and Effects of Very Large Eruptions

Although the effects of volcanic eruptions on climate are largest in the 2 years following a large stratospheric injection, and the winter warming effect in the NH has been supported by long-term records (Fischer et al., 2007), there is new work indicating extended volcanic impacts via long-term memory in the ocean heat content and sea level (Stenchikov et al., 2009; Gregory, 2010; Otterä et al., 2010). Zanchettin et al. (2012) found changes in the North Atlantic Ocean circulation that imply strengthened northward oceanic heat transport a decade after major eruptions, which contributes to the emergence of extensive winter warming over the continental NH along with persistent cooling over Arctic regions on decadal time scales, in agreement with Zhong et al. (2011) and Miller et al. (2012).

New work on the mechanisms by which a supereruption (Self and Blake, 2008) could force climate has focused on the 74,000 BP eruption of the Toba volcano (2.5°N, 99.0°E). Robock et al. (2009) used simulations of up to 900 times the 1991 Mt Pinatubo sulphate injection to show that the forcing is weaker than that predicted based on a linear relationship with the sulphate aerosol injection. The results agreed with a previous simulation by Jones et al. (2005). They also showed that chemical interactions with ozone had small impacts on the forcing and that the idea of Bekki et al. (1996) that water vapour would limit and prolong the growth of aerosols was not supported. Timmreck et al. (2010) however, incorporating the idea of Pinto et al. (1989) that aerosols would grow and therefore both have less RF per unit mass and fall out of the atmosphere more quickly, found much less of a radiative impact from such a large stratospheric input.

8.4.2.4 Future Effects

We expect large eruptions over the next century but cannot predict when. Ammann and Naveau (2003) and Stothers (2007) suggested an 80-year periodicity in past eruptions, but the data record is quite short and imperfect, and there is no mechanism proposed that would cause this. While the period 1912–1963 was unusual for the past 500 years in having no large volcanic eruptions, and the period 1250–1300 had the most globally climatically significant eruptions in the past 1500 years (Gao et al., 2008), current knowledge only allows us to predict such periods on a statistical basis, assuming that the recent past distributions are stationary. Ammann and Naveau (2003), Gusev (2008), and Deligne et al. (2010) studied these statistical properties and Ammann and Naveau (2010) showed how they could be used to produce a statistical distribution for future simulations. Although the future forcing from volcanic eruptions will depend only on the stratospheric aerosol loading for most forcing mechanisms, the future effects on reducing ozone will diminish as ozone depleting substances diminish in the future (Eyring et al., 2010b).

8.5 Synthesis of Global Mean Radiative Forcing, Past and Future

The RF can be used to quantify the various agents that drive climate change over the Industrial Era or the various contributions to future climate change. There are multiple ways in which RF can be attributed to underlying causes, each providing various perspectives on the importance of the different factors driving climate change. This section evaluates the RF with respect to emitted component and with respect to the ultimate atmospheric concentrations. The uncertainties in the RF

agents vary and the confidence levels for these are presented in this section. Finally, this section shows historical and scenarios of future time evolution of RF.

8.5.1 Summary of Radiative Forcing by Species and Uncertainties

Table 8.5 has an overview of the RF agents considered here and each of them is given a confidence level for the change in RF over the Industrial Era to the present day. The confidence level is based on the evidence (robust, medium, and limited) and the agreement (high, medium, and low; see further description in Chapter 1). The confidence level of the forcing agents goes beyond the numerical values available in estimates and is an assessment for a particular forcing agent to have a real

value within the estimated range. Some of the RF agents have robust evidence such as WMGHG with well documented increases based on high precision measurements as well as contrails as additional clouds which can be seen by direct observations. However, for some forcing agents the evidence is more limited regarding their existence such as aerosol influence on cloud cover. The consistency in the findings for a particular forcing agent determines the evaluation of the evidence. A combination of different methods, for example, observations and modeling, and thus the understanding of the processes causing the forcing is important for this evaluation. The agreement is a qualitative judgment of the difference between the various estimates for a particular RF agent. Figure 1.11 shows how the combined evidence and agreement results in five levels for the confidence level.

Table 8.5 | Confidence level for the forcing estimate associated with each forcing agent for the 1750–2011 period. The confidence level is based on the evidence and the agreement as given in the table. The basis for the confidence level and change since AR4 is provided. See Figure 1.11 for further description of the evidence, agreement and confidence level. The colours are adopted based on the evidence and agreement shown in Figure 1.11. Dark green is “High agreement and Robust evidence”, light green is either “High agreement and Medium evidence” or “Medium agreement and Robust evidence”, yellow is either “High agreement and limited evidence” or “Medium agreement and Medium evidence” or “Low agreement and Robust evidence”, orange is either “Medium agreement and Limited evidence” or “Low agreement and Medium evidence” and finally red is “Low agreement and Limited evidence”. Note, that the confidence levels given in Table 8.5 are for 2011 relative to 1750 and for some of the agents the confidence level may be different for certain portions of the Industrial Era.

	Evidence	Agreement	Confidence Level	Basis for Uncertainty Estimates (more certain / less certain)	Change in Understanding Since AR4
Well-mixed greenhouse gases	Robust	High	Very high	Measured trends from different observed data sets and differences between radiative transfer models	No major change
Tropospheric ozone	Robust	Medium	High	Observed trends of ozone in the troposphere and model results for the industrial era/Differences between model estimates of RF	No major change
Stratospheric ozone	Robust	Medium	High	Observed trends in stratospheric and total ozone and modelling of ozone depletion/Differences between estimates of RF	No major change
Stratospheric water vapour from CH ₄	Robust	Low	Medium	Similarities in results of independent methods to estimate the RF/Known uncertainty in RF calculations	Elevated owing to more studies
Aerosol–radiation interactions	Robust	Medium	High	A large set of observations and converging independent estimates of RF/Differences between model estimates of RF	Elevated owing to more robust estimates from independent methods
Aerosol–cloud interactions	Medium	Low	Low	Variety of different observational evidence and modelling activities/Spread in model estimates of ERF and differences between observations and model results	ERF in AR5 has a similar confidence level to RF in AR4
Rapid adjustment aerosol–radiation interactions	Medium	Low	Low	Observational evidence combined with results from different types of models/Large spread in model estimates	Elevated owing to increased evidence
Total aerosol effect	Medium	Medium	Medium	A large set of observations and model results, independent methods to derive ERF estimates/Aerosol–cloud interaction processes and anthropogenic fraction of CCN still fairly uncertain	Not provided previously
Surface albedo (land use)	Robust	Medium	High	Estimates of deforestation for agricultural purposes and well known physical processes/Spread in model estimates of RF	Elevated owing to the availability of high-quality satellite data
Surface albedo (BC aerosol on snow and ice)	Medium	Low	Low	Observations of snow samples and the link between BC content in snow and albedo/Large spread in model estimates of RF	No major change
Contrails	Robust	Low	Medium	Contrails observations, large number of model estimates/Spread in model estimates of RF and uncertainties in contrail optical properties	Elevated owing to more studies
Contrail-induced cirrus	Medium	Low	Low	Observations of a few events of contrail induced cirrus/Extent of events uncertain and large spread in estimates of ERF	Elevated owing to additional studies increasing the evidence
Solar irradiance	Medium	Medium	Medium	Satellite information over recent decades and small uncertainty in radiative transfer calculations/Large relative spread in reconstructions based on proxy data	Elevated owing to better agreement of a weak RF
Volcanic aerosol	Robust	Medium	High	Observations of recent volcanic eruptions/Reconstructions of past eruptions	Elevated owing to improved understanding

Notes:

The confidence level for aerosol–cloud interactions includes rapid adjustments (which include what was previously denoted as cloud lifetime effect or second indirect aerosol effect). The separate confidence level for the rapid adjustment for aerosol–cloud interactions is very low. For aerosol–radiation interaction the table provides separate confidence levels for RF due to aerosol–radiation interaction and rapid adjustment associated with aerosol–radiation interaction.

Evidence is robust for several of the RF agents because of long term observations of trends over the industrial era and well defined links between atmospheric or land surfaced changes and their radiative effects. Evidence is medium for a few agents where the anthropogenic changes or the link between the forcing agent and its radiative effect are less certain. Medium evidence can be assigned in cases where observations or modelling provide a diversity of information and thus not a consistent picture for a given forcing agent. We assess the evidence to be limited only for rapid adjustment associated with aerosol–cloud interaction where model studies in some cases indicate changes but direct observations of cloud alterations are scarce. High agreement is given only for the WMGHG where the relative uncertainties in the RF estimates are much smaller than for the other RF agents. Low agreement can either be due to large diversity in estimates of the magnitude of the forcing or from the fact that the method to estimate the forcing has a large uncertainty. Stratospheric water vapour is an example of the latter with modest difference in the few available estimates but a known large uncertainty in the radiative transfer calculations (see further description in Section 8.3.1).

used instead of confidence level. For comparison with previous IPCC assessments the LOSU is converted approximately to confidence level. Note that LOSU and confidence level use different terms for their rankings. The figure shows generally increasing confidence levels but also that more RF mechanisms have been included over time. The confidence levels for the RF due to aerosol–radiation interactions, surface albedo due to land use and volcanic aerosols have been raised and are now at the same ranking as those for change in stratospheric and tropospheric ozone. This is due to an increased understanding of key parameteres and their uncertainties for the elevated RF agents. For tropospheric and stratospheric ozone changes, research has shown further complexities with changes primarily influencing the troposphere or the stratosphere being linked to some extent (see Section 8.3.3). The rapid adjustment associated with aerosol–cloud interactions is given the *confidence level very low* and had a similar level in AR4. For rapid adjustment associated with aerosol–radiation interactions (previously denoted as semi-direct effect) the *confidence level is low* and is raised compared to AR4, as the evidence is improved and is now *medium* (see Section 7.5.2).

Figure 8.14 shows the development of the confidence level over the last four IPCC assessments for the various RF mechanisms. In the previous IPCC reports level of scientific understanding (LOSU) has been

Table 8.6 shows the best estimate of the RF and ERF (for AR5 only) for the various RF agents from the various IPCC assessments. The RF due to WMGHG has increased by 16% and 8% since TAR and AR4,

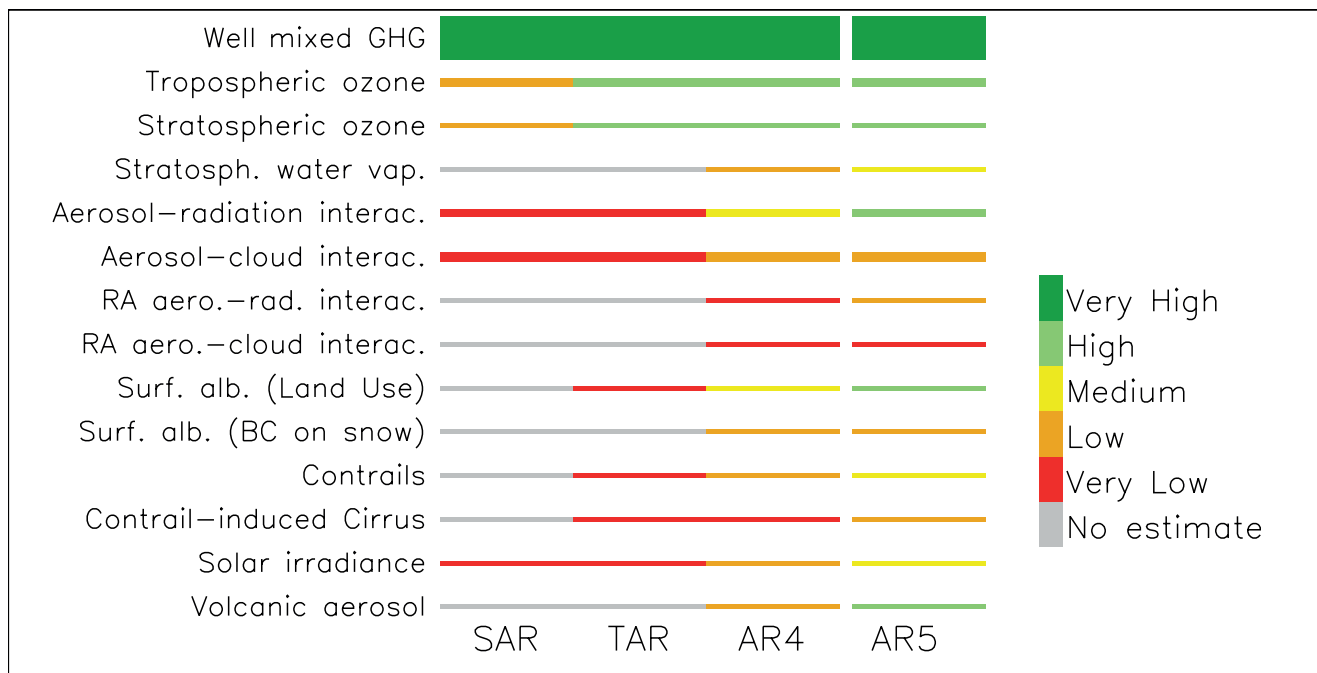


Figure 8.14 | Confidence level of the forcing mechanisms in the 4 last IPCC assessments. In the previous IPCC assessments the level of scientific understanding (LOSU) has been adopted instead of confidence level, but for comparison with previous IPCC assessments the LOSU is converted approximately to confidence level. The thickness of the bars represents the relative magnitude of the current forcing (with a minimum value for clarity of presentation). LOSU for the RF mechanisms was not available in the first IPCC Assessment (Houghton et al., 1990). Rapid adjustments associated with aerosol–cloud interactions (shown as RA aero.–cloud interac.) which include what was previously referred to as the second indirect aerosol effect or cloud lifetime effect whereas rapid adjustments associated with aerosol–radiation interactions (shown as RA aero.–rad. interac.) were previously referred to as the semi-direct effect (see Figure 7.3). In AR4 the confidence level for aerosol–cloud interaction was given both for RF due to aerosol–cloud interaction and rapid adjustment associated with aerosol–cloud interaction. Generally the aerosol–cloud interaction is not separated into various components in AR5, hence the confidence levels for ERF due to aerosol–cloud interaction in AR5 and for RF due to aerosol–cloud interaction from previous IPCC reports are compared. The confidence level for the rapid adjustment associated with aerosol–cloud interaction is comparable for AR4 and AR5. The colours are adopted based on the evidence and agreement shown in Figure 1.11. Dark green is “High agreement and Robust evidence”, light green is either “High agreement and Medium evidence” or “Medium agreement and Robust evidence”, yellow is either “High agreement and limited evidence” or “Medium agreement and Medium evidence” or “Low agreement and Robust evidence”, orange is either “Medium agreement and Limited evidence” or “Low agreement and Medium evidence” and finally red is “Low agreement and Limited evidence”.

respectively. This is due mainly to increased concentrations (see Section 8.3.2), whereas the other changes for the anthropogenic RF agents compared to AR4 are due to re-evaluations and in some cases from improved understanding. An increased number of studies, additional observational data and better agreement between models and observations can be the causes for such re-evaluations. The best estimates for RF due to aerosol–radiation interactions, BC on snow and solar irradiance are all substantially decreased in magnitude compared to AR4; otherwise the modifications to the best estimates are rather small. For the RF due to aerosol–radiation interaction and BC on snow the changes in the estimates are based on additional new studies since AR4 (see Section 8.3.4 and Section 7.5). For the change in the estimate of the solar irradiance it is a combination on how the RF is calculated, new evidence showing some larger earlier estimates were incorrect, and a downward trend observed during recent years in the solar activity that has been taken into account (see Section 8.4.1). The estimate for ERF due to aerosol–cloud interaction includes rapid adjustment but still this ERF is smaller in magnitude than the AR4 RF estimate due to aerosol–cloud interactions without rapid adjustments (a theoretical construct not quantified in AR5). The uncertainties for ERF due to CO₂ increase when compared to RF (see Section 8.3.2). We assume the relative ERF uncertainties for CO₂ apply to all WMGHG. For the short-lived GHG we do not have sufficient information to include separate ERF uncertainty to each of these forcing agents (see Section 8.1.1.3).

However, for these forcing mechanisms the RF uncertainties are larger than for the WMGHG and thus it is *unlikely* that rapid adjustments change the uncertainties substantially.

Figure 8.15 shows the RF for agents listed in Table 8.6 over the 1750–2011 period. The methods for calculation of forcing estimates are described in Section 8.3 and 8.4. For some of the components the forcing estimates are based on observed abundance whereas some are estimated from a combination of model simulations and observations and for others are purely model based. Solid bars are given for ERF, whereas RF values are given as (additional) hatched bars. Similarly the uncertainties are given for ERF in solid lines and dotted lines for RF. An important assumption is that different forcing mechanisms can be treated additively to calculate the total forcing (see Boucher and Haywood, 2001; Forster et al., 2007; Haywood and Schulz, 2007). Total ERF over the Industrial Era calculated from Monte Carlo simulations are shown in Figure 8.16, with a best estimate of 2.29 W m⁻². For each of the forcing agents a probability density function (PDF) is generated based on uncertainties provided in Table 8.6. The combination of the individual RF agents to derive total forcing follows the same approach as in AR4 (Forster et al., 2007) which is based on the method in Boucher and Haywood (2001). The PDF of the GHGs (sum of WMGHG, ozone and stratospheric water vapour) has a more narrow shape than the PDF for the aerosols owing to the much lower relative uncertainty.

Table 8.6 | Summary table of RF estimates for AR5 and comparison with the three previous IPCC assessment reports. ERF values for AR5 are included. For AR5 the values are given for the period 1750–2011, whereas earlier final years have been adopted in the previous IPCC assessment reports.

	Global Mean Radiative Forcing (W m ⁻²)				Comment	ERF (W m ⁻²)
	SAR (1750–1993)	TAR (1750–1998)	AR4 (1750–2005)	AR5 (1750–2011)		
Well-mixed greenhouse gases (CO ₂ , CH ₄ , N ₂ O, and halocarbons)	2.45 (2.08 to 2.82)	2.43 (2.19 to 2.67)	2.63 (2.37 to 2.89)	2.83 (2.54 to 3.12)	Change due to increase in concentrations	2.83 (2.26 to 3.40)
Tropospheric ozone	+0.40 (0.20 to 0.60)	+0.35 (0.20 to 0.50)	+0.35 (0.25 to 0.65)	+0.40 (0.20 to 0.60)	Slightly modified estimate	
Stratospheric ozone	–0.1 (–0.2 to –0.05)	–0.15 (–0.25 to –0.05)	–0.05 (–0.15 to +0.05)	–0.05 (–0.15 to +0.05)	Estimate unchanged	
Stratospheric water vapour from CH ₄	Not estimated	+0.01 to +0.03	+0.07 (+0.02, +0.12)	+0.07 (+0.02 to +0.12)	Estimate unchanged	
Aerosol–radiation interactions	Not estimated	Not estimated	–0.50 (–0.90 to –0.10)	–0.35 (–0.85 to +0.15)	Re-evaluated to be smaller in magnitude	–0.45 (–0.95 to +0.05)
Aerosol–cloud interactions	0 to –1.5 (sulphate only)	0 to –2.0 (all aerosols)	–0.70 (–1.80 to –0.30) (all aerosols)	Not estimated	Replaced by ERF and re-evaluated to be smaller in magnitude	–0.45 (–1.2 to 0.0)
Surface albedo (land use)	Not estimated	–0.20 (–0.40 to 0.0)	–0.20 (–0.40 to 0.0)	–0.15 (–0.25 to –0.05)	Re-evaluated to be slightly smaller in magnitude	
Surface albedo (black carbon aerosol on snow and ice)	Not estimated	Not estimated	+0.10 (0.0 to +0.20)	+0.04 (+0.02 to +0.09)	Re-evaluated to be weaker	
Contrails	Not estimated	+0.02 (+0.006 to +0.07)	+0.01 (+0.003 to +0.03)	+0.01 (+0.005 to +0.03)	No major change	
Combined contrails and contrail-induced cirrus	Not estimated	0 to +0.04	Not estimated	Not estimated		0.05 (0.02 to 0.15)
Total anthropogenic	Not estimated	Not estimated	1.6 (0.6 to 2.4)	Not estimated	Stronger positive due to changes in various forcing agents	2.3 (1.1 to 3.3)
Solar irradiance	+0.30 (+0.10 to +0.50)	+0.30 (+0.10 to +0.50)	+0.12 (+0.06 to +0.30)	+0.05 (0.0 to +0.10)	Re-evaluated to be weaker	

Notes:

Volcanic RF is not added to the table due to the periodic nature of volcanic eruptions, which makes it difficult to compare to the other forcing mechanisms.

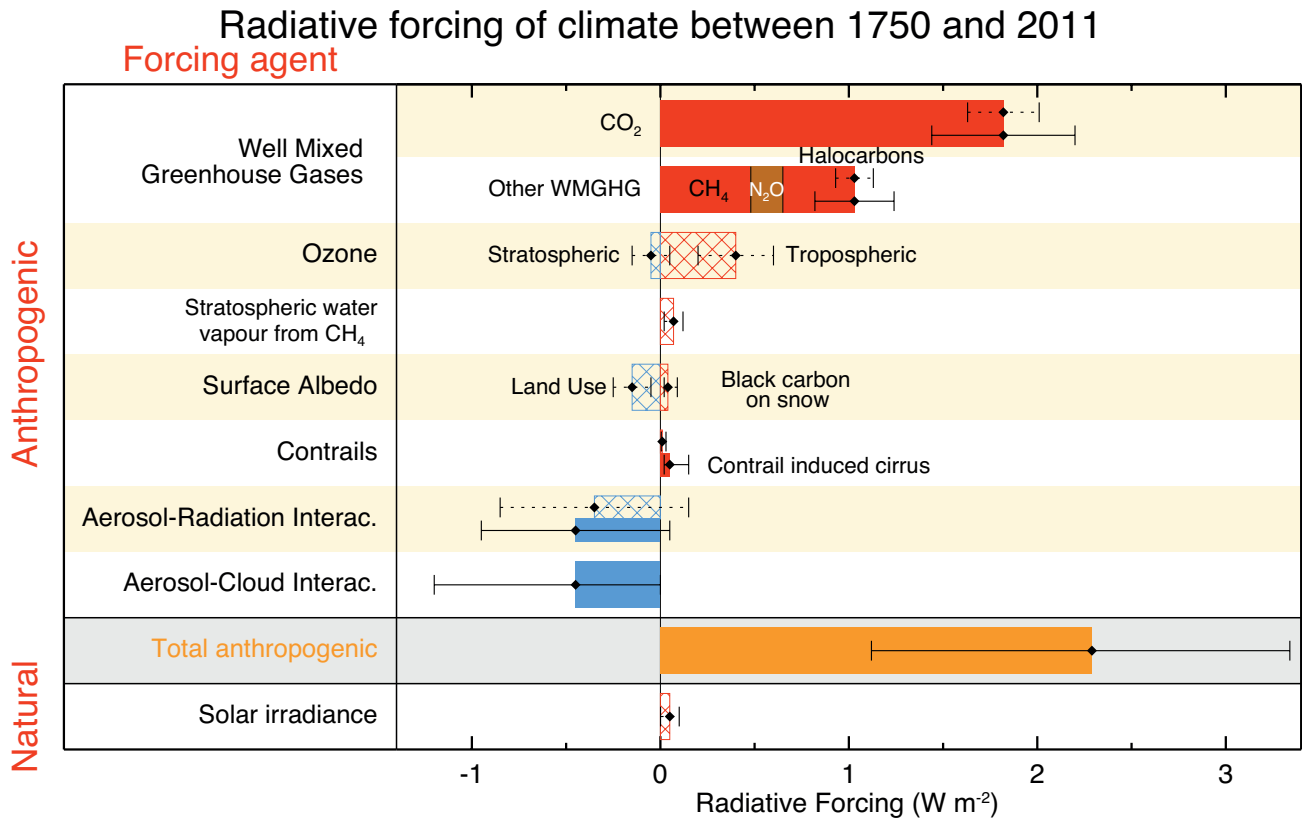


Figure 8.15 | Bar chart for RF (hatched) and ERF (solid) for the period 1750–2011, where the total ERF is derived from Figure 8.16. Uncertainties (5 to 95% confidence range) are given for RF (dotted lines) and ERF (solid lines).

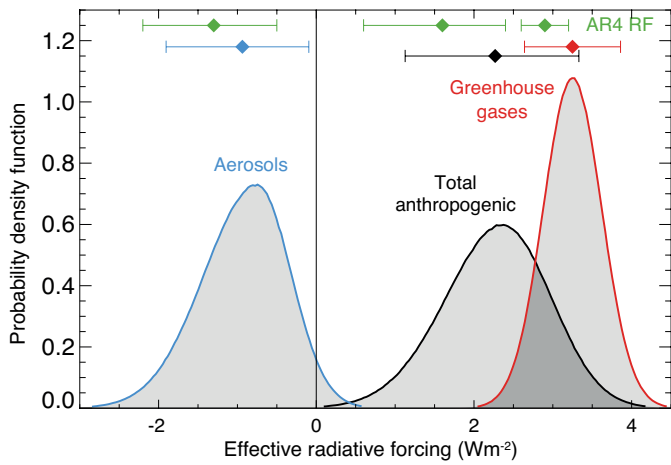


Figure 8.16 | Probability density function (PDF) of ERF due to total GHG, aerosol forcing and total anthropogenic forcing. The GHG consists of WMGHG, ozone and stratospheric water vapour. The PDFs are generated based on uncertainties provided in Table 8.6. The combination of the individual RF agents to derive total forcing over the Industrial Era are done by Monte Carlo simulations and based on the method in Boucher and Haywood (2001). PDF of the ERF from surface albedo changes and combined contrails and contrail-induced cirrus are included in the total anthropogenic forcing, but not shown as a separate PDF. We currently do not have ERF estimates for some forcing mechanisms: ozone, land use, solar, etc. For these forcings we assume that the RF is representative of the ERF and for the ERF uncertainty an additional uncertainty of 17% has been included in quadrature to the RF uncertainty. See Supplementary Material Section 8.SM.7 and Table 8.SM.4 for further description on method and values used in the calculations. Lines at the top of the figure compare the best estimates and uncertainty ranges (5 to 95% confidence range) with RF estimates from AR4.

Therefore, the large uncertainty in the aerosol forcing is the main cause of the large uncertainty in the total anthropogenic ERF. The total anthropogenic forcing is *virtually certain* to be positive with the probability for a negative value less than 0.1%. Compared to AR4 the total anthropogenic ERF is more strongly positive with an increase of 43%. This is caused by a combination of growth in GHG concentration, and thus strengthening in forcing of WMGHG, and weaker ERF estimates of aerosols (aerosol–radiation and aerosol–cloud interactions) as a result of these effects.

Figure 8.17 shows the forcing over the Industrial Era by emitted compounds (see Supplementary Material Tables 8.SM.6 and 8.SM.7 for actual numbers and references). It is more complex to view the RF by emitted species than by change in atmospheric abundance (Figure 8.15) since the number of emitted compounds and changes leading to RF is larger than the number of compounds causing RF directly (see Section 8.3.3). The main reason for this is the indirect effect of several compounds and in particular components involved in atmospheric chemistry (see Section 8.2). To estimate the RF by the emitted compounds in some cases the emission over the entire Industrial Era is needed (e.g., for CO₂) whereas for other compounds (such as ozone and CH₄) quite complex simulations are required (see Section 8.3.3). CO₂ is the dominant positive forcing both by abundance and by emitted compound. Emissions of CH₄, CO, and NMVOC all lead to excess CO₂ as one end product if the carbon is of fossil origin and is the reason why the RF of direct CO₂ emissions is slightly lower than the RF of abundance change of CO₂. For CH₄ the contribution from emission is estimated to be almost twice as large as that from the CH₄ concen-

tration change, 0.97 (0.80 to 1.14) $W m^{-2}$ versus 0.48 (0.43 to 0.53) $W m^{-2}$, respectively. This is because emission of CH_4 leads to ozone production, stratospheric water vapour, CO_2 (as mentioned above), and importantly affects its own lifetime (Section 8.2). Actually, emissions of CH_4 would lead to a stronger RF via the direct CH_4 greenhouse effect (0.64 $W m^{-2}$) than the RF from abundance change of CH_4 (0.48 $W m^{-2}$). This is because other compounds have influenced the lifetime of CH_4 and reduced the abundance of CH_4 , most notably NO_x . Emissions of CO (0.23 (0.18 to 0.29) $W m^{-2}$) and NMVOC (0.10 (0.06 to 0.14) $W m^{-2}$) have only indirect effects on RF through ozone production, CH_4 and CO_2 and thus contribute an overall positive RF. Emissions of NO_x , on the other hand, have indirect effects that lead to positive RF through ozone production and also effects that lead to negative RF through

reduction of CH_4 lifetime and thus its concentration, and through contributions to nitrate aerosol formation. The best estimate of the overall effect of anthropogenic emissions of NO_x is a negative RF (-0.15 (-0.34 to +0.02) $W m^{-2}$). Emissions of ammonia also contribute to nitrate aerosol formation, with a small offset due to compensating changes in sulphate aerosols. Additionally indirect effects from sulphate on atmospheric compounds are not included here as models typically simulate a small effect, but there are large relative differences in the response between models. Impacts of emissions other than CO_2 on the carbon cycle via changes in atmospheric composition (ozone or aerosols) are also not shown owing to the limited amount of available information.

For the WMGHG, the ERF best estimate is the same as the RF. The uncertainty range is slightly larger, however. The total emission-based ERF of WMGHG is 3.00 (2.22 to 3.78) $W m^{-2}$. That of CO_2 is 1.68 (1.33 to 2.03) $W m^{-2}$; that of CH_4 is 0.97 (0.74 to 1.20) $W m^{-2}$; that of stratospheric ozone-depleting halocarbons is 0.18 (0.01 to 0.35) $W m^{-2}$.

Emissions of BC have a positive RF through aerosol–radiation interactions and BC on snow (0.64 $W m^{-2}$, see Section 8.3.4 and Section 7.5). The emissions from the various compounds are co-emitted; this is in particular the case for BC and OC from biomass burning aerosols. The net RF of biomass burning emissions for aerosol–radiation interactions is close to zero, but with rather strong positive RF from BC and negative RF from OC (see Sections 8.3.4 and 7.5). The ERF due to aerosol–cloud interactions is caused by primary anthropogenic emissions of BC, OC and dust as well as secondary aerosol from anthropogenic emissions of SO_2 , NO_x and NH_3 . However, quantification of the contribution from the various components to the ERF due to aerosol–cloud interactions has not been attempted in this assessment.

8.5.2 Time Evolution of Historical Forcing

The time evolution of global mean forcing is shown in Figure 8.18 for the Industrial Era. Over all time periods during the Industrial Era CO_2 and other WMGHG have been the dominant term, except for shorter periods with strong volcanic eruptions. The time evolution shows an almost continuous increase in the magnitude of anthropogenic ERF. This is the case both for CO_2 and other WMGHGs as well as several individual aerosol components. The forcing from CO_2 and other WMGHGs has increased somewhat faster since the 1960s. Emissions of CO_2 have made the largest contribution to the increased anthropogenic forcing in every decade since the 1960s. The total aerosol ERF (aerosol–radiation interaction and aerosol–cloud interaction) has the strongest negative forcing (except for brief periods with large volcanic forcing), with a strengthening in the magnitude similar to many of the other anthropogenic forcing mechanisms with time. The global mean forcing of aerosol–radiation interactions was rather weak until 1950 but strengthened in the latter half of the last century and in particular in the period between 1950 and 1980. The RF due to aerosol–radiation interaction by aerosol component is shown in Section 8.3.4 (Figure 8.8).

Although there is *high confidence* for a substantial enhancement in the negative aerosol forcing in the period 1950–1980, there is much more uncertainty in the relative change in global mean aerosol forcing over the last two decades (1990–2010). Over the last two decades there has been a strong geographic shift in aerosol and aerosol precursor

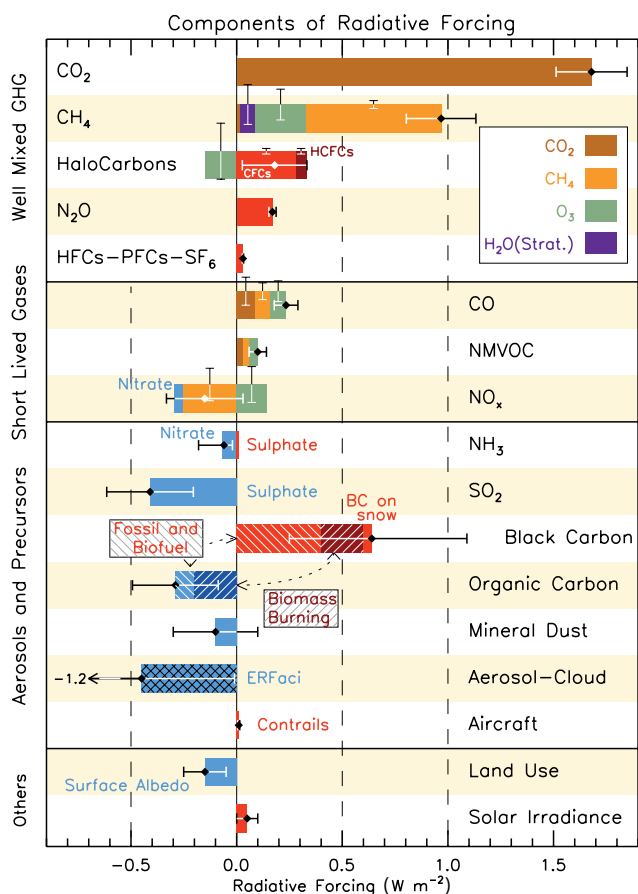


Figure 8.17 | RF bar chart for the period 1750–2011 based on emitted compounds (gases, aerosols or aerosol precursors) or other changes. Numerical values and their uncertainties are shown in Supplementary Material Tables 8.SM.6 and 8.SM.7. Note that a certain part of CH_4 attribution is not straightforward and discussed further in Section 8.3.3. Red (positive RF) and blue (negative forcing) are used for emitted components which affect few forcing agents, whereas for emitted components affecting many compounds several colours are used as indicated in the inset at the upper part of the figure. The vertical bars indicate the relative uncertainty of the RF induced by each component. Their length is proportional to the thickness of the bar, that is, the full length is equal to the bar thickness for a $\pm 50\%$ uncertainty. The net impact of the individual contributions is shown by a diamond symbol and its uncertainty (5 to 95% confidence range) is given by the horizontal error bar. ERFaci is ERF due to aerosol–cloud interaction. BC and OC are co-emitted, especially for biomass burning emissions (given as Biomass Burning in the figure) and to a large extent also for fossil and biofuel emissions (given as Fossil and Biofuel in the figure where biofuel refers to solid biomass fuels). SOA have not been included because the formation depends on a variety of factors not currently sufficiently quantified.

emissions (see Section 2.2.3), and there are some uncertainties in these emissions (Granier et al., 2011). In addition to the regional changes in the aerosol forcing there is also likely a competition between various aerosol effects. Emission data indicate a small increase in the BC emissions (Granier et al., 2011) but model studies also indicate a weak enhancement of other aerosol types. Therefore, the net aerosol forcing depends on the balance between absorbing and scattering aerosols for aerosol–radiation interaction as well as balance between the changes in aerosol–radiation and aerosol–cloud interactions. In the ACCMIP models, for example, the RF due to aerosol–radiation interaction becomes less negative during 1980 to 2000, but total aerosol ERF becomes more negative (Shindell et al., 2013c). There is a *very low confidence* for the trend in the total aerosol forcing during the past two to three decades, even the sign; however, there is *high confidence* that the offset from aerosol forcing to WMGHG forcing during this period was much smaller than over the 1950–1980 period.

The volcanic RF has a very irregular temporal pattern and for certain years has a strongly negative RF. There has not been a major volcanic eruption in the past decade, but some weaker eruptions give a current RF that is slightly negative relative to 1750 and slightly stronger in magnitude compared to 1999–2002 (see Section 8.4.2).

Figure 8.19 shows linear trends in forcing (anthropogenic, natural and total) over four different time periods. Three of the periods are the same as chosen in Box 9.2 (1984–1998, 1998–2011 and 1951–2011) and the period 1970–2011 is shown in Box 13.1. Monte Carlo simulations are performed to derive uncertainties in the forcing based on ranges given in Table 8.6 and the derived linear trends. Further, these uncertainties are combined with uncertainties derived from shifting time periods ± 2 years and the full 90% confidence range is shown in Figure 8.19 (in Box 9.2 only the total forcing is shown with uncertainties derived from the forcing uncertainty without sensitivity to time period). For the anthropogenic forcing sensitivity to the selection of time periods is very small with a maximum contribution to the uncertainties shown in Figure 8.19 of 2%. However, for the natural forcing the sensitivity to time periods is the dominant contributor to the overall uncertainty (see Supplementary Material Figure 8.SM.3) for the relatively short periods 1998–2011 and 1984–1998, whereas this is not the case for the longer periods. For the 1998–2011 period the natural forcing is *very likely* negative and has offset 2 to 89% of the anthropogenic forcing. It is *likely* that the natural forcing change has offset at least 30% of the anthropogenic forcing increase and *very likely* that it has offset at least 10% of the anthropogenic increase. For the 1998–2011 period both the volcanic and solar forcings contribute to this negative natural forcing, with the latter dominating. For the other periods shown in Figure 8.19 the best estimate of the natural is much smaller in magnitude than the anthropogenic forcing, but note that the natural forcing is very dependent on the selection of time period near the 1984–1998 interval. Over the period 1951–2011 the trend in anthropogenic forcing is almost 0.3 W m^{-2} per decade and thus anthropogenic forcing over this period is more than 1.5 W m^{-2} . The anthropogenic forcing for 1998–2011 is 30% higher and with smaller uncertainty than for the 1951–2011 period. Note that due to large WMGHG forcing (Section 8.3.2) the anthropogenic forcing was similar in the late 1970s and early 1980s to the 1998–2011 period. The reason for the reduced uncertainty in the 1998–2011 anthropogenic forcing

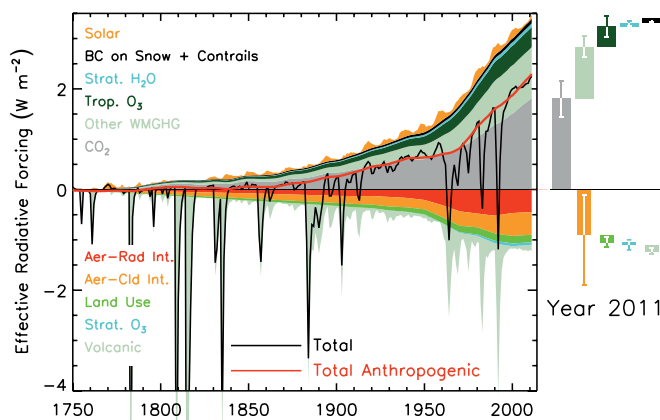


Figure 8.18 | Time evolution of forcing for anthropogenic and natural forcing mechanisms. Bars with the forcing and uncertainty ranges (5 to 95% confidence range) at present are given in the right part of the figure. For aerosol the ERF due to aerosol–radiation interaction and total aerosol ERF are shown. The uncertainty ranges are for present (2011 versus 1750) and are given in Table 8.6. For aerosols, only the uncertainty in the total aerosol ERF is given. For several of the forcing agents the relative uncertainty may be larger for certain time periods compared to present. See Supplementary Material Table 8.SM.8 for further information on the forcing time evolutions. Forcing numbers provided in Annex II. The total anthropogenic forcing was 0.57 (0.29 to 0.85) W m^{-2} in 1950, 1.25 (0.64 to 1.86) W m^{-2} in 1980 and 2.29 (1.13 to 3.33) W m^{-2} in 2011.

is the larger domination of WMGHG forcing and smaller contribution from aerosol forcing compared to previous periods. Similar to the results for 1970–2011 in Figure 8.19, Box 13.1 shows that the global energy budget is dominated by anthropogenic forcing compared to the natural forcing, except for the two major volcanic eruption in this period as can be easily seen in Figure 8.18.

Figure 8.20 shows the forcing between 1980 and 2011. Compared to the whole Industrial Era the dominance of the CO_2 is larger for this recent period both with respect to other WMGHG and the total anthropogenic RF. The forcing due to aerosols is rather weak leading

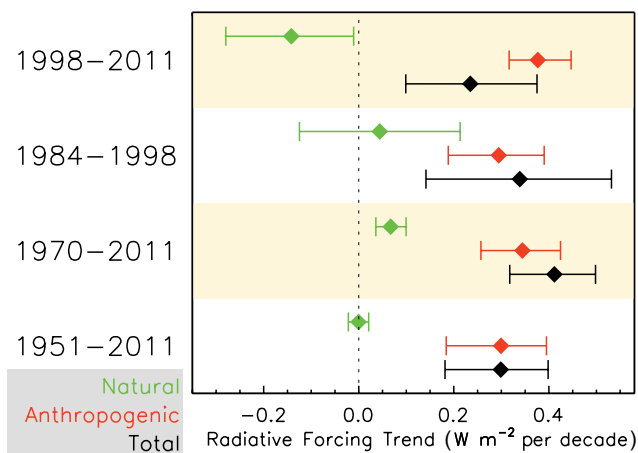


Figure 8.19 | Linear trend in anthropogenic, natural and total forcing for the indicated time periods. The uncertainty ranges (5 to 95% confidence range) are combined from uncertainties in the forcing values (from Table 8.6) and the uncertainties in selection of time period. Monte Carlo simulations were performed to derive uncertainties in the forcing based on ranges given in Table 8.6 and linear trends in forcing. The sensitivity to time periods has been derived from changing the time periods by ± 2 years.

Radiative forcing of climate between 1980 and 2011

Forcing agent

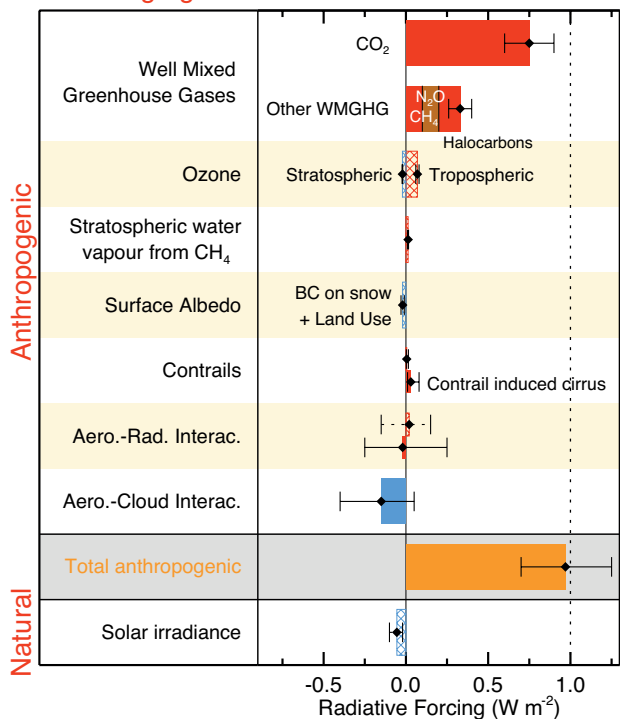


Figure 8.20 | Bar chart for RF (hatched) and ERF (solid) for the period 1980–2011, where the total anthropogenic ERF are derived from Monte-Carlo simulations similar to Figure 8.16. Uncertainties (5 to 95% confidence range) are given for RF (dotted lines) and ERF (solid lines).

to a very strong net positive ERF for the 1980–2011 period. More than 40% of the total anthropogenic ERF has occurred over the 1980–2011 period with a value close to 1.0 (0.7 to 1.3) W m^{-2} . The major contribution to the uncertainties in the time evolution of the anthropogenic forcing is associated with the aerosols (see Section 8.5.1). Despite this, anthropogenic ERF is *very likely* considerably more positive than the natural RF over the decadal time periods since 1950. This is in particular the case after 1980, where satellite data are available that provide important measurements to constrain the natural RF mechanisms (e.g., the volcanic RF change between 2007–2011 and 1978–1982 is 0.06 W m^{-2} and the representative change in solar irradiance over the 1980–2011 period is -0.06 W m^{-2}) with total natural RF of 0.0 (-0.1 to $+0.1$) W m^{-2} .

8.5.3 Future Radiative Forcing

Projections of global mean RF are assessed based on results from multiple sources examining the RF due to RCP emissions: the ACCMIP initiative (see Section 8.2) provides analysis of the RF or ERF due to aerosols and ozone (Shindell et al., 2013c), while WMGHG, land use and stratospheric water RFs are taken from the results of calculations with the reduced-complexity Model for the Assessment of Greenhouse-gas Induced Climate Change 6 (MAGICC6) driven by the RCP emissions and land use (Meinshausen et al., 2011a). While MAGICC6 also estimated ozone and aerosol RF, those values differ substantially from the ACCMIP values and are considered less realistic. Additional discussion of biases in the MAGICC6 results due to the simplified representations

of atmospheric chemistry and the carbon cycle, along with further discussion on the representativeness of the RCP projections in context with the broader set of scenarios in the literature, is presented in Section 11.3.5 and Section 12.3 (also see Section 8.2). As the ACCMIP project provided projected forcings primarily at 2030 and 2100, we hereafter highlight those times. Although understanding the relative contributions of various processes to the overall effect of aerosols on forcing is useful, we emphasize the total aerosol ERF, which includes all aerosol–radiation and aerosol–cloud interactions, as this is the most indicative of the aerosol forcing driving climate change. We also present traditional RF due to aerosol–radiation interaction (previously called direct aerosol effect) but do not examine further the various components of aerosol ERF. Aerosol forcing estimates, both mean and uncertainty ranges, are derived from the 10 ACCMIP models, 8 of which are also CMIP5 models. We analyze forcing during the 21st century (relative to 2000), and hence the WMGHG forcing changes are in addition to persistent forcing from historical WMGHG increases.

Analysis of forcing at 2030 relative to 2000 shows that under RCP2.6, total ozone (tropospheric and stratospheric) forcing is near zero, RF due to aerosol–radiation interaction is positive but small, and hence WMGHG forcing dominates changes over this time period (Figure 8.21). WMGHG forcing is dominated by increasing CO_2 , as declining CH_4 and increasing N_2O have nearly offsetting small contributions to forcing. Aerosol ERF was not evaluated for this RCP under ACCMIP, and values cannot be readily inferred from RF due to aerosol–radiation interaction as these are not directly proportional. Under RCP8.5, RF due to aerosol–radiation interaction in 2030 is weakly negative, aerosol ERF is positive with a fairly small value and large uncertainty range, total ozone forcing is positive but small ($\sim 0.1 \text{ W m}^{-2}$), and thus WMGHG forcing again dominates with a value exceeding 1 W m^{-2} . As with RCP2.6, WMGHG forcing is dominated by CO_2 , but under this scenario the other WMGHGs all contribute additional positive forcing. Going to 2100, ozone forcing diverges in sign between the two scenarios, consistent with changes in the tropospheric ozone burden (Figure 8.4) which are largely attributable to projected CH_4 emissions, but is small in either case. Ozone RF is the net impact of a positive forcing from stratospheric ozone recovery owing to reductions in anthropogenic ozone-depleting halocarbon emissions in both scenarios and a larger impact from changes in tropospheric precursors (Shindell et al., 2013c) which have a negative forcing in RCP2.6 and a positive forcing in RCP8.5.

The two scenarios are fairly consistent in their trends in RF due to aerosol–radiation interaction by component (Figure 8.21). There is positive RF due to aerosol–radiation interaction due to reductions in sulfate aerosol. This is largely offset by negative RF due to aerosol–radiation interaction by primary carbonaceous aerosols and especially by nitrate (though nearly all CMIP5 models did not include nitrate), leaving net aerosol RF due to aerosol–radiation interaction values that are very small, 0.1 W m^{-2} or less in magnitude, in either scenario at 2030 and 2100. Nitrate aerosols continue to increase through 2100 as ammonia emissions rise steadily due to increased use of agricultural fertilizer even as all other aerosol precursor emissions decrease (Figure 8.2), including sulphur dioxide which drives the reduction in sulphate aerosol that also contributes to additional formation of nitrate aerosols in the future (Bauer et al., 2007; Bellouin et al., 2011). Aerosol ERF is *likely* similar at this time in all scenarios given that they all have greatly

reduced emissions of all aerosols and aerosol precursors other than ammonia. Aerosol ERF shows a large positive value at 2100 relative to 2000, nearly returning to its 1850 levels (the 2100 versus 1850 ERF represents a decrease in ERF of 91% relative to the 2000 versus 1850 value), as is expected given the RCP emissions. Thus although some models project large increases in nitrate RF in the future, the reduction in overall aerosol loading appears to lead to such a strong reduction in aerosol ERF that the impact of aerosols becomes very small under these RCPs. Of course the projections of drastic reductions in primary aerosol as well as aerosol and ozone precursor emissions may be overly optimistic as they assume virtually all nations in the world become wealthy and that emissions reductions are directly dependent on wealth. The RCPs also contain substantially lower projected growth in HFC emissions than in some studies (e.g., Velders et al., 2009).

Although aerosol ERF becomes less negative by nearly 1 W m^{-2} from 2000 to 2100, this change is still small compared with the increased WMGHG forcing under RCP8.5, which is roughly 6 W m^{-2} during this time (Figure 8.21). Roughly 5 W m^{-2} of this WMGHG forcing comes from CO_2 , with substantial additional forcing from increases in both CH_4 and nitrous oxide and only a very small negative forcing from reductions in halocarbons. Under RCP2.6, the WMGHG forcing is only about 0.5 W m^{-2} during this time, as relatively strong decreases in CH_4 and halocarbon forcing offset roughly 40% of the increased CO_2 forcing, which is itself far less than under RCP8.5. Hence under this scenario, the projected future forcing due to aerosol reductions is actually stronger than the WMGHG forcing. Viewing the timeseries of the various forcings, however, indicates that aerosol ERF is returning to its pre-industrial levels, so that net forcing becomes increasingly dominated by WMGHGs regardless of scenario during the 21st century (Figure 8.22). As the forcing is so heavily dominated by WMGHGs at 2100, and the WMGHG concentrations (CO_2) or emissions (others) were chosen to match forcing targets, all the scenarios show net forcing values at that time that are fairly close to the scenarios' target values. The reduced aerosol forcing, with its large uncertainty, leads to a pronounced decrease in the uncertainty of the total net forcing by 2100. Based on the spread across ACCMIP models (using ERF for aerosols and converting to ERF for GHGs), the 90% confidence interval (CI) is about 20% for the 2100 net forcing, versus 26% for 2030 under RCP8.5 and 45–61% for 1980 and 2000 (Shindell et al., 2013c). The total ERF due to all causes has been independently estimated based on the transient response in the CMIP5 models and a linear forcing-response relationship derived through regression of the modelled response to an instantaneous increase in CO_2 (Forster et al., 2013). Uncertainties based on model spread behave similarly, with the 90% CI for net total ERF decreasing from 53% for 2003 to only 24 to 34% for 2100. Forcing relative to 2000 due to land use (via albedo only) and stratospheric water vapor changes are not shown separately as their projected values under the four RCPs are quite small: -0.09 to 0.00 and -0.03 to 0.10 W m^{-2} , respectively.

The CMIP5 forcing estimates (Forster et al., 2013) for the total projected 2030 and 2100 ERF are slightly smaller than the results obtained from the ACCMIP models (or the RCP targets; see Section 12.3.3). Examining the subset of models included in both this regression analysis and in ACCMIP shows that the ACCMIP subset show forcings on the low side of the mean value obtained from the full set of CMIP5

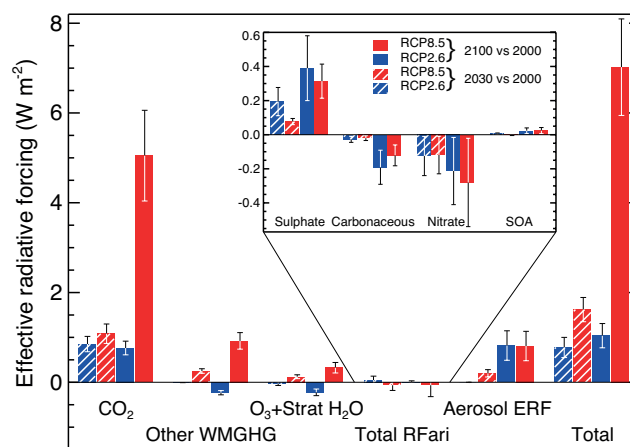


Figure 8.21 | Radiative forcing relative to 2000 due to anthropogenic composition changes based on ACCMIP models for aerosols (with aerosol ERF scaled to match the best estimate of present-day forcing) and total ozone and RCP WMGHG forcings. Ranges are one standard deviation in the ACCMIP models and assessed relative uncertainty for WMGHGs and stratospheric water vapor. Carbonaceous aerosols refer to primary carbonaceous, while SOA are secondary organic aerosols. Note that 2030 ERF for RCP2.6 was not available, and hence the total shown for that scenario is not perfectly comparable to the other total values. RFari is RF due to aerosol–radiation interaction.

analyzed, indicating that the discrepancy between the methods is not related to analysis of a different set of models. Instead, it may reflect nonlinearities in the response to forcing that are not represented by the regression analysis of the response to abrupt CO_2 increase experiments (Long and Collins, 2013) or differences in the response to other forcing agents relative to the response to CO_2 used in deriving the CMIP5 estimates (see also 12.3.3).

Natural forcings will also change in the future. The magnitudes cannot be reliably projected, but are *likely* to be small at multi-decadal scales (see Section 8.4). Brief episodic volcanic forcing could be large, however.

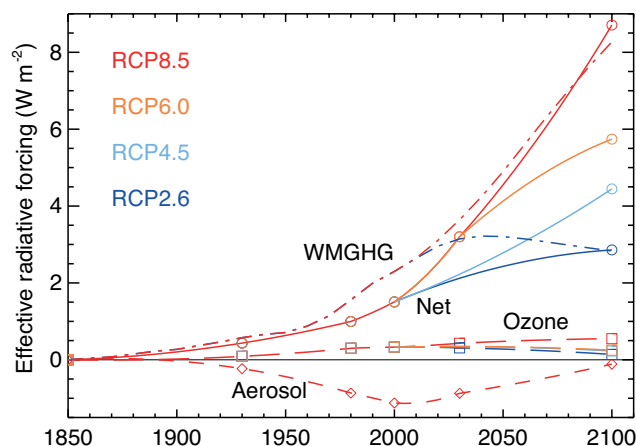


Figure 8.22 | Global mean anthropogenic forcing with symbols indicating the times at which ACCMIP simulations were performed (solid lines with circles are net; long dashes with squares are ozone; short dashes with diamonds are aerosol; dash-dot are WMGHG; colours indicate the RCPs with red for RCP8.5, orange RCP6.0, light blue RCP4.5, and dark blue RCP2.6). RCPs 2.6, 4.5 and 6.0 net forcings at 2100 are approximate values using aerosol ERF projected for RCP8.5 (modified from Shindell et al., 2013c). Some individual components are omitted for some RCPs for visual clarity.

8.6 Geographic Distribution of Radiative Forcing

The forcing spatial pattern of the various RF mechanisms varies substantially in space and in time, especially for the NTCFs. The spatial pattern is of interest to the extent that it may influence climate response (Section 8.6.2.2) as is being particularly investigated in the ACCMIP simulations.

8.6.1 Spatial Distribution of Current Radiative Forcing

The WMGHGs such as CO₂ have the largest forcing in the subtropics, decreasing toward the poles, with the largest forcing in warm and dry regions and smaller values in moist regions and in high-altitude regions (Taylor et al., 2011). For the NTCFs (Box 8.2) their concentration spatial pattern and therefore their RF pattern are highly inhomogeneous, and again meteorological factors such as temperature, humidity, clouds, and surface albedo influence how concentration translates to RF.

Figure 8.23 shows the RF spatial distribution of the major NTCFs together with standard deviation among the ACCMIP models (Shindell et al., 2013c) the net anthropogenic composition (WMGHG+ozone+aerosol) forcing is also shown (lower left panel). These models used unified anthropogenic emissions of aerosol and ozone precursors (Supplementary Material Figure 8.SM.2), so that the model diversity in RF is due only to differences in model chemical and climate features and natural emissions, and would be larger if uncertainty in the anthropogenic emissions were also included. In general, the confidence in geographical distribution is lower than for global mean, due to uncertainties in chemistry, transport and removal of species.

The negative RF due to aerosol–radiation interaction (first row; defined in Figure 7.3) is greatest in the NH and near populated and biomass burning regions. The standard deviation for the net RF due to aerosol–radiation interaction is typically largest over regions where vegetation changes are largest (e.g., South Asia and central Africa), due to uncertainties in biomass burning aerosol optical properties and in treatment of secondary organic aerosols. Carbonaceous aerosol forcing (second row) is greatest in South and East Asia and can be negative in biomass burning regions due to large weakly absorbing organic components. Absorbing aerosols also have enhanced positive forcing when they overlie high albedo surfaces such as cryosphere, desert or clouds, with as much as 50% of BC RF resulting from BC above clouds (Zarzycki and Bond, 2010).

Figure 8.24 compares the aerosol RFs for ACCMIP (Shindell et al., 2013c), which are representative of the CMIP5 experiments, with those from the AeroCom model intercomparison (Myhre et al., 2013) which includes sixteen models that used unified meteorology and are more extensively compared to measurements (e.g., Koch et al., 2009b; Koffi et al., 2012). The forcing results are very similar, establishing the representativeness and validity of the ACCMIP aerosol simulations.

The net aerosol ERF (Figure 8.23; third row), includes both aerosol–radiation and aerosol–cloud interactions. The spatial pattern correlates with the RF (first row), except with stronger effect in the outflow regions over oceans. The flux change is larger in the NH than the

SH (e.g., by nearly a factor of 3; Ming et al., 2007). Rapid adjustment associated with aerosol–radiation and aerosol–cloud interactions may enhance or reduce cloud cover depending on the region, cloud dynamics and aerosol loading (e.g., Randles and Ramaswamy, 2008; Koch and Del Genio, 2010; Persad et al., 2012). In general, the ocean–land forcing pattern differs from that reported in AR4, where the forcing due to aerosol–cloud interaction were larger over land than ocean (Forster et al., 2007), and this continues to be a source of uncertainty. Since AR4, Quaas et al. (2009) showed using satellite retrievals that the correlation between AOD changes and droplet number changes is stronger over oceans than over land and that models tend to overestimate the strength of the relation over land. Penner et al. (2011) showed that satellite retrievals, due to their dependence on present-day conditions, may underestimate the forcing due to aerosol–cloud interaction, especially over land, although this model analysis may overestimate the cloud condensation nucleus to AOD relation (Quaas et al., 2011). Wang and Penner (2009) also showed that if models include boundary layer nucleation and increase the fraction of sulphur emitted as a primary particle, the effect over land is increased relative to over ocean (see also Section 7.5.3). The aerosol ERF standard deviation is large in biomass burning regions, as for the RF, and in regions where cloud effects differ among models (e.g., northern North America, northeast Asia, Amazonia). The spread in aerosol ERF is much larger than for the RF alone, although the relative standard deviation is no larger (Shindell et al., 2013c).

For components that primarily scatter radiation, the radiative effect at the surface is similar to the RF (according to the definition in Section 8.1.1). However for components that absorb radiation in the atmosphere the radiation reaching the surface is reduced (Forster et al., 2007; Ramanathan and Carmichael, 2008; Andrews et al., 2010). This absorption of incoming solar radiation alters the vertical temperature profile in the atmospheric column and can thus change atmospheric circulation and cloud formation. The aerosol atmospheric absorption (Figure 8.23, bottom right), or the difference between ERF and the analogous radiative flux reaching the surface including rapid adjustments, has a spatial pattern that to lowest order tracks the carbonaceous aerosol forcing, but is also affected by cloud changes, where e.g., cloud loss could enhance atmospheric absorption. Atmospheric aerosol absorption patterns thus mirror the ERF due to aerosol–cloud interaction pattern, with larger forcing over continents.

Ozone RF is calculated using the methodology described in Shindell et al. (2013c), but applied to the larger set of models in ACCMIP (Stevenson et al., 2013). The net ozone RF (Figure 8.23; fourth row) is largest in subtropical latitudes, and is more positive in the NH than the SH. Pollution in the NH accounts for positive tropospheric forcing; stratospheric ozone loss has caused negative SH polar forcing. Model standard deviation is largest in the polar regions where lower stratosphere/upper troposphere changes differ in the models (Young et al., 2013).

Overall, the *confidence* in aerosol and ozone RF spatial patterns is *medium* and lower than that for the global mean due to the large regional standard deviations (Figure 8.23), and is exacerbated in aerosol ERF patterns due to uncertainty in cloud responses.

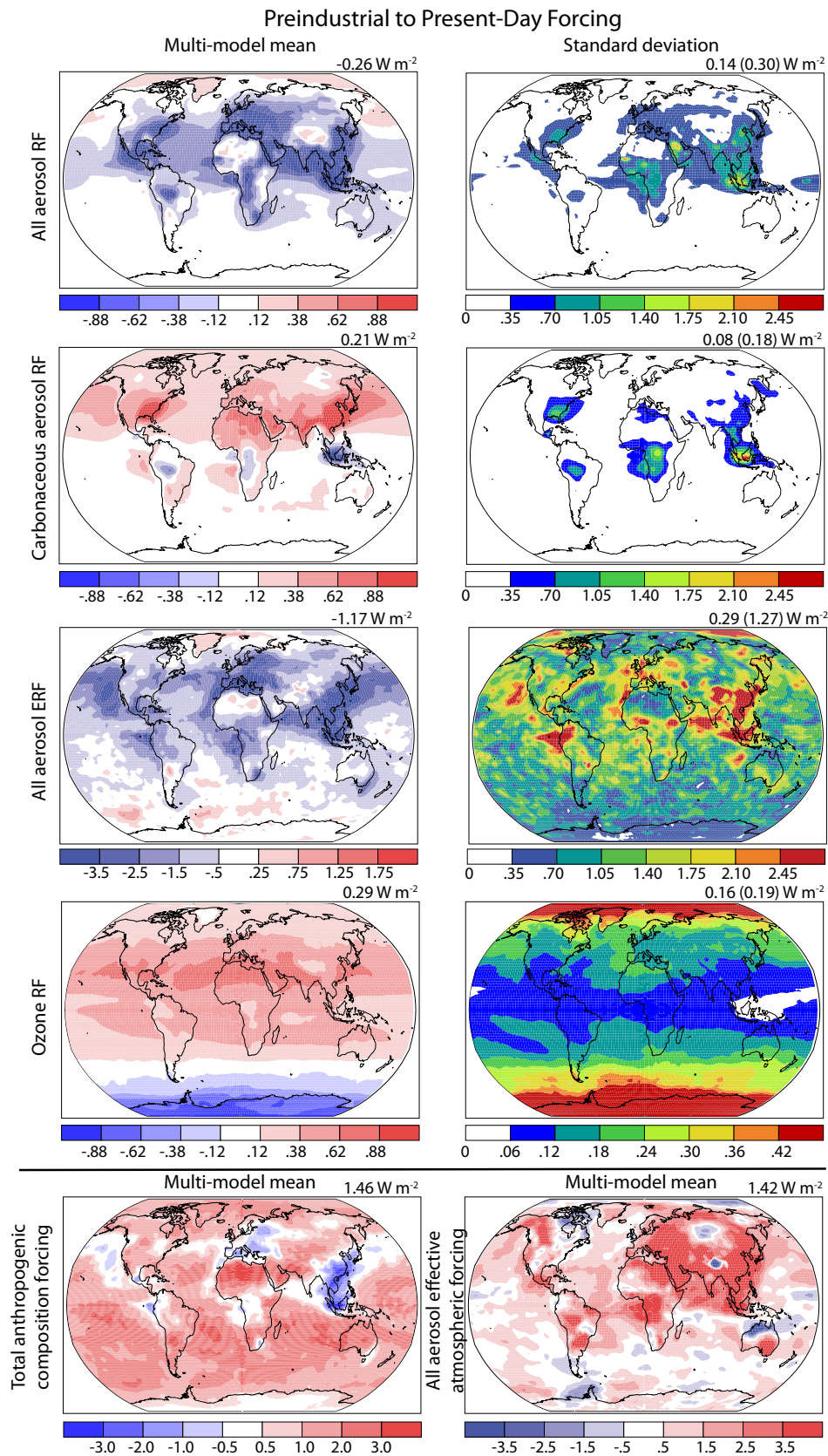


Figure 8.23 | Spatial pattern of ACCMIP models 1850 to 2000 forcings, mean values (left) and standard deviation (right) for aerosols and ozone (top four rows). Values above are the average of the area-weighted global means, with the area weighted mean of the standard deviation of models at each point provided in parenthesis. Shown are net aerosol RF due to aerosol–radiation interaction (top, 10 models), carbonaceous aerosol RF due to aerosol–radiation interaction (2nd row, 7 models), aerosol ERF (3rd row, 8 models), ozone (4th row, 11 models), total anthropogenic composition forcing (WMGHG+ozone+aerosols; bottom left), aerosol atmospheric absorption including rapid adjustment (bottom right, 6 models). Note that RF and ERF means are shown with different colour scales, and standard deviation colour scales vary among rows.